Self-assembled transmembrane protein-polymer conjugates for the generation of nano-thin membranes and micro-compartments

Dissertation

zur Erlangung des akademischen Grades

„doctor rerum naturalium“ (Dr. rer. nat.)

in der Wissenschaftsdisziplin "Kolloid- und Polymerchemie"

eingereicht an der

Mathematisch-Naturwissenschaftlichen Fakultät

der Universität Potsdam

von

M.Tech. Himanshu Charan

Potsdam, 11 September 2017

करत करत अभ्यास के, जड़मतत होत सुजान। रसरी आवत जात रे, तसल पर पडत तनसान।

- कबीर

“Practice makes a man perfect”

- Kabeer

Published online at the
Institutional Repository of the University of Potsdam:
URN urn:nbn:de:kobv:517-opus4-402060
http://nbn-resolving.de/urn:nbn:de:kobv:517-opus4-402060

Erklärung

Ich (Himanshu Charan) versichere, die hier vorliegende schriftliche Arbeit selbständig verfasst und keine anderen als die angegebenen Hilfsmittel benutzt zu haben. Die Stellen der Arbeit, die anderen Werken dem Wortlaut oder dem Sinn nach entstammen, wurden unter Angabe der Quellen kenntlich gemacht. Dies gilt auch für in der Arbeit enthaltenen Zeichnungen und Abbildungen. Ich erkläre hiermit, dass die Dissertation in der vorgelegten oder einer ähnlichen Fassung noch nicht zu einem früheren Zeitpunkt an einer anderen in- oder ausländischen Hochschule als Dissertation eingereicht worden ist.

Himanshu Charan

Prüfungsausschuss:
Prof. Dr. Alexander Böker (Erstgutachter)
Prof. Dr. Ulrich Schwaneberg (Zweitgutachter)
Prof. Dr. Svetlana Santer (Externer Gutachter)
Prof. Dr. André Laschewsky (Mitglied der Prüfungskommission)
Prof. Dr. Heiko M. Möller (Mitglied der Prüfungskommission)
Prof. Dr. Andreas Taubert (Vorsitz)

Acknowledgements

It is a pleasure to thank all the people who have accompanied and supported me throughout my scientific work. I am honored to show my sincere gratitude to my research supervisor Prof. Dr. Alexander Böker for giving me the opportunity to work in his research group on such an interesting and interdisciplinary topic. I also thank him for his persistent optimism and confidence in my abilities.

I most gratefully acknowledge that the work carried out in this project was considerably influenced by the deep insight and vision of my daily guide and supervisor, Dr. Ulrich Glebe. In addition to being a moral support all through the execution of my work, he was always a critical discussion partner. His meticulous approach towards my experimental work as well as daily life hacks have not only proved valuable for the project but also significantly molded my research acumen and personal wisdom, and for that I shall ever remain indebted to him.

I express my gratitude towards our collaboration partners, the group of Prof. Dr. Schwaneberg, particularly Julia, Deepak, Leilei, Tayebeh and Marco for a successful collaboration and insightful discussions.

I also thank all the past and present colleagues, from DWI, Aachen as well as Fraunhofer IAP. I also thank my office colleagues for a positive and amicable environment conducive for efficient work.

I would like to cheerfully thank my friends here at Fraunhofer IAP, in Aachen and abroad for the constant stimulus and optimism. I would like to specifically thank Abhishek Sanoria, Sampat Singh Bhati, Srinath Subramanian and Li Tan for always keeping me motivated. I would also like to thank my flatmates, Lynn and Uli for giving me a second home here in Germany.

Most importantly, I am ever so grateful to my dearest mother (Rajbala Charan), sister (Monika Charan) and father (Bhagirath Charan), without whose unconditional love, faith and enthusiasm this project would never have been possible.

Publications and posters

Parts of this thesis have already been published or submitted, as shown below:

- **Patent:**
  - "Poröse Dünnschichtmembran, Verfahren zu ihrer Herstellung sowie Verwendungsmöglichkeiten"
    H. Charan, U. Glebe, A. Böker, M. Tutus, U. Schwaneberg, L. Zhu, M. Bocola, T. Mirzaei Garakani, J. Kinzel, D. Anand
    EP16160714.8, application date: 16.3.2016
    PCT/EP2017/054764, application date 1.3.2017

- **Publications:**
  - "Nano-thin walled micro-compartments from transmembrane protein polymer conjugates"
    H. Charan, U. Glebe, D. Anand, J. Kinzel, L. Zhu, M. Bocola, T. Mirzae Garakani, U. Schwaneberg, A. Böker
    Soft Matter, **2017***,* DOI: 10.1039/C6SM02520J

  - "Dual-Stimuli Sensitive Hybrid Materials: Ferritin-PDMAEMA by grafting-from Polymerization"
    M. L. Tebaldi, H. Charan, L. Mavliutova, A. Böker, U. Glebe
    Macromolecular Chemistry and Physics, **2017**, DOI:10.1002/macp.201600529

  - "Grafting PNIPAAm from ß-barrel shaped transmembrane nanopores"
    H. Charan, J. Kinzel, U. Glebe, D. Anand, T. Mirzaei Garakani, L. Zhu, M. Bocola, U. Schwaneberg, A. Böker, *Biomaterials*, **2016**, *107*, 115-123

  - "Auf dem Weg zu chiralen Protein-Membranen"
    J. Kinzel, U. Glebe, D. Anand, H. Charan, T. Mirzaei Garakani, M. Bocola, L. Zhu, X. Dai, A. Böker, U. Schwaneberg, *18. Heiligenstädter Kolloquium*, **2016**, ISBN: 978-3-00-054165-0, 8 pp.

- **Conference posters:**
  - "Functional polymer-protein conjugates: grafting from a transmembrane protein"
    H. Charan, U. Glebe, T. Mirzaeigarakani, A. Böker, J. Kinzel, D. Anand, L. Zhu, M. Bocola, U. Schwaneberg,
    Functional Polymeric Materials Conference, Fusion Conferences, Ascot/UK, 06.08.2015.

  - "To transmembrane protein-polymer conjugates and beyond: Moving from proof-of-principles to applications"
    H. Charan, U. Glebe, A. Böker
    Polydays conference, Potsdam, 28.09.2016.

Table of contents

List of abbreviations

Materials and bioparticles

AQP	Aquaporin
BAL	Benzaldehyde lyase
BCA	Bicinchoninic acid
BiBA	2-Bromoisobutyric acid
BSA	Bovine serum albumin
CalB	Candida antarctica lipase B
DHB	2,5-Dihydroxybenzoic acid
DMAEMA	(2-Dimethylamino)ethyl methacrylate
DMIAAm	2-(Dimethyl maleinimido)-*N*-ethyl-acrylamide
DMMIBA	3,4-Dimethyl maleic imidobutyl acrylate
DNA	Deoxyribonucleic acid
E. Coli	Escherichia coli
EDC	3-(3-Dimethylaminopropyl)carbodiimide
EDTA	Ethylenediaminetetraacetic acid
FhuA	Ferric hydroxamate uptake protein component A
GOx	Glucose oxidase
HRP	Horseradish peroxidase
Me_6TREN	Tris[2-(dimethylamino)ethyl]amine
MI	Macroinitiator
MPD	2-Methyl-2,4-pentanediol
MtX_n/L	Transition metal-ligand complex used in ATRP
NHS	*N*-hydroxysuccinimide
NIPAAm	*N*-isopropylacrylamide
OmpA	Outer membrane protein A
OmpF	Outer membrane protein F
PBS	Phosphate buffered saline
PDMAEMA	Poly((2-dimethylamino)ethyl methacrylate)
PDMIAAm	Poly(2-(dimethyl maleinimido)-*N*-ethyl-acrylamide)

PDMMIBA	Poly(3,4-dimethyl maleic imidobutyl acrylate)
PE-PEG	Polyethylene-polyethyleneglycol
PES	Polyether sulfone
PFD	Perfluorodecalin
PNIPAAm	Poly(*N*-isopropylacrylamide)
RNA	Ribonucleic acid
SDS	Sodium dodecyl sulfate
Super-DHB	9:1 Mixture of DHB and 2-hydroxy-5-methoxybenzoic acid
TEV	Tobacco etch virus

Technical terms

SFM	Scanning force microscopy
AIDS	Acquired immunodeficiency syndrome
AGET	Activators generated by electron transfer
ARGET	Activator regenerated by electron transfer
ATRP	Atom transfer radical polymerization
AUC	Analytical ultracentrifugation
BBTP	Building blocks based on transmembrane proteins
CD	Circular dichroism
CRP	Controlled radical polymerization
CRDRP	Controlled reversible-deactivation radical polymerization
CTA	Chain transfer agent
DLS	Dynamic light scattering
DP	Degree of polymerization
FTIR	Fourier transform infra-red
IUPAC	International union of pure and applied chemistry
LCST	Lower critical solution temperature
MALDI-ToF	Matrix assisted laser desorption ionization time of flight
MS	Mass spectrometry
MW	Molecular weight
MWCO	Molecular weight cut-off
NMR	Nucleic magnetic resonance

NMP	Nitroxide-mediated polymerization
PDB	Protein data bank
PDI	Polydispersity index
RAFT	Reversible addition fragmentation chain transfer
RDRP	Reversible-deactivation radical polymerization
RT	Room temperature
SARA	Supplemental activator and reducing agent
SDS-PAGE	Sodium dodecyl sulfate polyacrylamide gel electrophoresis
SEC	Size exclusion chromatography
SEM	Scanning electron microscopy
SET-LRP	Single electron transfer living radical polymerization
TEM	Transmission electron microscopy
UV-Vis	Ultraviolet – visible
WT	Wild type
XPS	X-ray photoelectron spectroscopy

Units and unitary terms

a.u.	Arbitrary units
kDa	Kilodalton
mM	Milimolar
m/z	Mass to charge ratio
nm	Nanometer
ns	Nanoseconds
ppm	Parts per million

1 Summary

This project was focused on generating ultra-thin stimuli-responsive membranes with an embedded transmembrane protein to act as the pore. The membranes were formed by crosslinking of transmembrane protein-polymer conjugates. The conjugates were self-assembled on air-water interface and the polymer chains crosslinked using a UV-crosslinkable comonomer to engender the membrane. The protein used for the studies reported herein was one of the largest transmembrane channel proteins, ferric hydroxamate uptake protein component A (FhuA), found in the outer membrane of Escherichia coli (*E. coli*). The wild type protein and three genetic variants of FhuA were provided by the group of Prof. Schwaneberg in Aachen. The well-known thermo-responsive poly(*N*-isopropylacrylamide) (PNIPAAm) and the pH and thermo-responsive polymer poly((2-dimethylamino)ethyl methacrylate) (PDMAEMA) were conjugated to FhuA and the genetic variants via controlled radical polymerization (CRP) using *grafting-from* technique. These polymers were chosen because they would provide stimuli handles in the resulting membranes. The reported polymerization was the first ever attempt to attach polymer chains onto a membrane protein using site-specific modification.

The conjugate synthesis was carried out in two steps – a) FhuA was first converted into a macroinitiator by covalently linking a water soluble functional CRP initiator to the lysine residues. b) Copper-mediated CRP was then carried out in pure buffer conditions with and without sacrificial initiator to generate the conjugates.

The challenge was carrying out the modifications on FhuA without denaturing it. FhuA, being a transmembrane protein, requires amphiphilic species to stabilize its highly hydrophobic transmembrane region. For the experiments reported in this thesis, the stabilizing agent was 2-methyl-2,4-pentanediol (MPD). Since the buffer containing MPD cannot be considered a purely aqueous system, and also because MPD might interfere with the polymerization procedure, the reaction conditions were first optimized using a

model globular protein, bovine serum albumin (BSA). The optimum conditions were then used for the generation of conjugates with FhuA.

The generated conjugates were shown to be highly interfacially active and this property was exploited to let them self-assemble onto polar-apolar interfaces. The emulsions stabilized by particles or conjugates are referred to as Pickering emulsions. Crosslinking conjugates with a UV-crosslinkable co-monomer afforded nano-thin micro-compartments. Interfacial self-assembly at the air-water interface and subsequent UV-crosslinking also yielded nano-thin, stimuli-responsive membranes which were shown to be mechanically robust. Initial characterization of the flux and permeation of water through these membranes is also reported herein. The generated nano-thin membranes with PNIPAAm showed reduced permeation at elevated temperatures owing to the resistance by the hydrophobic and thus water-impermeable polymer matrix, hence confirming the stimulus responsivity.

Additionally, as a part of collaborative work with Dr. Changzhu Wu, TU Dresden, conjugates of three enzymes with current/potential industrial relevance (candida antarctica lipase B, benzaldehyde lyase and glucose oxidase) with stimuli-responsive polymers were synthesized. This work aims at carrying out cascade reactions in the Pickering emulsions generated by self-assembled enzyme-polymer conjugate.

2 Zusammenfassung

Im Rahmen dieses Projekts wurden ultradünne Stimuli-responsive Membranen hergestellt, in die ein Transmembranprotein als Pore eingebettet ist. Die Membranen wurden durch das Verlinken von Transmembranprotein-Polymer Konjugaten an Grenzflächen hergestellt. Dazu wurden Konjugate an der Luft-Wasser-Grenzfläche selbstassembliert und die Polymerketten unter Verwendung eines UV-vernetzbaren Comonomers vernetzt. Als Protein wurde einer der größten Transmembran-Proteinkanäle, welcher sich in der Natur in der äußeren Membran von Escherichia coli (E. coli) findet, verwendet, nämlich ferric hydroxamate uptake protein component A (FhuA). Das Wildtyp-Protein und drei genetische Varianten von FhuA wurden von der Gruppe von Prof. Schwaneberg in Aachen zur Verfügung gestellt. Das bekannte thermo-responsive Poly(*N*-isopropylacrylamid) (PNIPAAm) und das pH- und thermo-responsive Polymer Poly((2-dimethylamino) ethylmethacrylat) (PDMAEMA) wurden über kontrollierte radikalische Polymerisationen (CRP) via der *grafting-from* Technik an FhuA und die genetischen Varianten konjugiert. Diese responsiven Polymere wurden ausgewählt, weil die Eigenschaften der resultierenden Membranen folglich durch äußere Einflusse verändert werden können. Dabei handelt es sich um das erste Beispiel, Polymerketten von einem Membranprotein ortsspezifisch zu synthetisieren.

Die Konjugatsynthese wurde in zwei Schritten durchgeführt - a) zuerst wurde ein FhuA Makroinitiator durch Anbinden funktioneller CRP Initiatoren an die Lysinreste des Proteins dargestellt. B) durch Kupfer-vermittelte CRP wurden dann in Pufferlösung sowohl mit als auch ohne Opferinitiator die Konjugate synthetisiert.

Die Herausforderung bestand darin, FhuA zu modifizieren ohne das Protein dabei zu denaturieren. Als Transmembranprotein benötigt FhuA amphiphile Agentien, um seine hydrophobe Transmembran Region zu stabilisieren. Für die im Rahmen dieser Arbeit durchgeführten Experimente war das stabilisierende Agens 2-Methyl-2,4-pentandiol (MPD). Da der MPD-Puffer nicht als rein wässriges Medium betrachtet werden kann,

und auch, weil MPD das Polymerisationsverfahren beeinflussen könnte, wurden die Reaktionsbedingungen zunächst unter Verwendung eines globulären Modellproteins, nämlich Rinderserumalbumin (BSA), optimiert. Die optimalen Bedingungen wurden dann für die Erzeugung von Konjugaten mit FhuA verwendet.

Die Konjugate zeigten eine hohe Grenzflächenaktivität und diese Eigenschaft wurde für die Selbstassemblierung an polaren/apolaren Grenzflächen ausgenutzt. Wurden Emulsionen durch die Konjugate stabilisiert, so bezeichnet man dies als Pickering-Emulsionen. Das Vernetzen von Konjugaten mit einem UV-vernetzbaren Co-Monomer führt zu nano-dünnen Mikrokompartimenten. Die Selbstassemblierung an der Luft-Wasser-Grenzfläche und anschließende UV-Vernetzung ergaben nano-dünne, Stimuli-responsive Membranen, die sich als mechanisch robust erwiesen. Eine erste Charakterisierung des Flusses und der Permeation von Wasser durch die Membranen wird ebenfalls in dieser Arbeit beschrieben. Die erzeugten nano-dünnen Membranen mit PNIPAAm zeigten eine verminderte Permeation bei erhöhten Temperaturen aufgrund der nun hydrophoben und damit wasserundurchlässigen Polymermatrix.

Darüber hinaus wurden für eine Kooperation mit Dr. Changzhu Wu, TU Dresden, Konjugate von drei Enzymen mit industrieller Relevanz (Candida antarctica Lipase B, Benzaldehydlyase und Glucose-Oxidase) synthetisiert. Diese Arbeit zielt auf Kaskadenreaktionen in Pickering-Emulsionen, die durch selbstassemblierte Enzym-Polymer Konjugate katalysiert werden.

3 Motivation

Biomimicry, a term that gained scientific relevance since the 1960s, refers to the study of structures and functions of biological systems as models for designing solutions to challenging problems in engineering.[1] Biomimicry can provide very effective solutions because they are derived from systems and processes that underwent millions of years of evolutionary perfection. Biological systems are organized in a hierarchical manner, with intricate architecture ultimately giving rise to functional components. A unique interplay of these functional components with the nature around gives rise to multi-functionalities and hence commercial interest.[2] Cells and cell membranes have provided a lot of impetuous for biomimetic and bioinspired membrane research.[1, 3]

Cells and their components, such as the phospholipids, liposomes and membrane proteins etc., have been the utopian standard for many membrane scientists to reach in synthetic membranes. Cell membranes show outstanding permselectivity and contain a lot of pores controlling and facilitating the transfer of water, ions, soluble and insoluble substrates and many other compounds critical to the survival of the cell and cellular functions. Many of these critical tasks are performed by integral membrane proteins.[4]

Integral membrane proteins, despite challenging purification and characterization, have inspired awe from scientists and engineers alike.[5] Aquaporins (AQPs) such as AQP1 allow water to move freely and bidirectionally out of and into the cell, while at the same time restricting other small organic, inorganic molecules, ions and even protons.[6-8] Another interesting example are ion channels, some which have remarkable properties. For instance, K^+ ion channel allows the larger K^+ ions (radius 1.35 Å) to pass at high throughputs (10^8 ions per second) while restricting the smaller Na^+ ions (radius 0.95 Å) by a factor of 1 to 10,000 compared to K^+.[5, 9] Such properties, if incorporated in synthetic membranes, would have great scientific and commercial value.

The development of biotechnology in the last decades has provided us with remarkable tools to sculpt proteins in a number of interesting ways such as using rational redesign

(site-directed mutagenesis)[10, 11] or directed evolution technology.[12, 13] Hence, it is possible to tailor desired residues in desired location in a protein to be suitable, for instance, for efficient grafting-from polymerization.[14]

If transmembrane channel proteins could be incorporated into synthetic membranes, the resulting membrane might be used for a lot of interesting applications. These applications may reach beyond the function of the membrane proteins. For example, with appropriate modification (genetic or chemical) to incorporate a chiral region in the protein channel, the membrane may be used for enantiomeric separation; a task either quite inefficient, or plagued with low yields and expensive at the moment. It would prove very useful in pharmaceutical,[15, 16] agrochemical, food and fragrance industry.[17, 18]

Attempts to generate biomimetic membranes with incorporated membrane channel proteins have been made before.[1] However, either the membranes are thick[19, 20] (hence deviating too far from their biological counterparts) or too weak to sustain stress (and additionally plagued by low incorporation of the protein into the membrane).[21-25] Inspired by the work of Rijn *et al*.,[26] the work presented in this thesis attempted to generate biomimetic membranes containing genetically tailored transmembrane proteins as the pore. The membranes were aimed to be mechanically stable, stimuli-responsive, nano-thin, and yet have a far larger area than any of those synthesized using polymer vesicles. This required generating transmembrane protein-polymer conjugate. Although interest in generating conjugates from membrane proteins has been shown before, it was not yet achieved.[27, 28] This thesis presents for the first time, growth of polymer chains from a membrane protein using controlled radical polymerization.

4 Fundamentals

4.1. Proteins and FhuA

4.1.1. Introduction to proteins and their structure

Polysaccharides, polynucleotides (DNA and RNA) and proteins represent the three life sustaining bio-macromolecules for all known life forms on our planet. While polysaccharides serve as food and building material, polynucleotides serve as the repository of genetic information which helps define the structure and functioning of the body. Proteins perform a whole range of tasks of the cellular life: providing structural strength to the cell, catalyzing bio-chemical reactions and recognition of foreign bodies and their cleanup. Membrane proteins and signal proteins receive signals from outside the cell and mobilize intracellular response, while, proteins like histones are crucial for the proper 'reading' of genetic data from the DNA / RNA. Proteins are the workhorse macromolecules of the cell and are as diverse as the tasks they perform.[4]

The structure of proteins is critically important for the function they perform. At the most elementary molecular level, proteins are polymers of amino acids. A primary amine and an acid add releasing a water molecule and the resulting bond is called a peptide bond. For this reason, proteins are also referred to as polypeptides. Out of theoretically infinite number of possible amino acids, only 20 specific amino acids build up all the proteins in all the creatures on planet earth.[5] Hence, they are called proteinogenic amino acids. Each proteinogenic amino acid consists of a primary amine group, a carboxylic acid group, an α-hydrogen and a side chain group, called the residue (Figure 4.1).

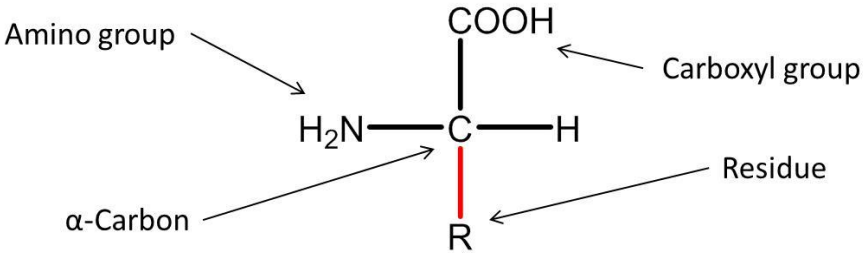

Figure 4.1: *The Fischer projection of the structure of a proteinogenic amino acid.*

The molecular structures of the residues of all 20 proteinogenic amino acids are shown in Figure 4.2. In nomenclature of the residues, there are two common abbreviation

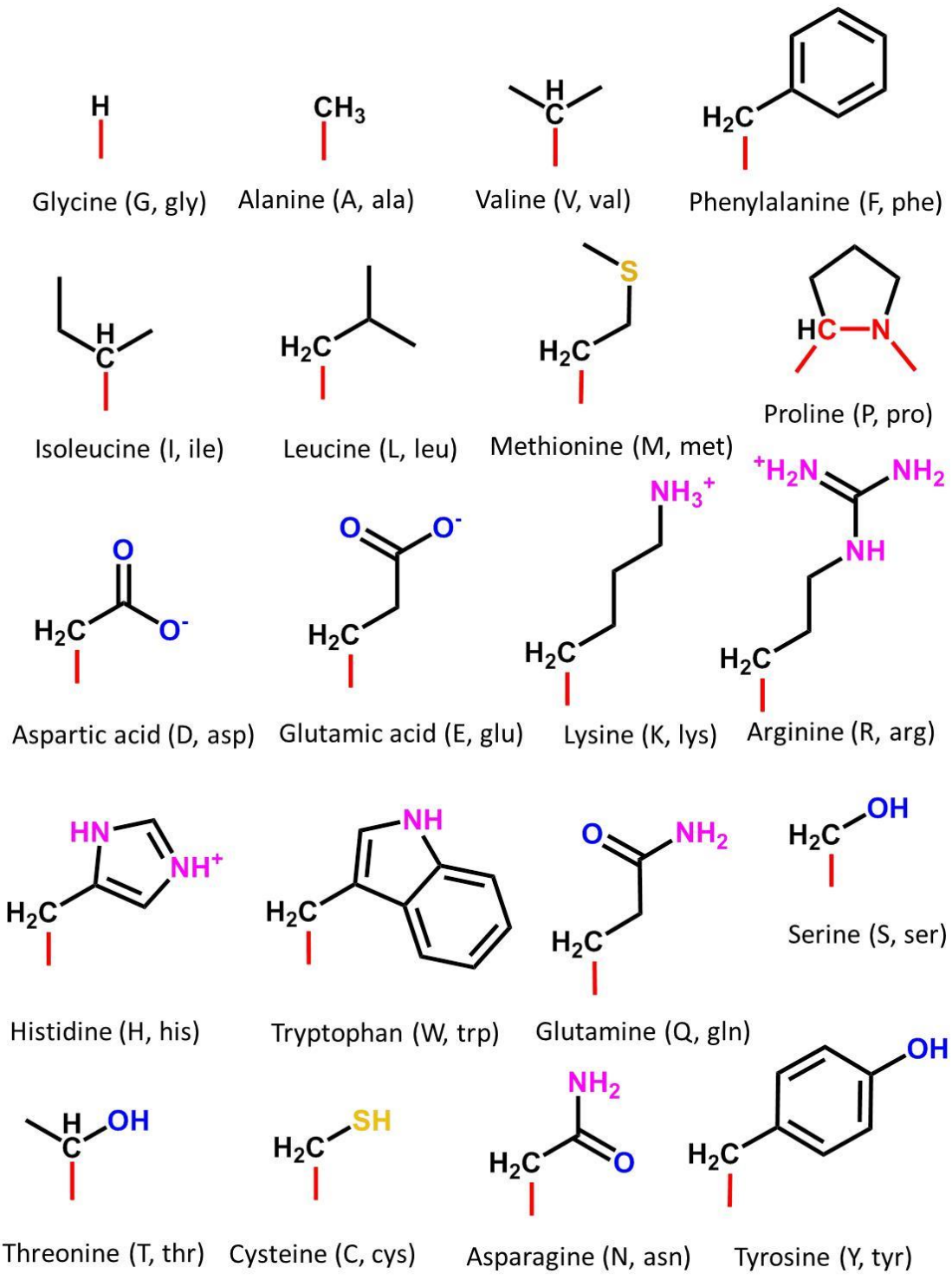

Figure 4.2: *Residues of the proteinogenic amino acids. The residues in the image have been ordered as having non-polar (G, A, V, F, I, L, M, P), acidic (L, R), basic (H, W, Q) and non-charged but polar (S, T, C, N, Y) side chains.*

systems; one using three letter acronym and another using a single letter representing the different residues and they are also illustrated in Figure 4.2.

The sequence of the residues of the amino acids making up the polypeptide chain is referred to as the primary structure of a protein.[5] However, proteins are much more complex than just linear polymer chains. Because of a number of charged and polar residues and polar main chain, different residues interact, resulting in complex 3-D structures. The second order of the structure is called the secondary structure, most common of which are α-helix and β-sheet (Figure 4.3). As the name suggests, α-helixes

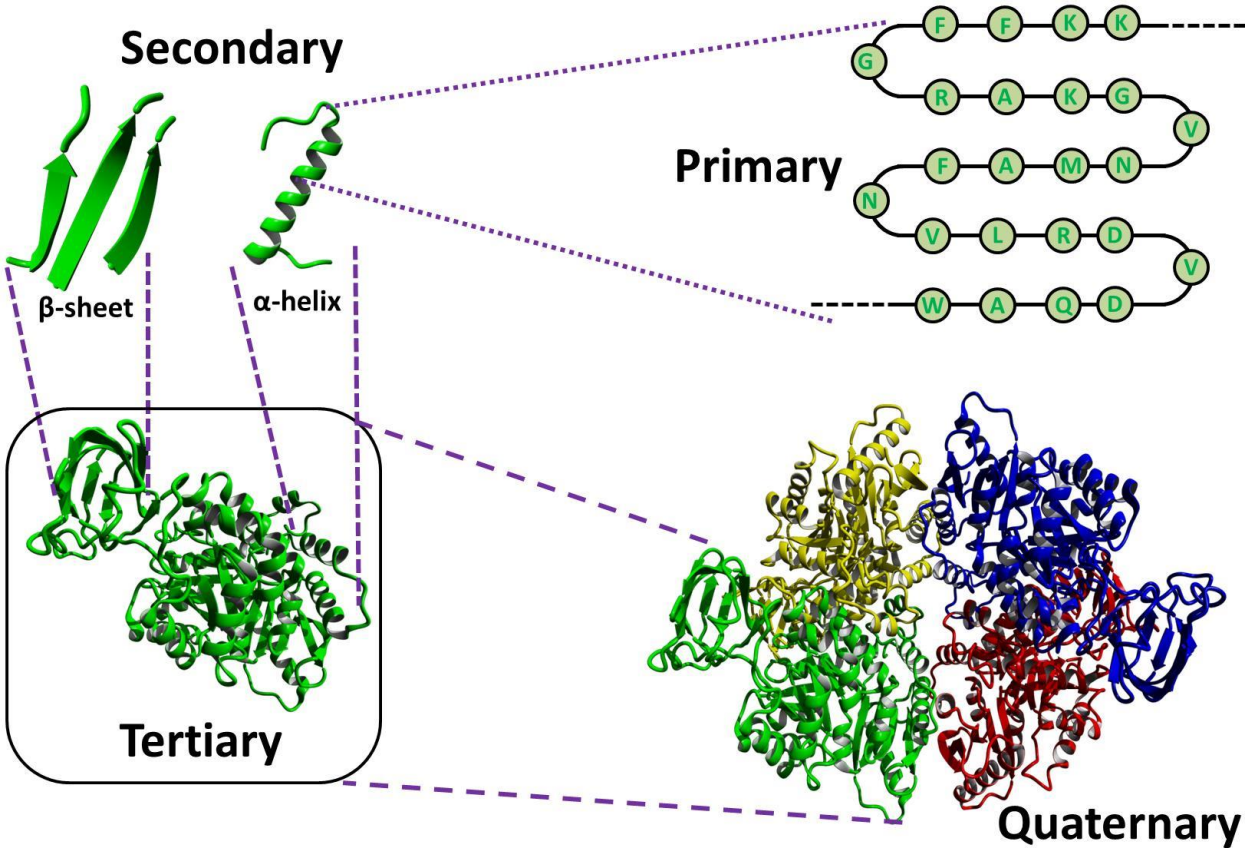

Figure 4.3: *Illustration of the four different levels of protein structures with the exemplary protein, human pyruvate kinase M2 mutant C424A (PDB ID 4wj8). The primary structure is the composition of polypeptide chain when stretched like a polymer. Self-assembly into medium-range order results in secondary structures such as α-helix and β-sheet. Tertiary structure is the folded form of a protein chain that can perform a function. The higher order structures resulting from multiple monomer units generate a fully functional protein. Not all proteins have a quaternary structure.*

are helical rod-like arrangement (see Figure 4.3) and β-sheets resemble sheet or planar arrangement. The secondary structures result from the hydrogen bonding between the carbonyl groups and amine groups in the main polypeptide chain.[5] A combination of these secondary structures is called a domain when it is a functional entity. The tertiary structure, which might have one or more than one domains, is the 3-D arrangement of the protein, in which residues much farther away in the primary sequence of the protein may come in very close proximity of each other and hence generate complex tertiary structures (Figure 4.3). In fact, despite substantial progress in protein science as well as the computing power in the last decades, predicting the tertiary structure of a protein based on the primary sequence is still one of the unsolved basic scientific enigmas of our time.[5] Quite often, more than one polypeptide chains arrange in complex architectures, displaying the quaternary structure in some proteins. The quaternary structures may be from the identical polypeptide chains (homo-oligomeric protein – Figure 4.3) or different polypeptide chains (hetero-oligomeric protein) arranging into complex architectures.

Interactions between various residues are very common, and they are crucial for the stability of secondary, tertiary and quaternary structure of proteins. Two of the most important interactions are disulfide bridges and salt bridges. The cysteine residues are capable of forming covalent bonds with other cysteine residues to generate what is called a disulfide bridge (Figure 4.4A). Disulfide bridges are very important for the structural stability of some proteins.[5] Another important type of interaction is the non-covalent interaction between charged residues. For instance, lysine and arginine residues show electrostatic interactions (including hydrogen bonding between residues) with residues like glutamic acid and aspartic acid. These interactions are termed as a salt-bridge if the oppositely charged units are less than 4.0 Å apart from each other.[29]
Even though non-covalent, salt bridges are very crucial to the structure of a protein. For instance, a small mutation in the natural structure of the protein lamin A IG-like domain (Figure 4.5a and Figure 4.5b) resulted in the destruction of a salt bridge (Figure 4.5c). The patients with this mutation, from a very early age, suffered multiple tragic syndromes like postnatal growth retardation, skeletal abnormalities and many more.[30]

This study demonstrates that it is very crucial to keep the salt bridges intact and stabilized when chemically modifying or genetically reengineering a protein.

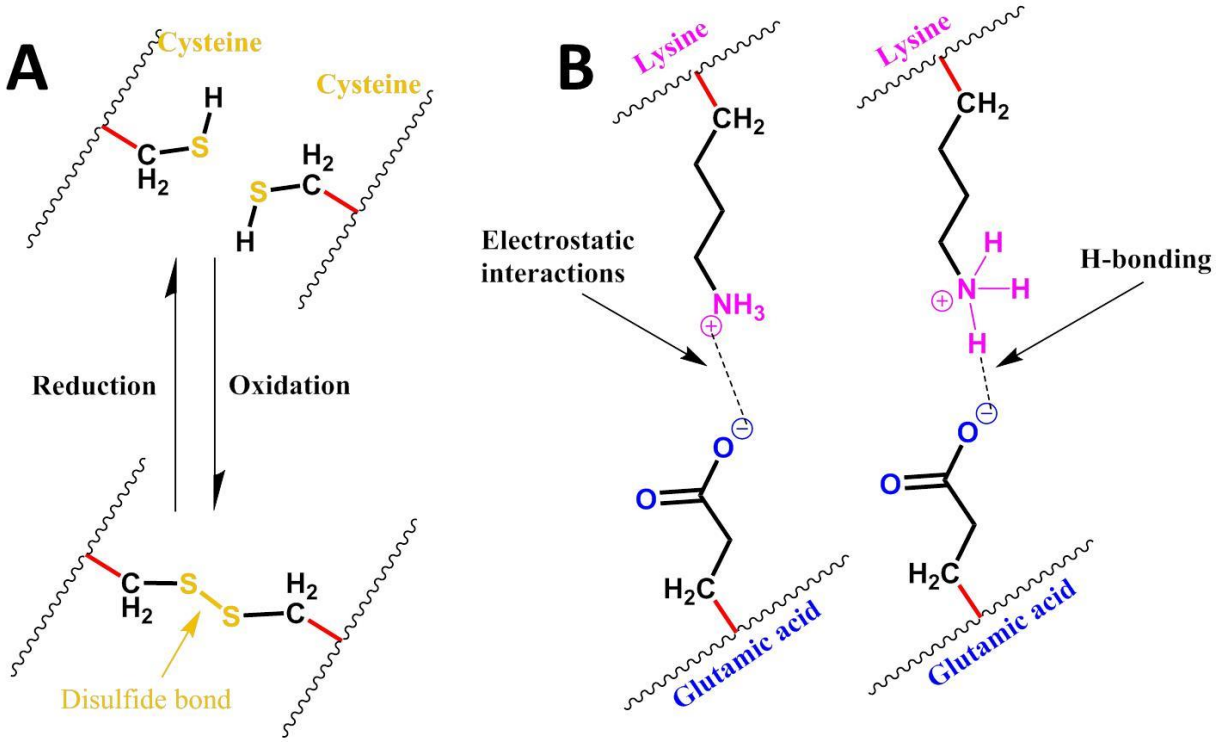

Figure 4.4: *The formation of a disulfide bond (A) provides structural stability to many proteins. Salt bridges (B), commonly formed between oppositely charged residues also provide stability to the tertiary and quaternary structure of many proteins.*

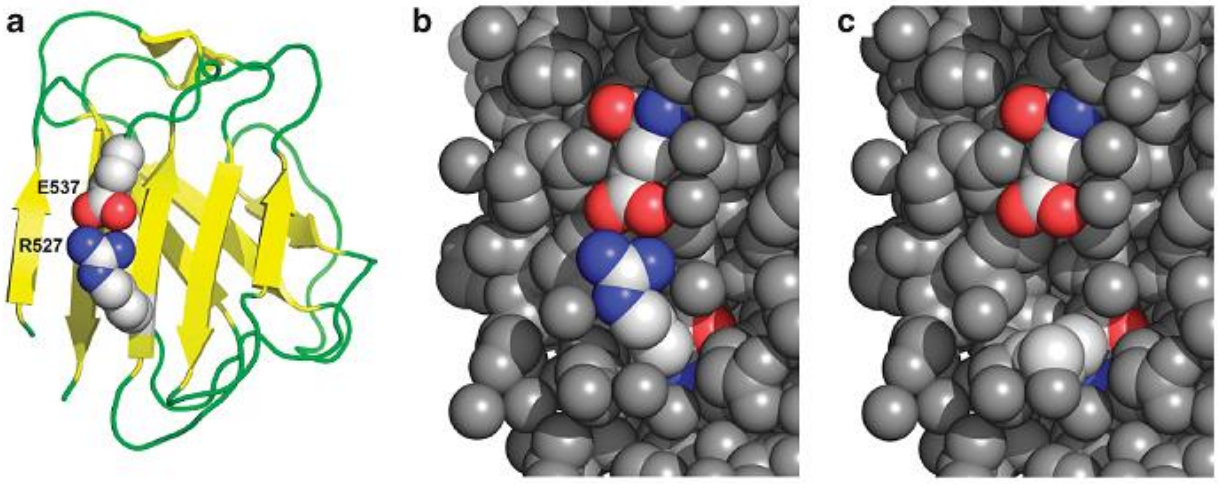

Figure 4.5: *Salt bridges play a very important role in protein structure and hence healthy body. Image adapted with permission from the reference.*[30]

4.1.2. Membrane proteins and FhuA

In gram negative bacteria, nearly 50 % of the outer membrane mass is composed of proteins (Figure 4.6).[31] This could be either lipoproteins or integral membrane proteins such as outer membrane protein A (OmpA), outer membrane protein F (OmpF) or ferric hydroxamate protein component A (FhuA). Membrane proteins have vital functions in various biological processes, such as cell signaling-transduction pathways and in controlling a wide array of gradients such as chemical, electrical, and mechanical gradients.[14] They can act as channels which enable highly selective transport of substrates or energy. Protein classes like aquaporin exhibit some remarkable characteristics like high speed transfer ($3 \cdot 10^9$ molecules per protein per second) of water across the cell membranes, while inhibiting other small molecules.[6-8] Another class, the ion channels are responsible for maintaining potential gradients

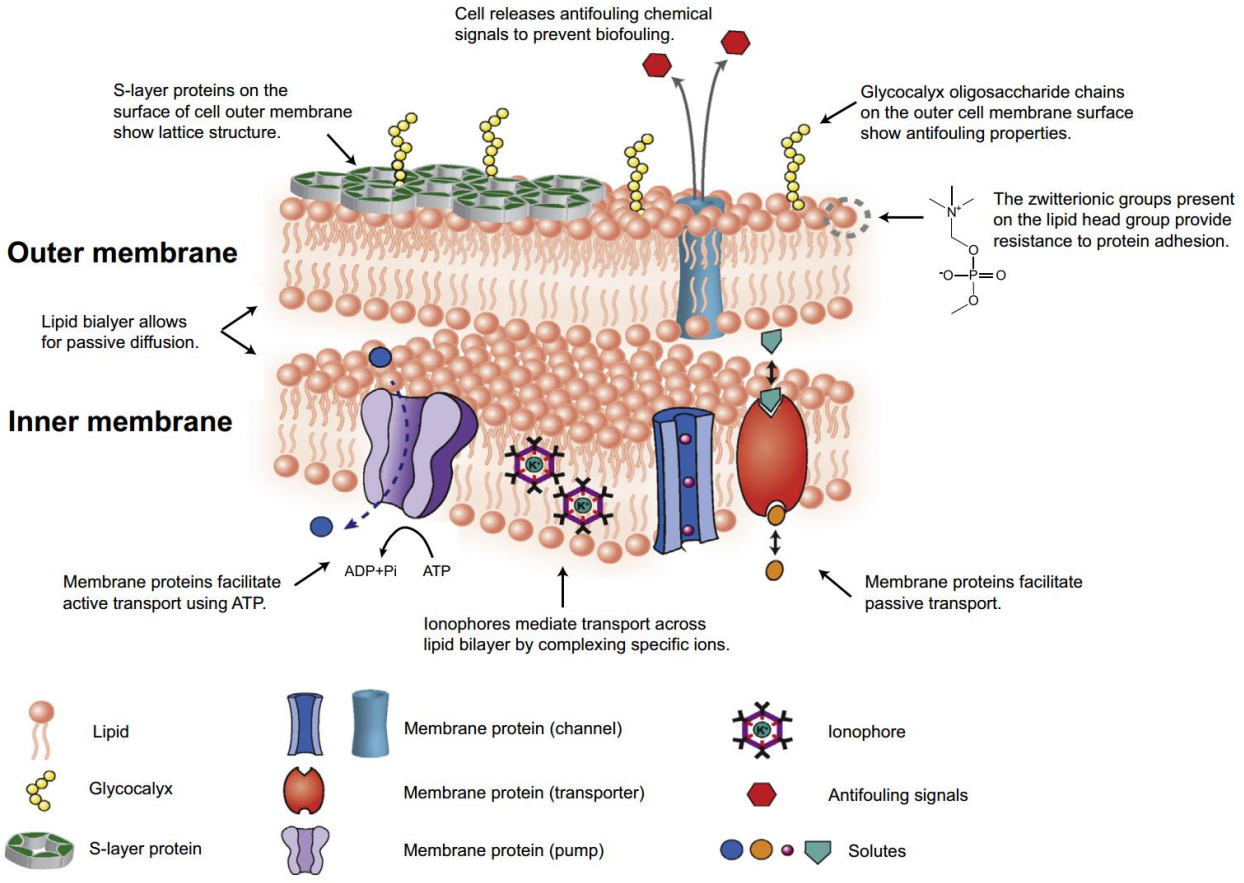

Figure 4.6: *A scheme of cell membrane and the typical functions. Image adapted with permission from the reference.*[32]

across the cell membrane (i.e. between the inside and outside of the cell).[5, 9]

Structurally, integral membrane proteins, especially transmembrane proteins, contain a highly hydrophobic middle part, as a consequence of their location spanning across the hydrophobic part of the phospholipid bilayer (Figure 4.7). *In vitro*, this hydrophobic part needs to be stabilized with the use of amphipathic stabilizers. Reader is referred to **Section 7.3** for more details about such stabilizers.

FhuA, the largest of monomeric β-barrel transmembrane proteins (Figure 4.8), functions as siderophore-mediated iron transporter, receptor for the antibiotic albomycin and bacteriophages like T1, T5.[31, 33] FhuA is located in the outer membrane of Escherichia coli (E. coli) (Figure 4.7). In its natural form (FhuA wild type or FhuA WT), it has an elliptical cross section of 39-46 Å, a height of 69 Å[33] and has a highly hydrophobic region in the middle (2-3 nm) to enable the anchoring in the outer membrane (Figure 4.9).[31] It consists of 22 β-sheets forming a barrel (C-terminus) and the N-terminal cork

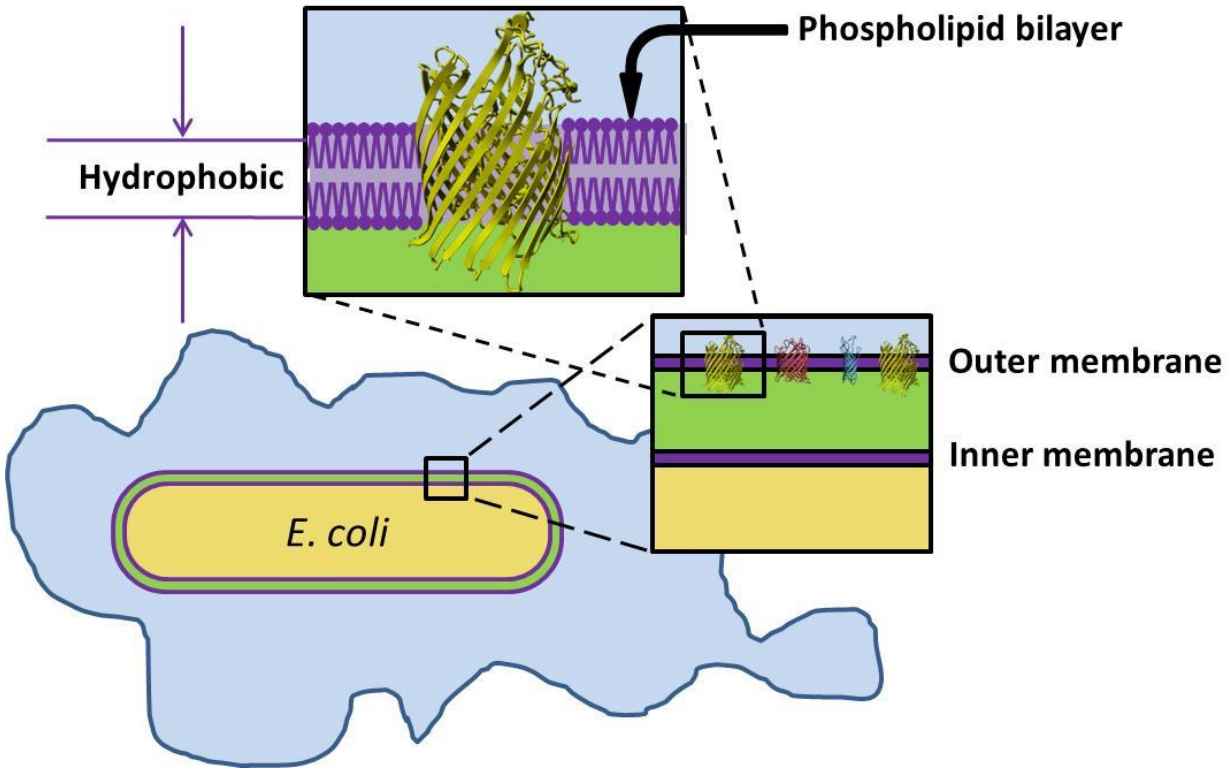

Figure 4.7: *Location of FhuA in the outer membrane of E. coli results in a hydrophobic patch in the middle of the FhuA barrel.*

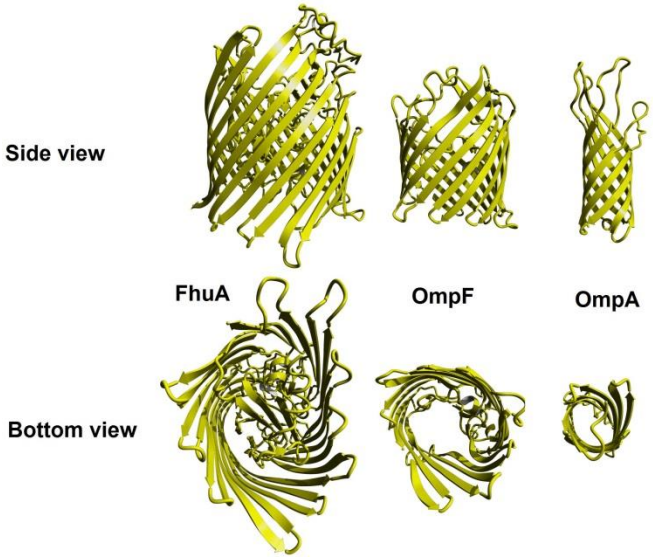

Figure 4.8: *Comparison of the structure of FhuA (PDB ID: 1by3), the largest transmembrane protein of E. coli, with OmpF (PDB ID: 2omf) and OmpA (PDB ID: 1bxw).*

domain which is blocking the channel.[34] After genetic modification, FhuA, without this cork domain (FhuA Δ1-159), can function as a passive diffusion channel and has been used as a nanopore integrated in liposome/polymersome membranes for the translocation of compounds.[35-37] *In vitro*, FhuA shows remarkable resistance towards high temperature, alkaline pH[38] and robustness in genetic modification.[36, 39-41]

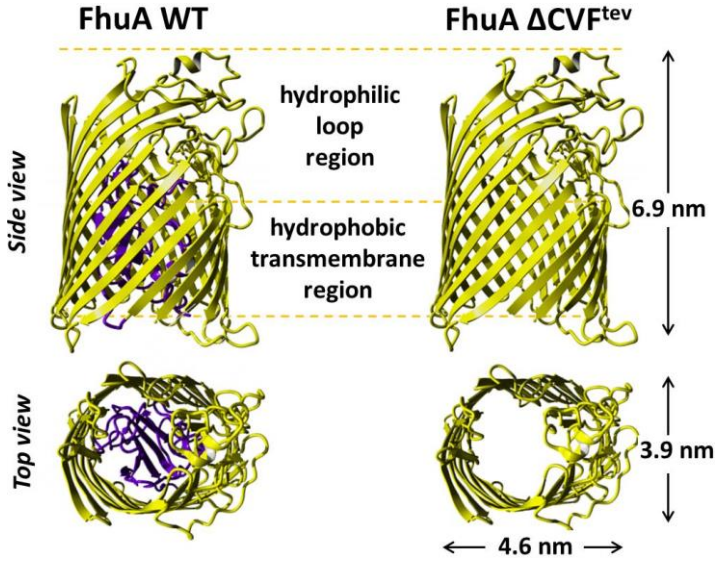

Figure 4.9: *The cork domain of FhuA WT (shown in purple) was removed to generate an open channeled FhuA ΔCVF^{tev}. See chapter 7 for more details.*

After genetic modification, another FhuA variant (FhuA ΔCVF^{tev}) has been generated that has two cleavage sites for protease from Tobacco Etch Virus (TEV), and can be used to cleave two beta-sheets for easier analysis using MALDI-ToF MS (see **Section 7.4** for more details). All these characteristics motivated us to choose FhuA as the transmembrane protein to carry out the work reported in this thesis.

4.2. Bioconjugation

For many applications, it is needed to chemically modify a protein. However, since a protein's function depends on its secondary and tertiary structure, the modification should be done in a way not to affect these structures. Various conjugation chemistries on various residues of the proteins have been tested in the last five decades. One of the primary factors in choosing a desired target residue for modification is its accessibility. Many residues such as methionine are usually deep in the core of the protein structure and hence not easily accessible for chemical modification.[42] The other factor is its reactivity. While lysines are highly nucleophilic and can be used in nucleophilic substitution reactions, aliphatic residues like leucine or proline are not reactive at all and hence cannot be the candidates for bioconjugation reactions. Another important factor is the relative abundance of the residue in the protein structure. It is crucial in deciding the amount of modification per protein. For instance, lysine has an average natural abundance of 5.85 % as opposed to 1.08 % for tryptophan.[42]

Lysine, with its relative abundance of 5.85 %, average surface accessibility of 0.607 and a high reactivity, is unsurprisingly one of the residues most often targeted for bioconjugation reactions.[42, 43] Using reactions with activated carboxylic acids is the most common technique to modify lysine residues. Particularly, *N*-hydroxysuccinimidyl (NHS) esters are frequently utilized in addition to other carboxylic acid derivatives such as NHS carbonates, NHS carbamates, anhydrides and acid halides.[42, 44] Figure 4.10 shows the most common reaction products when targeting lysines.

Although, cysteine is present only in very small relative amounts in proteins and further less that are not in a disulfide bridge, it has been frequently used for protein modification.[42, 44, 45] One advantage of having a low relative abundance is the less polydispersity of the resultant protein-polymer conjugate. Additionally, cysteine modification is beneficial when the more common lysine residue is in the active center of an enzyme. Michael addition and thiol-ene coupling are the two most commonly used conjugation chemistries for targeting cysteines (Figure 4.10).

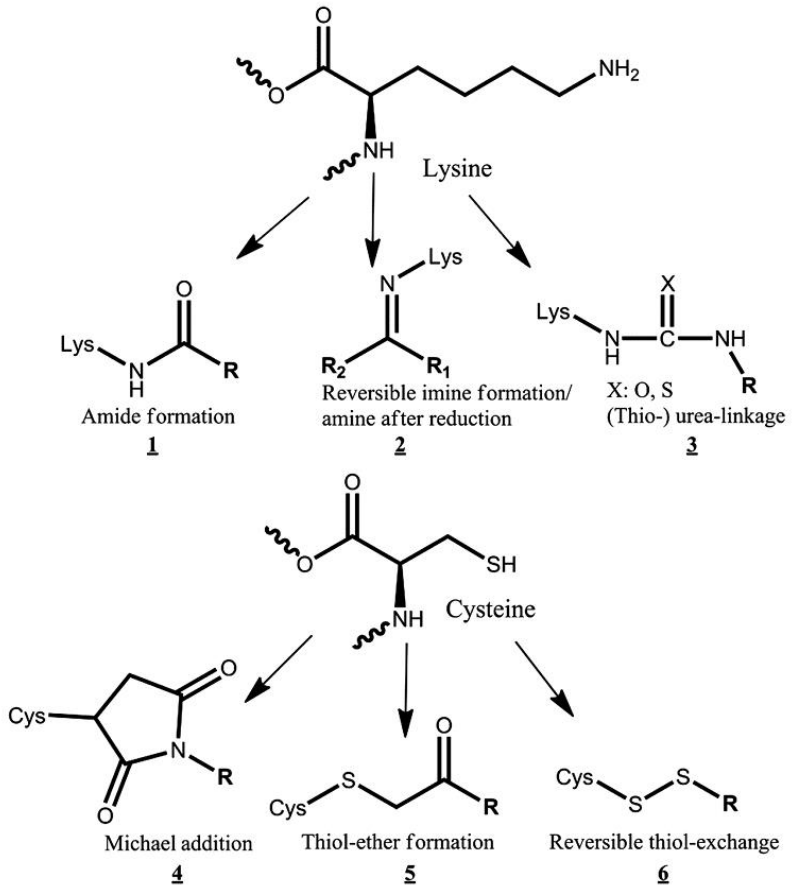

Figure 4.10: *Reaction products of two most frequently used amino acid residues, lysine (1, 2 and 3) and cysteine (4, 5 and 6). Lysine reaction with NHS esters results in amide bond formation (product 1), while reactions of cysteine with α-halocarbonyl compunds or Michael addition results in stable thiol-ether bond formation (product 4 and 5). Reported with permission from reference.*[46]

4.3. Controlled radical polymerization

Controlled radical polymerization (CRP), or IUPAC recommended terms reversible-deactivation radical polymerization (RDRP) or controlled reversible-deactivation radical (CRDR) polymerization,[47, 48] refer to radical polymerization that contains much lower concentration of propagating radicals as compared to conventional free radical polymerization. Consecutively, these polymerizations offer much greater control over the polymerization kinetics and hence, substantially lower polydispersities. Three main approaches, namely nitroxide-mediated polymerization (NMP), reversible addition fragmentation chain transfer (RAFT) polymerization and atom transfer radical polymerization (ATRP) have become popular in the last two decades. Figure 4.11 shows the number of citations (entries in Chemical Abstract Services, CAS) per year since 1994. ATRP and RAFT are the two most widespread RDRP used for synthesis of a number of polymer architectures in the last two decades, and are discussed below.

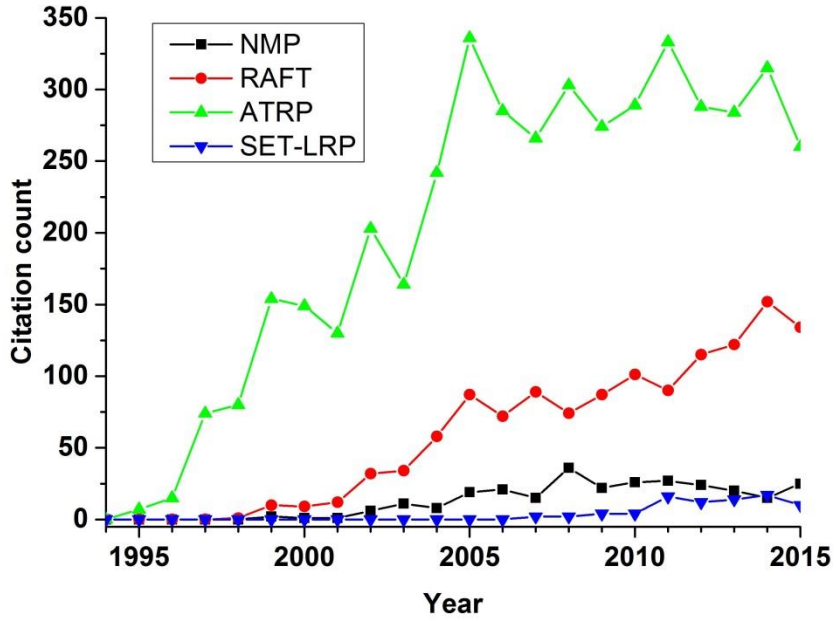

Figure 4.11: *Number of CAS entries per year for the four popular RDRP methods. ATRP and RAFT are by far the most used RDRP.*

4.3.1. ATRP and related techniques

ATRP is usually carried out from an alkyl halide initiator which is converted to a radical by a catalyst system (usually transition metal complexes) to initiate and propagate the polymerization (Figure 4.12a). The catalyst (metal-ligand complex, MtX_n/L; copper being the most common transition metal for the use), with the help of an inner-sphere electron transfer process, activates the alkyl halide initiator and engenders the radicals.[49] Active radicals are deactivated by the catalyst in its higher oxidation state to generate the polymer chains in the dormant state (Figure 4.12a). Since, most chains remain in the dormant state statistically longer than propagating chains at any given time, undesired reactions such as termination, self-coupling or disproportionation of active radical species are significantly minimized.[49] Hence, the polymer chains grow in a controlled fashion and the resulting polymer has a substantially low polydispersity as compared to

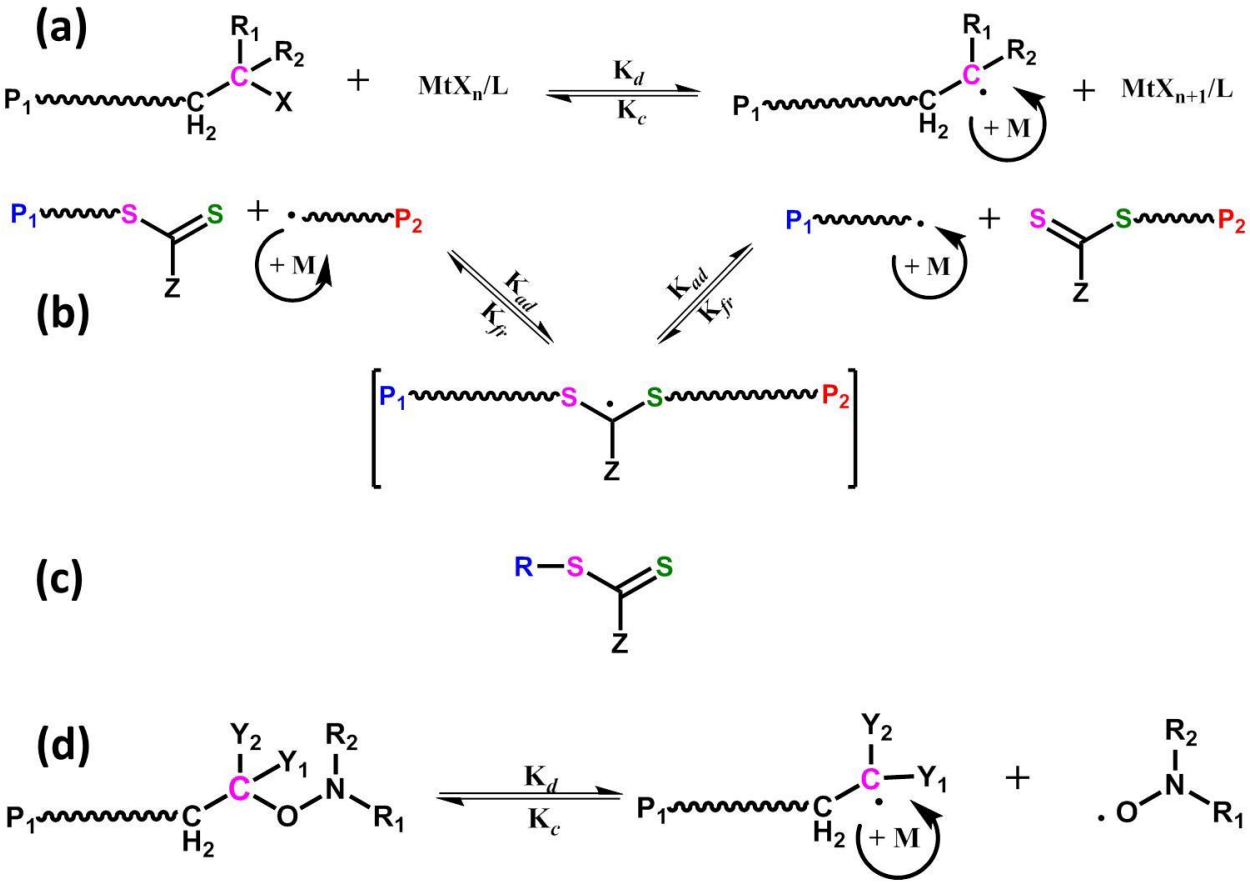

Figure 4.12: *Main propagation mechanisms of a) ATRP, b) RAFT and d) NMP. A typical CTA (c).*

the one from conventional free radical polymerization. However, as the polymerization proceeds, some termination reactions keep occurring (since it is not an ideal “living” radical polymerization), resulting in accumulation of the catalyst in higher oxidation state (MtX_{n+1}/L). As a result, the rate of propagation continuously drops, eventually stopping, because of the so-called persistent radical effect.[50] Activators generated by electron (such as Sn^{II} compounds,[51] ascorbic acid[52] or phenols[53]) is added to “reactivate” the catalyst to its lower oxidation state (MtX_n/L).[54] As a result, substantially lower amounts of catalyst could be used in conjugation with the reducing agent. When using a reducing agent that cannot generate polymer chains as a slow continuous feed to the reaction mixture, the mechanism has been termed as activators regenerated by electron transfer (ARGET) ATRP.[55] These approaches have been proposed to be beneficial for biological and healthcare applications.[54]

More recently, copper-mediated CRP have been termed as single electron transfer living radical polymerization (SET-LRP)[56] or supplemental activator and reducing agent atom transfer radical polymerization (SARA ATRP)[57], depending on weather Cu(0) or Cu(I) plays the dominant role in radical generation. The reactants (monomer and catalysts) as well as resulting products from both the routes are identical, but a fierce debate about the mechanism of activation, particularly for polymerizations in water, is still ongoing.[58-63] The ATRP technique is compatible with a wide range of monomers,[64] and across various reaction conditions.[48, 49, 65] The initiators, transition metal catalysts and ligands employed in the ATRP can be easily commercially procured. These facts make ATRP one of the most popular choices for RDRP, as seen in the number of publications per year on ATRP (Figure 4.11).

4.3.2. RAFT

RAFT polymerization is a controlled radical polymerization mediated by a RAFT agent or CTA. CTA is typically a thiocarbonylthio derivative with a stabilizing Z-group and a reinitiating R-group (Figure 4.12c). In early stages of polymerization, the attachment of the CTA to a propagating polymer chain followed by fragmentation of the intermediate radical results in the formation of a dormant polymer-CTA compound and R·radical.[66]

Reaction of the R·radical with monomer results in another propagating polymer chain. Eventually, the equilibrium depicted in Figure 4.12b is established and the polymerization propagates. Hence, the CTA converts the polymerization into a controlled one by continuously and reversibly deactivating one chain while the complementary chain is propagating, in addition to rapid exchange between similar propagating chains (Figure 4.12b).[64, 66] RAFT is tolerant to a variety of functional groups, can be performed under mild conditions and chain end of the resultant polymer is easily modifiable.[67-69] Although compatible with most common vinyl monomers from conventional radical polymerization, RAFT is not suitable for monomers with primary amino groups.[66] Furthermore, RAFT CTAs are not commonly commercially available and their synthesis can be quite complex.[70] RAFT has also gained prominence in the last decade and a half as one of the most important RDRP techniques (Figure 4.11).

4.3.3. NMP

NMP utilizes nitroxide radicals as the reversible deactivator for the propagating polymer chains (Figure 4.12d).[71, 72] Since most of the polymer chains exist in the dormant state, the propagation, and hence, the polymerization is substantially more controlled than free radical polymerization. Being a monomolecular polymerization system, it is the most straightforward of the three approaches being discussed here. However, despite being one of the first RDRP techniques, it suffers from significant challenges such as high temperatures required for homolysis of the alkoxyamines and their limited commercial availability.[73] Consecutively, research with NMP as a RDRP has not reached the same prominence as ATRP or RAFT.

4.4. Smart polymers

4.4.1. Stimuli-responsive polymers

In the beginning of the 20th century, extraordinary works carried out by Staudinger and others led to the establishment of polymer science as a proper field of chemistry as

opposed to the trial and error fringe part of science till then.[74] The macromolecular theory established that polymers are macromolecules made from covalently linked monomeric units. Meticulous use of polymer chemistry and plastics engineering has completely changed the lifestyle that modern humans lead.

The advent of CRP afforded the ability to control the properties of resultant polymer to a much higher level than ever before. In parallel, a new class of polymers, which respond to their environment by changing their physical and/or chemical properties, has been emerging (Figure 4.13).[75, 76] These polymers are referred to as stimuli-responsive or smart polymers and have been synthesized to be responsive to a variety of physical (mechanical force,[77] electric/magnetic fields,[78, 79] and light[80, 81]) as well as chemical (pH,[82, 83] temperature,[84] presence of various small molecules and biomolecules[85]) stimuli. Stimuli-responsive polymers have found many applications such as their use as sensors and biosensors,[86] as controlled and triggered drug delivery agents,[87] as environmental remediation agents,[88] chemo-mechanical actuators,[89, 90] matrix in smart membranes[26] and for many other applications.[91-93]

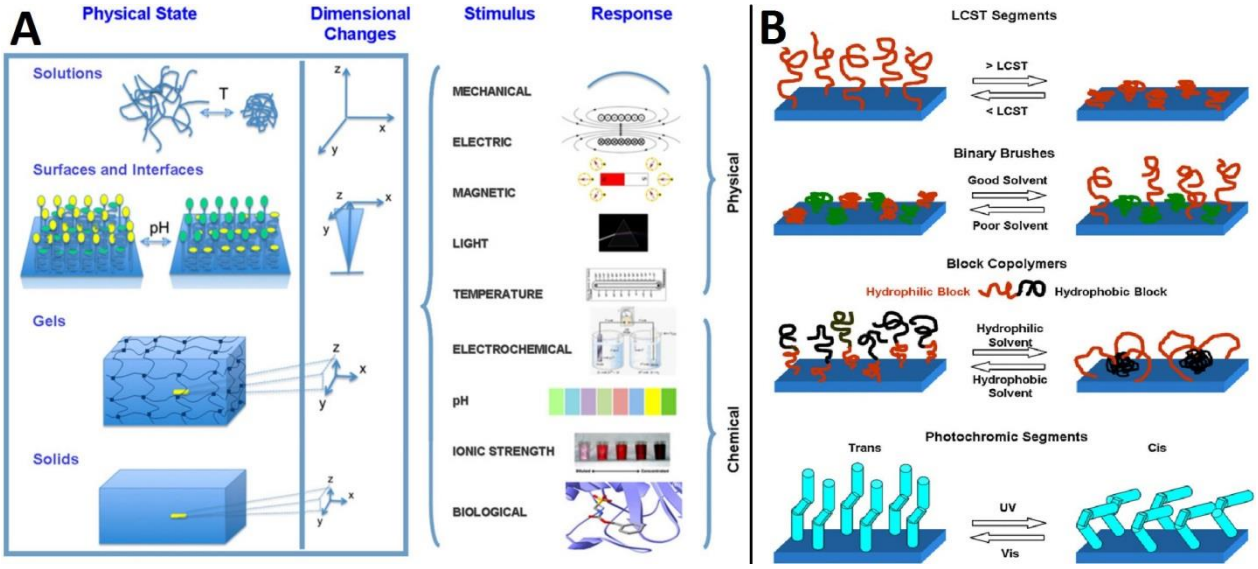

Figure 4.13: *The stimuli-responsive polymers may respond to a range of stimuli (A). Grafting of stimuli-responsive LCST segments, binary brushes, block copolymers and photo-chromic segments using CRP (B). Images adapted with permission from reference.*[76]

Of the plethora of stimuli possible, the most well-researched and understood response is towards temperature. Some polymers exhibit a lower critical solution temperature (LCST),[94] which is the lowest temperature at which temperature induced demixing occurs. That means below the LCST, the polymer chains and solvent molecules are in one homogeneous mixed phase. However, above the LCST, phase separation occurs via an entropically driven process. The opposite phenomenon where phase separation occurs below a temperature is indicated by upper critical solution temperature (UCST). Poly(*N*-isopropylacrylamide) (PNIPAAm), owing to its LCST (~32 °C) being close to the physiological temperature,[95] is one of the most extensively researched thermo-responsive polymers. The LCST of PNIPAAm has been reported to be independent of the MW or architecture of the polymer chains and over a wide range of concentrations, also independent of PNIPAAm concentration.[96-99] As the solution temperature rises above the LCST, PNIPAAm chains undergo a transition from an extended (solvated) random coil conformation to a compact (desolvated) globular conformation (called the coil-globule transition). The coil to globule transition can be thermodynamically controlled by adjusting the polymer composition, i.e., the LCST can be increased or decreased by copolymerization with a hydrophilic or hydrophobic monomer, respectively.[100] There are a variety of polymers that exhibit LCST.[100] Furthermore, multi-responsive polymers exist that respond to more than one stimulus. A possible combination is pH- and thermo-sensitivity. pH-responsivity results from an ionizable functional groups capable of donating or accepting protons upon environmental pH changes (Figure 4.14). Some common examples are polyacrylic acid (PAAc; pH-responsive and UCST in solutions with high ionic strength)[101] and poly(*N,N*-dimethylaminoethyl methacrylate) (PDMAEMA; pH-responsive and ionic strength dependent LCST).[102-105]

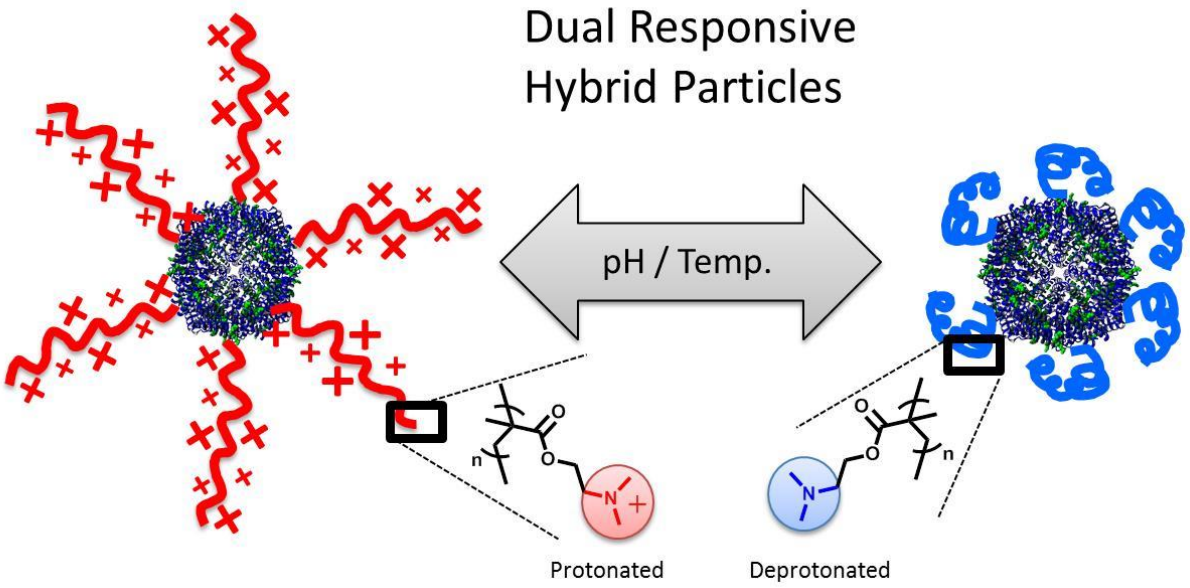

Figure 4.14: *Dual-responsive particles created using PDMAEMA. Image adapted with permission from the reference.*[104]

4.4.2. Polymers with UV-crosslinkable monomers

Copolymers of crosslinkable monomers and stimuli-responsive polymers have given rise to a promising class of materials for applications in multiple applications, for instance in stimuli-responsive hydrogels. Of these, UV-crosslinkable monomers are perhaps the smartest ones since they offer very simple approach to crosslinking (exposure to UV light) and require no post-crosslinking purification.[106] In the late 90's, 2-(dimethyl maleinimido)-*N*-ethyl-acrylamide (DMIAAm) was synthesized by Ling *et al*.[107] DMIAAm is an acrylamide monomer containing a light sensitive dimethylmaleimide (DMI) group, which can undergo a [2+2] cycloaddition with high quantum yield,[108, 109] leading to the crosslinking of the resultant polymer chains (Figure 4.15). Recently, more monomers containing DMI group have been synthesized.[105, 110] However, the crosslinking does not always result in a [2+2] cycloaddition. In fact, in aqueous systems, the formation of asymmetric dimer (Figure 4.15B) is much more likely.[111] Initially, sensitizers, such as thioxanthone, were commonly used to photo-initiate the reactions. However, later on, it was realized that the crosslinking can also be achieved without any sensitizer, simply by

bringing polymer chains in close proximity and irradiating the DMI group. This could be achieved for instance by evaporating the solvent, resulting in a copolymer film and irradiating it.[112] When using a smart polymer (such as PNIPAAm), its responsivity could be used to precipitate the polymer and then irradiate the resulting aggregate.[113, 114] Finally, self-assembled systems, resulting in polymer chains being in close proximity, could be irradiated to induce the dimerization and hence crosslinking.[26, 106, 110, 115, 116]

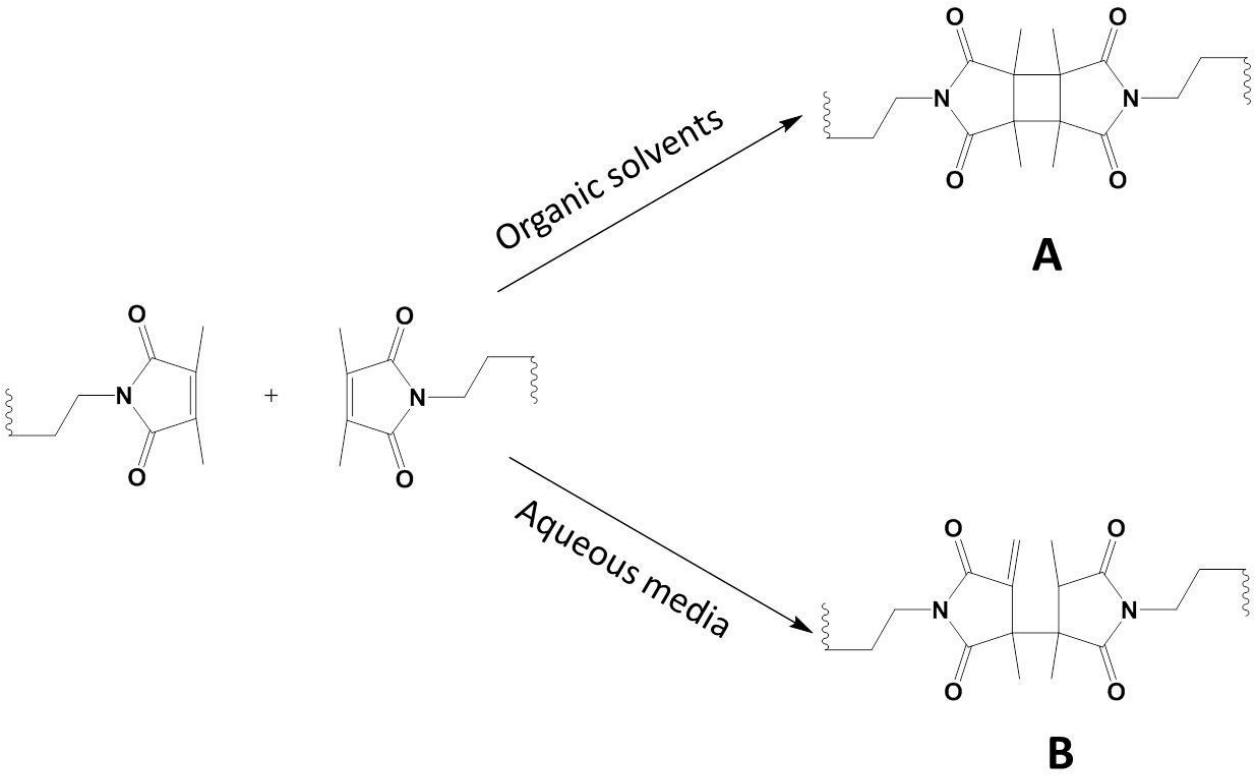

Figure 4.15: *Dimerization of the DMI group. Cyclobutane derivative (A) is the sole product in organic media, however only a side product in aqueous media, where asymmetric dimer is the major product (B).*[111]

It was shown by Langmuir Blodgett experiments that in the case of self-assembled systems, the crosslinking does not occur in the bulk solvent phase, and only at the interface.[115] While there is enough literature about crosslinking the DMI group using UV light in the aqueous environment,[26, 106, 110, 112, 114, 115, 117] copolymerization to generate these polymers in aqueous conditions is very scarce.[26, 117] Most of the copolymerizations in these reports were carried out in dioxane, THF or DMF. In fact, the only report that I could find about copolymerization of a crosslinkable monomer with DMI group in water,

apart from those by the group of Prof. Böker, was this.[118] It was a conventional free radical polymerization with NIPAAm and DMIAAm.

4.5. Protein-polymer conjugates: Preparation and applications

Perhaps the most important example for the applicability and need of protein-polymer conjugates are demonstrated by enzymes. In their natural habitat, they perform a myriad of chemical reactions at impeccable rates with high stereo-selectivity, regio-selectivity and chemo-selectivity[119-122] Use of enzymes for organic synthesis can quite often remove the requirement of high temperatures or extreme pH ranges, while at the same time affording increased reaction specificity, product purity and reduced environmental impact.[123] For this reason, since 1960's, many enzymes have been increasingly utilized to catalyze organic reactions in industries like pharmaceuticals, food and feed, detergent manufacturing, paper and textile industry.[124] Enzymes like lipases, esterases, peptidases and amidases, acylases, glycosidases, glycosyltransferases, epoxidases, hydrolases, aldolases, nitrilases, oxynitrilases and nitrile hydratases have been extensively used.[120, 125, 126] However, enzymes, being proteins, pose certain limitations on the universal applicability and the replacement of conventional chemicals. Enzymes get denatured under stringent reaction conditions such as extreme pH and temperature, limiting their usability.[124, 127, 128] One possible method to overcome these limitations is immobilizing the enzymes using polymer support, for instance by making protein-polymer conjugates. Basak *et al.* compiled a nice review summarizing the recent trends in the application of protein-polymer conjugates for biocatalysis.[129] Immobilization and conjugation often improve pH and temperature resistance of the enzymes, and sometimes augment reaction specificity,[130-133] hence making them more efficient and more usable for applications in organic synthesis.

However, proteins with enzymatic activity are not the only ones that have been employed for generation of conjugates. Protein-polymer conjugates represent an active research field that has been steadily growing in prominence over the last ten years.[14, 27, 28, 44, 45, 134-141] Linkage of polymers can prepare proteins for specific applications and confer them with properties they cannot offer on their own. The effect of covalently

attached polymer chains to the protein ranges from improved solubility, enhanced biocompatibility and stability to tunable enzyme activity.[42, 46, 142, 143] Protein-polymer conjugates find versatile applications in biomedicine as nano-carrier systems for drug delivery, especially in cancer therapy.[144, 145] There are multiple uses in bio-sensing and diagnostics and they have been successfully used as biomimetic protocells.[145, 146] Moreover, they have been employed in electronic devices as functional materials and in ultra-thin membranes with the protein acting as a sacrificial template.[26, 46, 145]

Two methods have been well established for the synthesis of protein-polymer conjugates (Figure 4.16). Using the grafting-to technique, pre-synthesized polymers with protein-reactive end groups are attached to the protein. However, steric hindrance around the protein often results in low attachment yields. Moreover, the isolation of conjugates from unreacted polymers and proteins is challenging. The second strategy, the grafting-from technique, focusses on polymerizing monomers directly from a protein. Here, a higher yield of attached polymer chains can be reached as the steric hindrance around the protein is lower for small monomers. Furthermore, the purification is easier

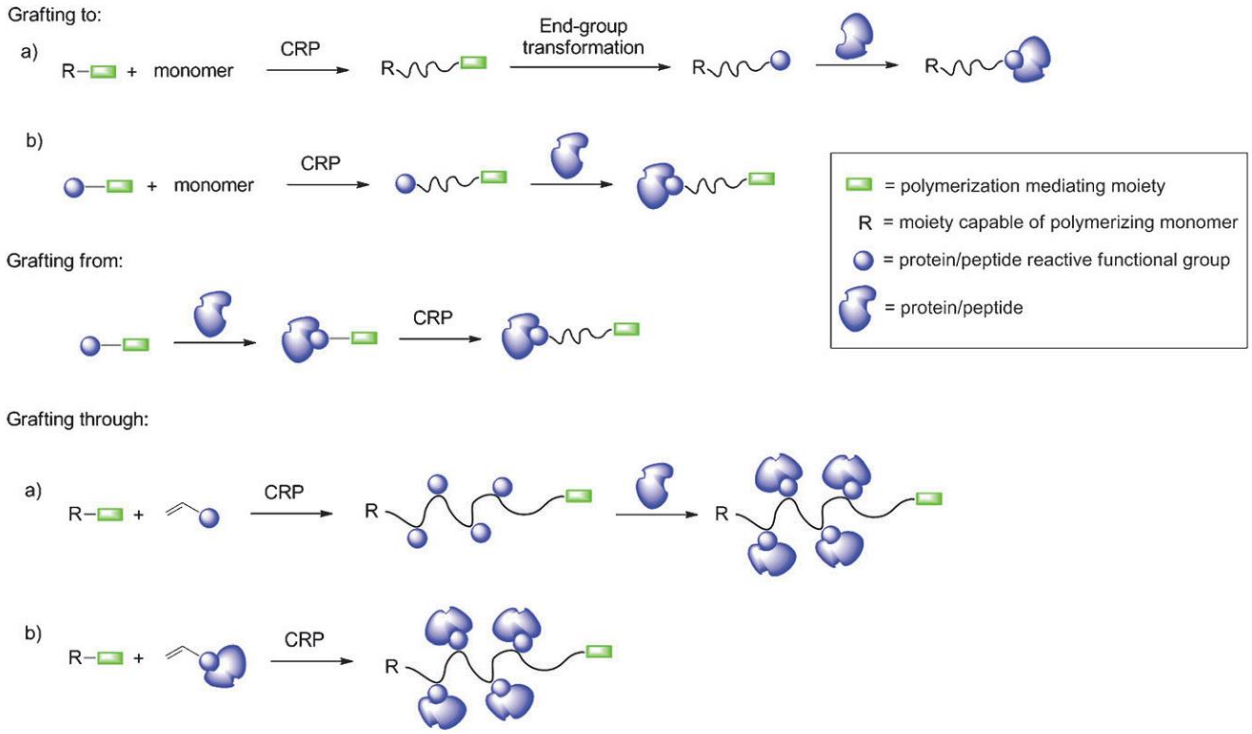

Figure 4.16: *Strategies to prepare protein-polymer conjugates. Image from reference*[138] *reproduced with the permission of RSC publishing.*

as only small molecular components need to be removed. These advantages favor the grafting-from strategy; however, there have not yet been as many reports as for the more traditional grafting-to approach. For the sake of completeness, grafting-through approach should also be mentioned. In this approach, multiple proteins are connected through a single polymer chain either by incorporating a protein reactive functional group in the polymer chain and attaching proteins post polymerization or by first attaching a monomer onto the protein and then polymerizing with free monomer, hence, resulting in the same architecture.

CRP, particularly ATRP[117, 147-154] and RAFT polymerization[155-159] have been commonly used to synthesize protein-polymer conjugates via grafting-from strategy. Performing the CRP in pure aqueous environment (without addition of an organic co-solvent) is a challenging task because the reaction in water is highly accelerated, instability of the catalyst complex is a major issue, and additionally, the loss of terminal bromine can occur.[54] Nonetheless, the reaction conditions of ATRP and related techniques, namely AGET ATRP, ARGET ATRP, and SET-LRP were recently optimized to develop procedures for CRP under biologically relevant conditions.[160-163]

Diverse polymeric architectures have been synthesized on the surface of proteins ranging from a variety of stimuli-responsive polymers[14, 117, 143, 150, 155, 156, 164] to block-copolymers synthesized by sequential polymerization steps.[143, 150, 156, 165] Moving on to more sophisticated protein structures, the groups of Finn and Douglas used virus-like particles as scaffold to independently modify the inside and the outside of a viral capsid.[166-169] The hence generated conjugates can be specifically tailored for desired applications like targeted drug delivery. Although many globular proteins like bovine serum albumin, ferritin, lysozyme or chymotrypsin have been extensively studied for conjugation,[117, 152, 156, 158] the studies shown in this thesis (and corresponding publications) remain the only ones to have employed transmembrane proteins for generating protein-polymer conjugates.[14, 105] The latter can likely be attributed to challenges in purification (incl. e.g. extraction from membrane fractions) and handling of purified samples.

4.6. Micro-/macro-structures from nanoscopic building blocks

4.6.1. Micro-compartments and micro-reactors

In an interesting article,[170] Stephen Mann suggests that instead of trying to learn more about the last universal common ancestor (LUCA) of most life forms on earth by trying to decode the molecular archives of the ribosomal RNA,[171] it might be more prudent to use the bottoms up approach towards the question of origin of life on earth. Generating synthetic constructs resembling the protocells, he argues, might lead us in the right direction (Figure 4.17).

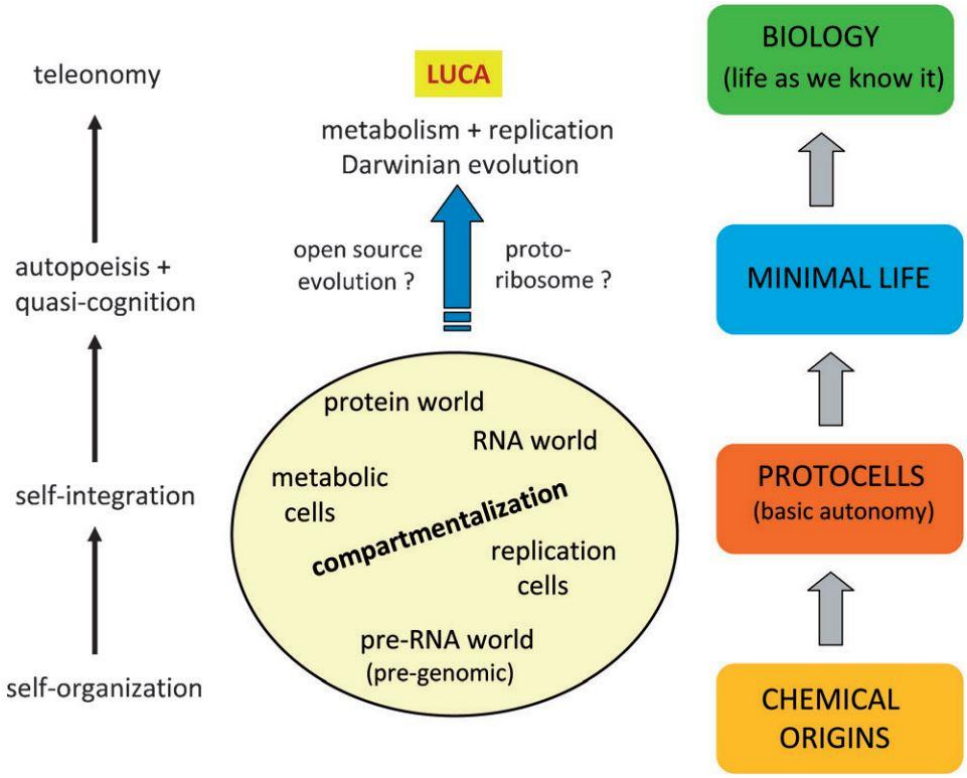

Figure 4.17: *A scheme representing possible scenarios of protobiological events prior to the emergence of LUCA. Scheme adapted with permission from the reference.*[170]

Although we are far away from synthesizing the first protocells, basic elements of a protocell are slowly being reported. A significant amount of research about the synthetic counterparts of lipid vesicles (liposomes), the biomimetic polymer vesicles (polymersomes), has now been reported.[22, 110, 172-174] Similarly, research about the

synthesis of micro-compartments has recently been reported, which may one day act as the protocell membrane.[116, 117, 146] Some compartmentalization, resembling proto-organelles, has also been reported.[175-177] Although, we are far away from the first protocells, the so-far generated polymersomes and micro-compartments have already shown many other potential applications such as in drug delivery,[22, 178] cancer therapeutics and theranostics,[22, 178] and nano-/micro-reactors[179, 180] (Figure 4.18).

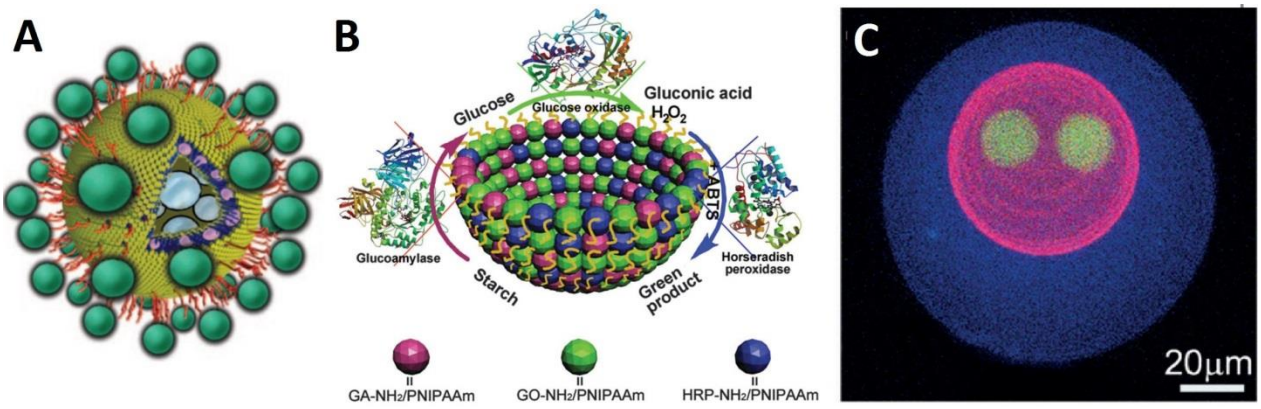

Figure 4.18: *A) A nano-reactor generated using polymersomes.[180] B) A micro-reactor generated using protein polymer conjugate stabilized micro-compartment.[179] C) A custom made multi-level micro-compartment with programmed release capabilities.[177] Figures adapted with respective permissions.*

One of the upcoming ways to synthesize a micro-compartment is using polymer-protein conjugate stabilized Pickering emulsions.[116, 117, 146, 177, 181] Emulsions stabilized by particles, instead of surfactant molecules, are referred to as Pickering emulsions.[182] Protein-polymer conjugates have been shown to be highly interfacially active[181] and their self-assembly at polar-apolar interfaces in turn shown to generate Pickering emulsions.[116] Furthermore, these Pickering emulsions afford a covalently linked stable system upon crosslinking.[116, 117, 146, 177] Pickering emulsions stabilized by conjugates of membrane proteins and polymers are expected to be next step towards protocells. While embedding membrane proteins into polymersomes and liposomes was shown to be possible,[21, 22, 35-37, 172, 173, 183-189] the amount of incorporated protein was limited.[21] For Pickering emulsions with conjugates of membrane proteins and polymers, the number of protein channels per unit area are expected to be significantly higher and the system more stable as a result of covalent crosslinking.[105] Particularly interesting works[146, 175-

[177, 179] in this respect show the generation of biomimetic protocells, the so-called proteinosomes (Figure 4.18C), which show guest molecule encapsulation, membrane gated enzyme catalysis, as well as multi-compartmentalization of the individual proteinosomes with selective release capabilities. Synthesis of such proteinosomes using transmembrane channel proteins like FhuA or OmpF could bring us one step closer to synthesizing the functional replicas of a protocell,[170] with the membrane proteins acting as the gates allowing the (selective) transfer of substrates and energy to and from the proteinosomes.

4.6.2. Stimuli-responsive nano-thin membranes

Incorporation of stimuli-responsiveness into membranes provides a very promising approach to a host of new applications such as stimuli-responsive permeation[190] (Figure 4.19B), stimuli-responsive separation (Figure 4.19C) and self-cleaning

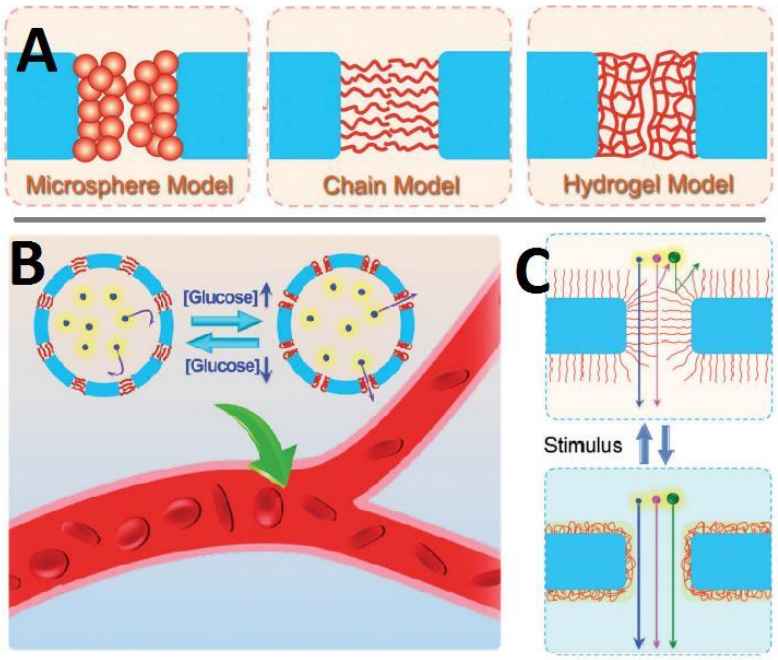

Figure 4.19: *Different approaches to synthesize porous membranes with stimuli-responsiveness (A), smart micro-capsule membrane with glucose-responsive gates for controlled release (B) and schematic illustration of the stimuli-responsive size-sieving-based separation (C).Figures adapted with permission from reference.*[191]

mechanisms.[191] Different approaches to modify membrane matrices (Figure 4.19A) have been suggested to incorporate stimuli-responsiveness.[191] In all approaches, the membrane matrix is covered by stimuli-responsive material, such as surface grafted polymer chains or a hydrogel. Upon addition of stimulus, the polymer chains undergo stimuli-mediated coil-globule transition and shrink, letting the pore open. **Section 4.4.1** details the possible stimuli responses these membranes could in principle be imparted.

Another upcoming class of membranes is ultrathin membranes. These membranes are very important for applications such as ultrafiltration of sensitive proteins at low transmembrane pressures.[192] When developing materials with pore sizes in the range of a few nanometers, even high resolution lithographic methods such as X-ray, electron beam and interference lithography suffer from limitations such as their inability to provide sufficient pore density.[192] Xu *et al.* reported synergistic co-assembly of nanotube subunits into a nanotube by heating-mediated hydrogen bond formation (Figure 4.20B).[193] Although, these are all promising approaches, none of them demonstrated flux or permeation data through the generated membranes.

Combining the best of both the membranes described above, Yameen *et al*. devised synthetic pH-responsive ion channels with modified nanotubes (Figure 4.20A). While the idea is very appealing, it did not engender a membrane, just some channels. Recently, van Rijn *et al.* reported the synthesis of ultrathin stimuli-responsive membranes using a new pore forming strategy: employing high interfacial activity of ferritin-PNIPAAm conjugates to self-assemble them at air-water interface.[26] After the self-assembly, the polymer chains were crosslinked and the protein cage denatured to leave holes in its place (Figure 4.21). While, the membranes mentioned earlier were thick, ferritin-PNIPAAm membranes reported by van Rijn *et al*. were nano-thin. Such nano-thin membranes have many advantages over conventional membranes such as high throughput at lower transmembrane pressure, while still having the ability to incorporate desired stimuli-responsivities.[192, 194] Furthermore, since proteins are monodisperse molecules, the generated holes are also expected to be of more uniform size than conventional membranes.

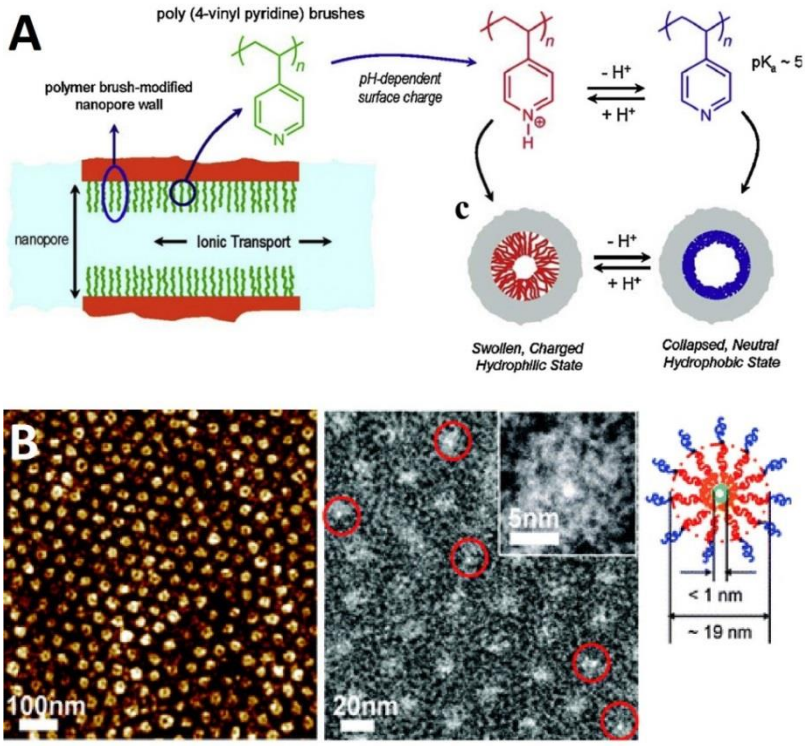

Figure 4.20: *A) pH-responsive ion channels with nanometer dimensions. Image adapted from reference.*[190] *B) Membrane with sub-nanometer sized pores, synthesized using co-assembly of nanotube subuints and block copolymers. Image adapted with permission from reference.*[193]

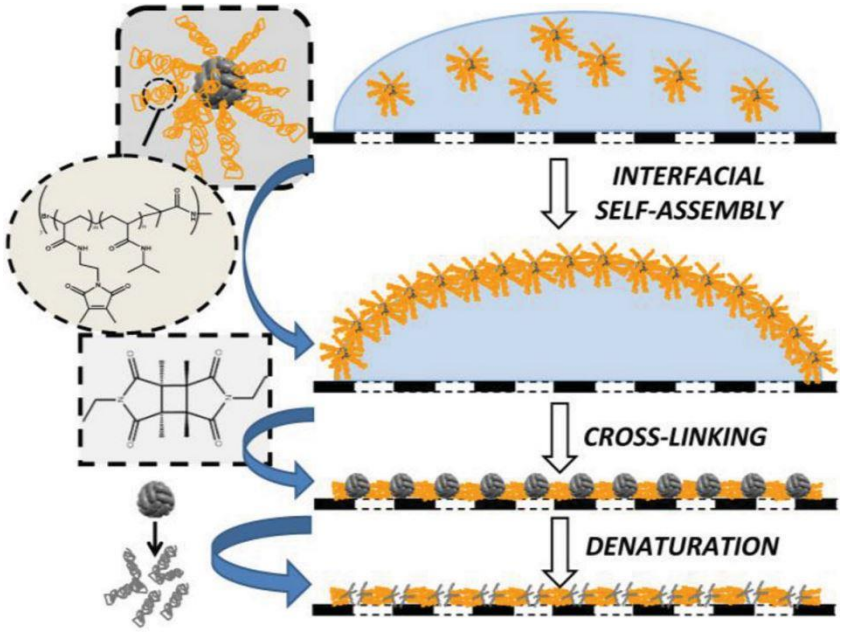

Figure 4.21: *Approach of van Rijn et al. to generate stimuli-responsive membranes. Reproduced with permission from reference.*[26]

However, the denaturing process may introduce some non-uniformity in the membrane morphology and pore size. As an alternative, spreading polymersomes with incorporated transmembrane proteins has been suggested and giant polymeric layers with incorporated membrane proteins might be used.[22, 25] These systems offer a nano-thin membrane with highly uniform pore size in the nanometer scale (the dimensions of the transmembrane channel proteins). However, these systems do not have sufficient mechanical stability to sustain most pressure regimes relevant for the industrial applications. Additionally, the incorporation of protein in such polymersomes and polymer membranes is inefficient; resulting in low number of pores and, hence, reduced effective permeation area.[21, 22] Hence, it would be desirable to use the self-assembly of conjugates of transmembrane channel proteins instead, which rather than being denatured eventually like ferritin conjugate membranes, could serve as an integral part of the membrane. This approach would also result in much more transmembrane pores per unit area in the membrane as compared to the polymersomes or lipid layers with incorporated channel proteins. Furthermore, the channel proteins can be genetically and chemically tailored to suit desired needs. For instance, upon incorporation of a chiral region in the protein, the membranes can be used for resolution of racemic mixtures or isolation a desired enantiomeric component.

5 Characterization techniques

The fundamentals of techniques such as NMR spectroscopy, TEM, DLS and mass spectrometry have not been included here on implicit understanding that a chemist or material scientist reading this thesis should be already well informed and experienced about these methods. This chapter details the characterization techniques more commonly used in biotechnology and biochemistry, but not so frequently in chemistry or material science. Other non-conventional characterization techniques used during the course of this work have been described briefly with the respective data in the following chapters.

5.1. BCA Assay

The BCA assay, short for bicinchoninic acid assay, is a technique to determine the total concentration of proteins in a given sample.[195] The typical range of measurement is from 20 to 2000 µg/ml. Commercially available assays, like Thermo Scientific™ Pierce™ BCA Protein Assay,[196] are typically detergent-compatible formulations based on bicinchoninic acid (BCA) for the colorimetric detection and quantitation of total protein content.

The underlying principle is a two-step reaction as shown in Figure 5.1. First step is the Biuret reaction, that is, reduction of Cu^{2+} to Cu^{+} by protein in an alkaline medium. The second step is the complexation of the freshly generated Cu^{+} with bicinchoninic acid, which enables an extremely sensitive and selective colorimetric detection of the resultant complex.[195] The purple product of this reaction is generated by the chelation of two molecules of BCA with one Cu^{+} ion (Figure 5.1, step 2). This water-soluble complex displays a strong absorbance at 562 nm and has a nearly linear relationship with the protein concentrations over the range around 20 to 2000 µg/ml.[196] The BCA assay is not a true end-point method; that is, the final color continues to develop. However, after prolonged incubation, the rate of color change is sufficiently low, allowing a large number of samples to be assayed together.

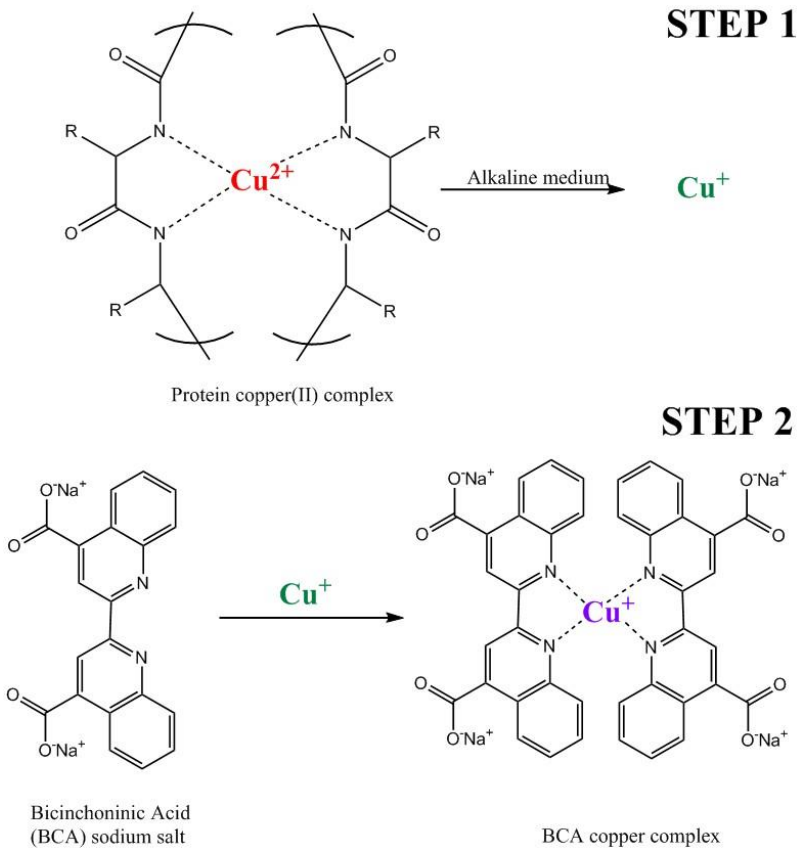

Figure 5.1: *The chemical reactions behind BCA assay to access protein concentration. Step 1 is the reduction of Cu^{2+} to Cu^{+} under alkaline conditions and the second step is the complexation of Cu^{+} with BCA, which results in the color that is quantified to access the protein concentration.*

The secondary and tertiary structure of protein, the length of the polypeptide chain and the presence of four particular amino acids (cysteine, cystine, tryptophan and tyrosine) have been reported to be responsible for color formation with BCA.[197] Furthermore, studies with di-, tri- and tetra peptides suggested that the final extent of formed color is more than the sum of the color produced by individual functional groups.[197] Hence, it is not possible to treat BCA assay as an absolute measurement tool such as NMR, rather a comparative tool. Protein concentrations are generally determined and reported with reference to a standard protein such as bovine serum albumin (BSA). A series of dilutions of known concentration are prepared from the standard protein and assayed alongside the unknown(s). Consecutively, the concentration of each unknown is determined based on the standard curve generated by dilutions of the standard protein.

If precise quantitation of an unknown protein is vital, it is prudent to select a standard protein similar (and in best identical) to the unknown protein being measured. This may not always be so easily doable, for instance when needed to measure concentration of a transmembrane protein or complex proteins.

5.2. SDS-PAGE

Polyacrylamide gel electrophoresis (PAGE) is a technique commonly used in biochemistry, genetics, molecular biology and biotechnology to separate bio-macromolecules based on their electrophoretic mobility.[4] Electrophoretic mobility is the movement of a charged entity under the effect of an electric field. There are two major approaches of PAGE. One of the variants is called native PAGE, in which the secondary / tertiary structure of the protein is retained as the macromolecule passes through the gel. The other, more common, approach is to use a denaturant like sodium dodecyl sulfate (SDS) to linearize the protein (Figure 5.2B). SDS attaches to the hydrophobic parts of the protein and imparts the polypeptide chain a nearly uniform charge per unit mass ratio. Hence, SDS-denatured proteins can be considered to be fractionated according to their mass when being fractionated according to electrophoretic mobility.[4] Usually, a mixture of various proteins of known masses is run as a comparison or standard (called protein marker or protein ladder) for identifying the range of mass of unknown samples of proteins.

The separation occurs because of two opposing phenomenon - the resistance or drag provided by a crosslinked polyacrylamide gel and the mobility provided by the electric field. The mobility can be increased by increasing the electric field. By varying the amount of crosslinking, the resistance can be varied: higher the crosslinking higher the resistance. Hence, for higher molecular weight proteins (100-400 kDa), the amount of crosslinking should be kept low – for instance 6 %. Similarly, for resolving lower molecular weight proteins, higher crosslinking is required to provide ample resistance, and hence efficient resolution. For smaller proteins (15-30 kDa), for instance, 15 % gels are more commonly used. When higher as well as lower molecular weight

macromolecules are anticipated in the same sample, gradient gels may be used. Gradient gels don't have a uniform crosslinking degree, rather the degree of crosslinking slowly increases along the length of the gel. For instance, many of the SDS-PAGE in this thesis were performed on 4-15 % gradient gels.

Figure 5.2A shows the basic setup of an SDS-PAGE cell used for electrophoresis. The samples are loaded onto the gels in the gel casket and affixed with the electrode assembly. After filling the inside of the electrode assembly with the cathode buffer, and the mini-tank with anode buffer, electric field is applied making use of the banana plug jacks (not shown in the image). Anode buffer and the cathode buffer were identical for

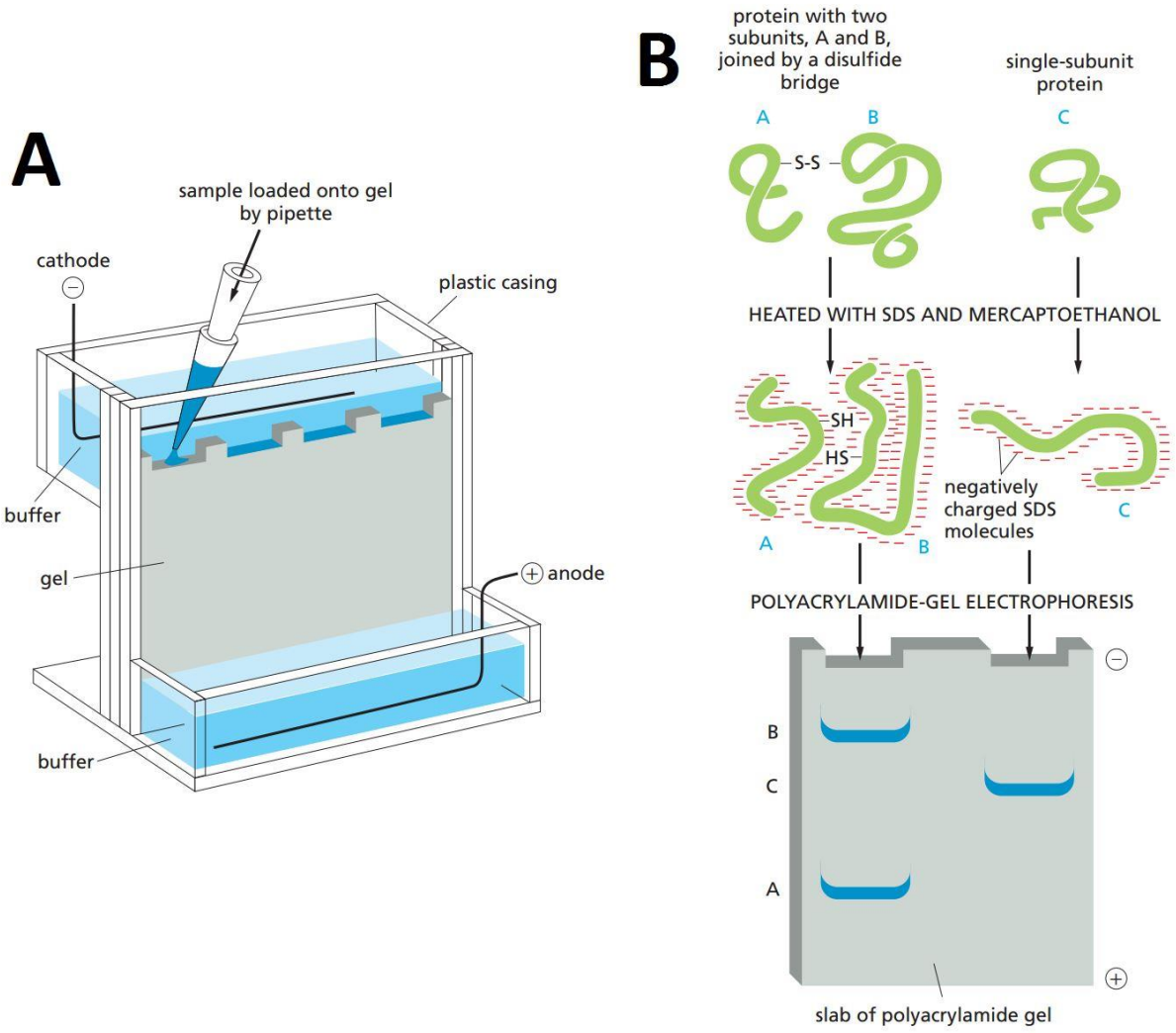

Figure 5.2: *Scheme of SDS-PAGE cell assembly (A) and mechanism of protein linearization and electrophoresis (B). Image adapted with permission from reference.*[4]

the work done during this thesis. After the run is complete, gels are removed from the gel casket and staining is done to visualize the proteins. The most common method of staining is to use the dye coomassie brilliant blue, which initially stains the protein as well as the gel, but upon destaining with acetic acid, the gel loses the color but the protein retains it.[198] Another very common approach is silver staining, where silver nitrate is used for staining. Silver staining, although, more sensitive to low amounts of protein as compared to coomassie staining, has more risks for measurement artefacts.[199, 200] Many protocols of silver staining have been investigated in this reference.[200]

5.3. Fluorescence microscopy

Luminescence, that is the phenomenon of emission of light from any substance, is divided into two types - phosphorescence and fluorescence.[201] The difference between the two is the time duration of the lifetime of the phenomenon, with phosphorescence being longer than fluorescence. Fluorescence is the property of some atoms and molecules to absorb light at a particular wavelength (called the excitation wavelength) resulting in excitation of the molecule to a higher energy state.[201] After a brief time interval, termed as the fluorescence lifetime, the molecules return to another stable state and in the process emitting light of longer wavelength (called the emission wavelength). Typically, fluorescence lifetime is near 10 ns ($10 \cdot 10^{-9}$ s). Fluorescence microscopy, that is using the fluorescence of fluorophores to visualize selective areas of a macro-structure under a microscope, has gained significant impetuous in the last three decades in biotechnology.[201, 202] Unless the fluorophore is irreversibly destroyed in the excited state (an important phenomenon known as photobleaching), the same fluorophore can be excited and detected repeatedly.[202] Most commonly employed fluorophores are aromatic compounds, for instance fluorescein or Nile red (Figure 5.3B). Also, it is worth noticing that for fluorescein, the excitation maxima and emission maxima are quite close, while for Nile red, these are quite far apart. The farther apart the excitation and emission maximum, the more efficient is the detection of signals. These

compounds can either be directly used for showing desired area or be covalently linked to the region of interest and then visualized using the microscope as explained below.

A basic setup of a fluorescence microscope is shown in Figure 5.3A. The excitation filter limits the wavelength of light falling onto the sample to the desired wavelength. The fluorescent light from the sample is then detected using an emission filter which cuts off the 'undesired' light beyond the emission spectrum of the sample. By changing the excitation and emission filters, fluorophores of various ranges may be easily imaged. In case of sample containing more than one fluorophore, images are acquired using respective filter and later overlaid using a software. The final overlaid image shows each fluorophore with a different color and when combined with the image of bright field can be used to deduce useful information.

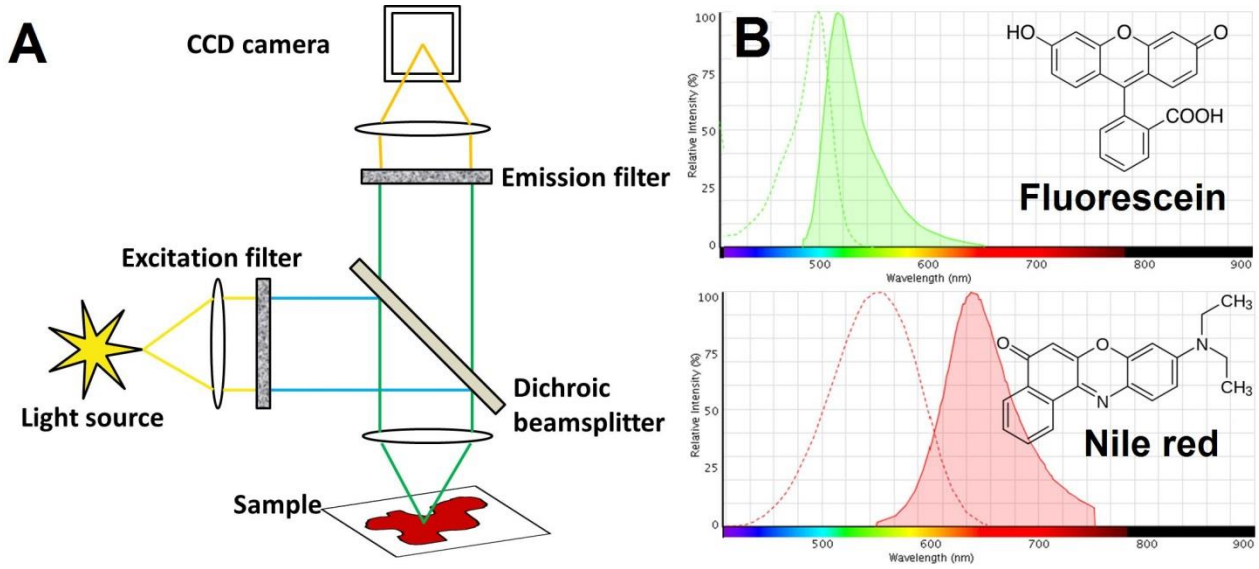

Figure 5.3: *Schematic representation of the construction of a fluorescence microscope (A) and the structure and excitation (dotted) / emission (full) spectra of fluorescein and Nile red (B).*

5.4. CD spectroscopy

Circular dichroism (CD) spectroscopy is a technique commonly used for the analysis of the secondary structure of proteins.[203] It is a highly sensitive, non-destructive technique that requires a very little amount of the sample. The underlying principle behind CD is

the differential absorption of the left and right circularly polarized components of a plane-polarized radiation. This effect occurs when the sample is chiral (optically active) either intrinsically by virtue of its structure, or because of being covalently linked to a chiral center. When plotted against wavelength, the generated curve gives meaningful information about the long range order of chiral units, for instance in proteins. CD in the far-UV region (178–260 nm) arises from the amides of the protein backbone and is sensitive to the conformation of the protein.[202] Depending on the type of secondary structure of a protein, its CD spectrum is characteristically different. Figure 5.4 shows typical CD spectra of an α-helix, a β-barrel and an irregularly structured protein.[203] The CD spectrum of a protein having predominantly α-helical structure would have positive maximum around 195 nm and a double negative minimum as shown in Figure 5.4. For a protein with predominantly β-sheets, the CD spectrum shows a positive maximum around 195 nm (which is significantly less intense than that for an α-helix) and a single negative minimum around 215 nm (Figure 5.4). Based on the location and intensity of the peaks, the process of deconvolution of the spectra gives the percent of α-helix or β-barrel content in the protein structure.

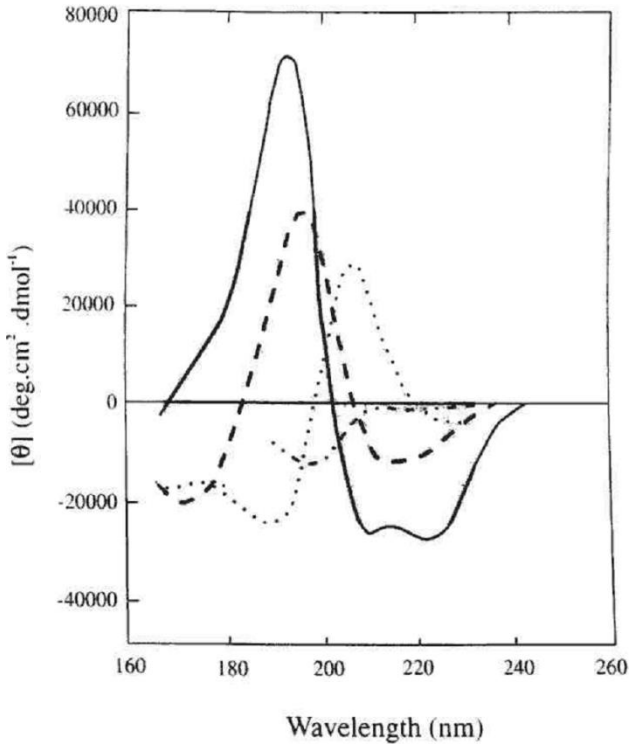

Figure 5.4: *Typical far UV CD spectra of an α-helix (solid curve); antiparallel β-sheet (long dashes), type I β-turn (dots), irregular structure (dots & short dashes).*[203]

This value may be used as an indication to track the stability of the structure of protein as it undergoes chemical modification or endures harsh conditions.

Although, the technique is simple and straightforward for most analyses, in the far UV region (below 200 nm), the data is prone to significant noise. This is especially the case when the buffer contains absorbing salts[203] or when the protein has been modified with an entity highly absorbing in this region. For very difficult cases, protein NMR spectroscopy and sophisticated FTIR spectroscopy may be more helpful. However, for proteins, these techniques require elaborate sample preparation and complex post-measurement data analysis.[204, 205]

6 Optimizing the CRP for a transmembrane protein

6.1. Introduction

The aim of the work presented in this thesis was to generate conjugates of proteins, particularly FhuA (**Chapter 7**), and using them for generation of micro- and macro-structures (**Chapter 9** and **Chapter 10**). Although many globular proteins like bovine serum albumin (BSA), ferritin, lysozyme or chymotrypsin have been extensively studied for conjugation,[117, 152, 156, 158] there is no literature regarding synthesis of conjugates from a transmembrane protein like FhuA. The hydrophobic transmembrane region of FhuA requires stabilizing agents (such as the small amphiphatic molecule MPD)[14] to keep the protein solubilized and correctly folded in water. The phosphate buffer in the presence of such molecules cannot be considered as purely aqueous system, with MPD possibly influencing the polymerization. Hence, optimization of the protocol of polymerization was required to obtain conjugates with FhuA without destroying its secondary or tertiary structure. Since, FhuA is not commercially available and very difficult to extract and purify, optimization of the reaction conditions was done utilizing model substrates. Hence, homopolymerization of PNIPAAm and PDMAEMA with 2-bromoisobutyric acid (BiBA) as initiator in MPD buffer was optimized first. Using PNIPAAm would provide temperature-responsivity and PDMAEMA would provide temperature- as well as pH-responsivity to the generated conjugates (**Chapter 9**). Furthermore, 2-(dimethyl maleinimido)-*N*-ethyl-acrylamide (DMIAAm) and 3,4-dimethyl maleic imidobutyl acrylate (DMMIBA), UV-crosslinkable monomers were copolymerized with NIPAAm and DMAEMA, which would later result in stable structures as a result of covalently crosslinked polymer chains (**Chapter 9**). Secondly, BSA was chosen as the model protein to optimize the reaction conditions for FhuA. A recently reported water soluble functional CRP initiator was synthesized and used for generating the BSA macroinitiator (MI).[164] MALDI-ToF MS was used to exact the reaction conditions optimum for maximum modification. BSA MI was consecutively used for growing polymers: PNIPAAm, PDMAEMA and their copolymers with DMMIBA or DMIAAm from the protein surface, using BiBA as a sacrificial initiator (see **Section 6.4.2**). Conjugates

generated without the use of any sacrificial initiator enabled the use of more characterization techniques such as analytical ultracentrifugation (AUC) for the analysis of generated conjugates.

6.2. Preparation and characterization

6.2.1. Materials

All chemicals used were of analytical reagent grade or higher quality, purchased from Applichem (Darmstadt, Germany), Alfa Aesar (Karlsruhe, Germany) or Sigma-Aldrich Chemie (Taufkirchen, Germany), if not stated otherwise. *N*-2-bromo-2-methylpropanoyl-β-alanine N'-oxysuccinimide ester (functional CRP initiator) was synthesized according to reference.[164] 2-(Dimethyl maleinimido)-*N*-ethyl-acrylamide (DMIAAm) was synthesized according to reference.[107] BSA was purchased from Sigma-Aldrich and dissolved in PBS or MPD buffer immediately before use. Once in solution, BSA and modified BSA were always stored at 4 °C. NIPAAm was purified by two successive recrystallizations from a mixture of *n*-hexane and benzene (4:1 v:v). CuBr was purified by stirring in acetic acid overnight. After filtration, it was washed successively with ethanol and diethylether and then dried in vacuum. 3,4-dimethyl maleic imidobutyl acrylate (DMMIBA) was synthesized according to a procedure for similar compounds in the reference.[105, 110] (2-Dimethylamino)ethyl methacrylate (DMAEMA) was passed through basic alumina twice, before use, to remove the inhibitor.

In this chapter, MPD buffer is defined as the buffer containing 50 mM MPD, 10 mM sodium phosphate and 1 mM EDTA at pH 7.4

Polymerization from BiBA: BiBA and monomers (NIPAAm or DMAEMA and when used, DMMIBA or DMIAAm) were dissolved in 2 ml MPD buffer and deoxygenated by three freeze-pump-thaw cycles and finally cooled to 0 °C in an ice bath or kept at RT. Simultaneously, a solution of Cu(I)Br and tris[2-(dimethylamino)ethyl]amine (Me_6TREN) in Millipore water (catalyst solution) was also deoxygenated by three freeze-pump-thaw

cycles and finally put in an ice bath (0 °C) or kept at RT, respectively. The typical final ratio of components for the reaction was BiBA : monomer : CuBr : Me_6TREN = 1 : 121 : 1.3 : 1.9. After 30 minutes of stirring, the initiator/monomer solution was transferred to the catalyst solution via cannula transfer. After 24 h, the reaction was quenched by allowing the air into the reaction mixture and products purified by two times dialysis (against water using dialysis membrane with a MWCO of 3 kDa for 24 h) and lyophilized to isolate the polymer. The lyophilized powder was stored at -20 °C. Alternatively, after 24 hours, the reaction mixture was lyophilized and the lyophilized powder dissolved in DCM and the polymer purified by precipitation in diethyl ether or petroleum ether for PNIPAAm or PDMAEMA, respectively. Solvent evaporation under high vacuum yielded the pure polymer, which was stored at -20 °C.

Formation of BSA macroinitiator (MI): The macroinitiators were prepared in MPD buffer in the range of pH 6.4 to pH 9.4. BSA was dissolved in the buffer of respective pH and then 25 molar excess of functional CRP initiator to lysine residues was added. Buffers of different pH were prepared by adding aq. HCl or aq. NaOH to MPD buffer for obtaining the desired pH. In all cases, the reaction was carried out on a shaking platform for 12 h at 12 °C. BSA MI was purified by two times dialysis (against MPD buffer using dialysis membrane with a MWCO of 12-14 kDa for 24 h) and stored at 12 °C before characterization or further modification.

Synthesizing conjugates from BSA MI: For making conjugate, the monomers (and BiBA when doing reaction with sacrificial initiator) were added to 2 ml BSA MI solution and purged with N_2 for 30 min in ice bath. Simultaneously, CuBr and Me_6TREN were added to 1 ml Millipore water (catalyst solution) and purged with N_2 for 30 min in ice bath. After that, the monomer solution was transferred to catalyst solution via cannula transfer and allowed to polymerize for 24 h. The typical final ratio of components for the reaction was initiator (BSA MI) : monomer : CuBr : Me_6TREN = 1 : 121 : 1.3 : 1.9 when using no sacrificial initiator, and initiator (BSA MI + BiBA) : monomer : CuBr : Me_6TREN = 1 :121 : 13 : 19 when using sacrificial initiator. The ratio of sacrificial initiator to lysine was kept 10 : 1. After that, the reaction was quenched by allowing air into the reaction mixture and products purified by two times dialysis (against MPD buffer using dialysis

membrane with a MWCO of 12-14 kDa for 24 h). The conjugate samples were stored at 4 °C before further characterization.

6.2.2. Characterization techniques

Proton nuclear magnetic resonance: ^{1}H-NMR spectra were recorded on an INOVA 500 spectrometer from Varian Inc. at 500 MHz. $CDCl_3$ and D_2O were used as solvents. Measurements were performed at room temperature. For measuring the conversion of a polymerization, the samples of product were taken before dialysis or purification, and mixed with D_2O 50:50 v/v. The signal of non-deuterated solvent was then used as internal standard.

MALDI-ToF mass spectrometry: Spectra were acquired using a 337 nm laser Bruker UTX MALDI-ToF mass spectrometer (Bruker, Bremen, Germany) with pulsed ion extraction. The masses were determined in positive ion linear mode. The sample solutions were applied on a ground steel target using the dried droplet technique. For analyzing BSA and BSA MI, ZipTipC4 pipette tips (Millipore, Darmstadt, Germany) were used. Super-DHB, a 9:1 mixture of 2,5 dihydroxybenzoic acid (DHB) and 2-hydroxy-5-methoxybenzoic acid, was used as matrix substance in a 50 mg/ml solution in Millipore water:acetonitrile 1:1 with 0.1 % trifluoroacetic acid. For analyzing just polymer, sample (5 mg/ml in THF) was mixed with sodium trifluoroacetate (10 mg/ml in THF), and the matrix dithranol (10 mg/ml in THF) in the ratio 5 : 1 : 25 and 0.5-2 µl of the mixture were applied on the ground steel target. Mass calibration was performed with external calibration.

Gel permeation chromatography: The purified polymers were characterized using GPC with attached RI detector on a Brookhaven device with DMF as solvent. The flow rate was 1 ml/min, injection volume 100 µl and samples were calibrated against polystyrene standards.

SDS-PAGE: BSA conjugates were analyzed on a 4-15 % gradient polyacrylamide gel (90 V, ca. 2.5 h, Mini-PROTEAN® Electrophoresis System-Bio-Rad, München,

Germany). Samples were prepared by denaturing the protein using 2 mercaptoethanol at 65 °C for 3 min. Then, 8 µl of each sample was loaded onto the gel. Silver as well as coomassie staining were used to resolve the gel. For coomassie staining, the gels were put on a shaking platform in staining solution *[1 g/l R-250 (Coomassie brilliant blue), 1 g/l CBB, 50 v/v % methanol, 10 v/v % acetic acid and 40 v/v % distilled water]* for 10-12 min and then 3-4 times in destaining solution *(30 v/v % ethanol, 10 v/v % acetic acid and 60 v/v % distilled water)* for 30 min each until destaining was complete. For silver staining, gels were first put on a shaking platform in Fix 1 *(30 v/v % ethanol, 10 v/v % acetic acid and 60 v/v % distilled water)* for 15 min and then in Fix 2 *(0.4 M sodium acetate, 0.5 v/v % acetic acid, 30 v/v % ethanol, 0.5 v/v % glutaraldehyde, 0.1 % sodium thiosulfate)* for 30 min. After this, the gels were washed with distilled water three times for 10 min each time. Then, the gel was put on a shaking platform in silver staining solution *(6 mM silver nitrate, 0.01 w/v % formaldehyde)* for 45 min in the dark *(container covered in aluminum foil)*. Afterwards, the gel was resolved using freshly prepared developing solution *(3.75 w/v % sodium carbonate, 0.022 w/v % formaldehyde)* for ca. 2-5 min until protein bands were sufficiently visible, after which the gel was put in the stop solution *(50 mM EDTA, pH 7.5)* for 10 min. The gel could be stored indefinitely in stop solution.

Analytical ultracentrifugation: AUC was performed with an Optima XL-I centrifuge from Beckman Coulter (Krefeld, Germany) equipped with an interference optical detection system and AN60Ti rotor. The protein concentration of the samples was 0.2 mg/ml and the centrifugation speed 31,000 rcf. Three parallel runs for 16 h at 20 °C were averaged to get the final spectra. The software XL-I 3.01h, SEDFIT V14.81 (2015) and Mathematica 10 were used for data analysis.

6.3. Reactions in MPD buffer with BiBA as the initiator

6.3.1. Homopolymerization of NIPAAm

In order to find suitable reaction conditions for the polymerization in MPD buffer, copper-mediated living radical polymerization of NIPAAm with BiBA as the initiator was carried out in MPD buffer, and the effect of temperature and other parameters investigated. In agreement with the observation in this reference,[206] $CuBr_2$ was not required as it was generated *in situ* anyway as a result of disproportionation of Cu(I). Based on optimization experiments, the ratio of 1 : 1.3 : 0 : 1.9 for BiBA : CuBr : $CuBr_2$: Me_6TREN resulted in near complete conversion and reproducible results for MPD buffer system (Figure 6.1B). The ratio of the monomer was varied while keeping the other ratios the same, depending on the desired polymer chain length. The temperature of the reaction proved to be another crucial factor, with no conversion at RT (Figure 6.1A). Hence, all further reactions were carried out in an ice bath at 0 °C, to ensure complete conversion (Figure 6.1B). Another very important factor was the disproportionation of Cu(I), in absence of which the polymerization either terminated too soon or the resultant

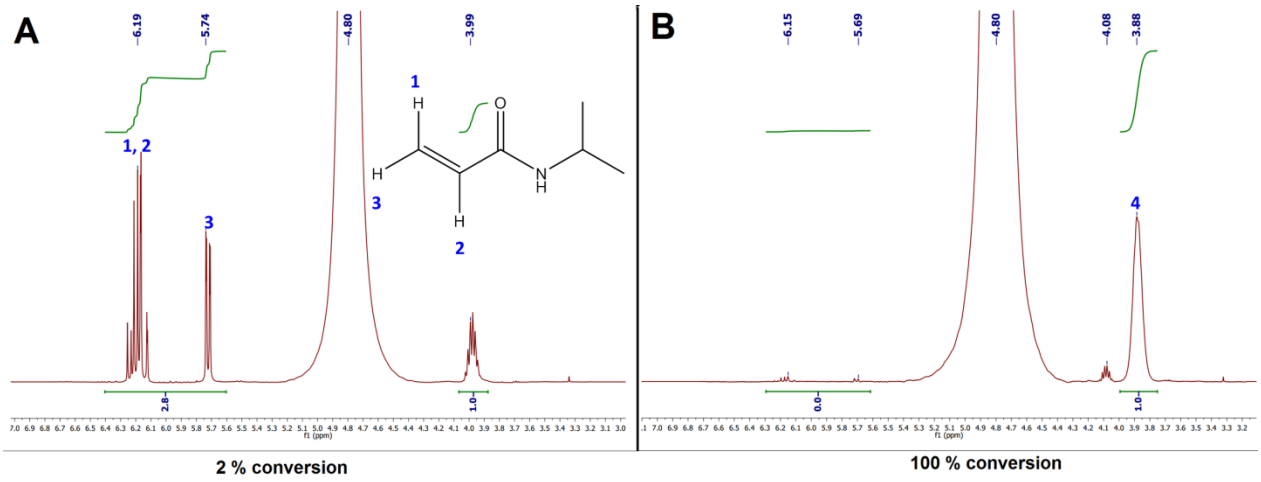

Figure 6.1*: NMR spectra showing conversion for polymerizations of NIPAAm carried out at RT (A) and 0 °C (B), and otherwise identical conditions (explained in* ***Section 6.2.1****). The reaction mixture was directly taken before purification, diluted with D2O (hence the large signal from water at 4.80 ppm). The signals of vinyl hydrogen atoms (1, 2 and 3) are shifted to lower ppm (4) upon polymerization, as shown in the image.*

PNIPAAm was highly polydisperse. Hence, the reaction mixtures were stirred 30 minutes before being mixed to ascertain complete disproportionation. GPC chromatograph with polymer chain length of around 200 repeat units shows that the generated PNIPAAm was with a polydispersity of 1.29 and a M_n of 15200 g/mol (Figure 6.2A). MALDI-ToF mass spectrum of PNIPAAm with lower chain length (50 repeat units) shows a MW around 5000 g/mol (Figure 6.2B). Hence, the MALDI-ToF MS data and GPC data are close to the theoretically expected values.

6.3.2. Homopolymerization of DMAEMA

Being a pH as well as thermo-responsive polymer, PDMAEMA stands out as an interesting candidate for usage in protein-polymer conjugates. Hence, polymerization of DMAEMA was optimized from the initiator BiBA in MPD buffer, and the same ratio of reactants as used for PNIPAAm resulted in efficient conversion. Figure 6.3B shows the NMR spectrum of PDMAEMA and disappearance of the signals of vinyl hydrogen atoms at 6.04 ppm and 5.48 ppm (Figure 6.3A) upon complete conversion to polymer (Figure 6.3B). For reactions to grow DMAEMA from FhuA variants, similar conditions

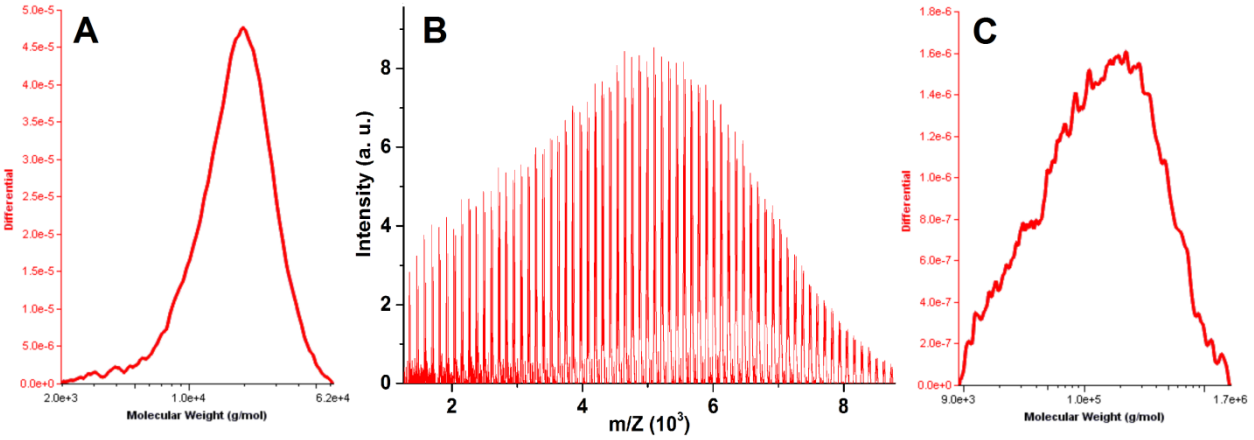

Figure 6.2: *Mass distribution of PNIPAAm from GPC chromatogram (A) and from MALDI-ToF mass spectrum (B). GPC chromatogram of PDMAEMA (C). It was not possible to obtain MALDI-ToF mass spectrum for PDMAEMA.*

were successfully used (Chapter 9). The GPC chromatogram for PDMAEMA with a polymer chain length of around 200 repeat units shows M_n around 68000 g/mol as shown in Figure 6.2C and PDI of 2.95. The molecular weight is much higher than the theoretically expected value and this deviation is much more pronounced than for PNIPAAm. GPC calibration was done against polystyrene standards; it is a common phenomenon in GPC that the apparent MW can show significant deviation from the real MW, especially when the standards have different properties than the sample.

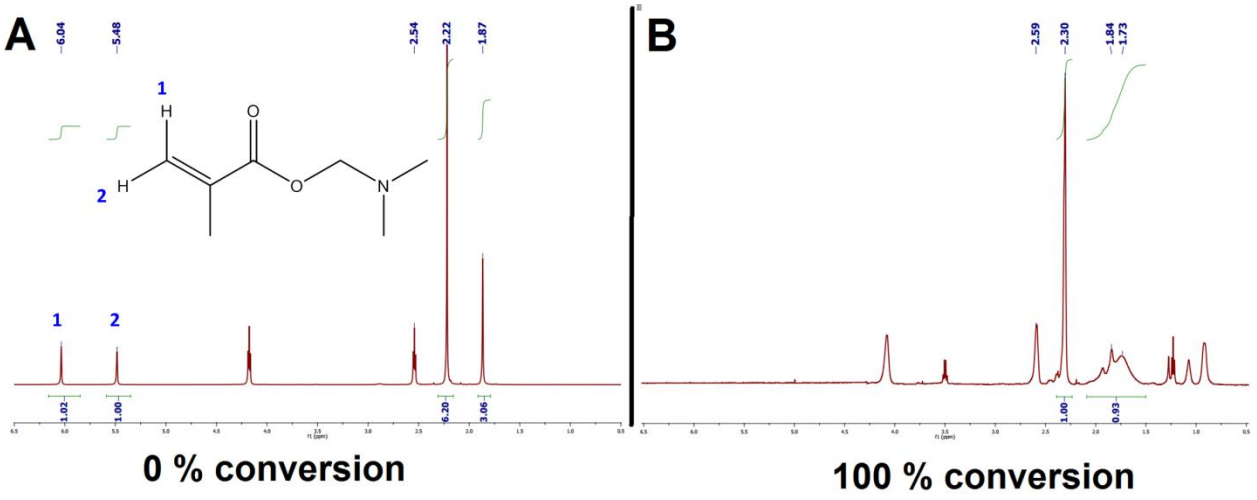

Figure 6.3: *NMR spectra of DMAEMA (A) and PDMAEMA (B). The signals at 6.04 ppm and 5.48 ppm of the vinyl hydrogen atoms (1 and 2) disappear upon polymerization.*

6.3.3. Statistical copolymerization of NIPAAm and DMMIBA

Since the final goal of the work done during the course of this thesis was to generate covalently stable macrostructures from protein-polymer conjugates (**Chapter 9** and **Chapter 10**), crosslinkable monomer units provide an interesting handle. UV-crosslinkable monomers provide a very efficient method of crosslinking since they don't require any additional crosslinking agent, whose presence may later contaminate the macrostructures. DMIAAm, a UV-crosslinkable monomer, has previously been employed for generation of ferritin-polymer conjugates, which were then crosslinked.[26, 116, 117] DMMIBA is another UV-crosslinkable monomer that was synthesized for the study shown in this thesis based on a protocol similar to that used in the reference.[105, 110] DMMIBA contains a longer spacer than DMIAAm and is hence expected to be more

efficient at UV-crosslinking. The length of the spacer unit can be varied and different crosslinking agents synthesized if needed. However, the water solubility needs to be carefully checked for longer spacer units. Furthermore, the synthesis of DMMIBA is much easier, faster and reaches higher yields compared to DMIAAm. Figure 6.4 shows a comparison of the chemical structures of DMIAAm and DMMIBA.

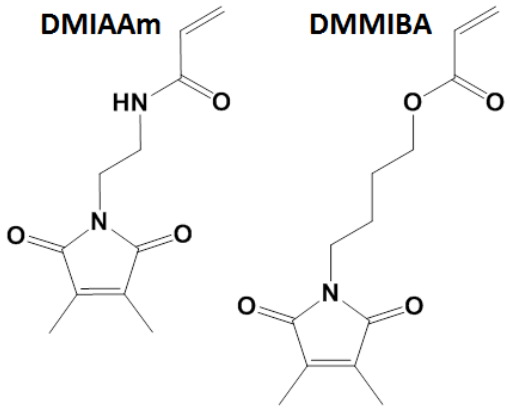

Figure 6.4: *DMMIBA has a longer spacer than DMIAAm and hence is expected to be better suited for UV-crosslinking when incorporated in copolymer chains.*

Copolymerization of DMMIBA and NIPAAm was more challenging than homopolymerization of NIPAAm, since DMMIBA has a low miscibility in water. The ratio of reactants was kept the same as in the homopolymerization of NIPAAm. Four reactions were carried out with increasing DMMIBA amount: 5 %, 10 %, 20 % and 40 % of the monomers. NMR analysis showed that up to 7 % crosslinker can be incorporated into the copolymer (Figure 6.5). Although up to 7 % of DMMIBA could be incorporated, there was significant loss in polymerization yield at higher ratio of DMMIBA in the reaction mixtures, most likely because at higher amounts there is significant amount of immiscible DMMIBA. Hence, 5 % DMMIBA was used for the synthesis of conjugates with BSA and FhuA.

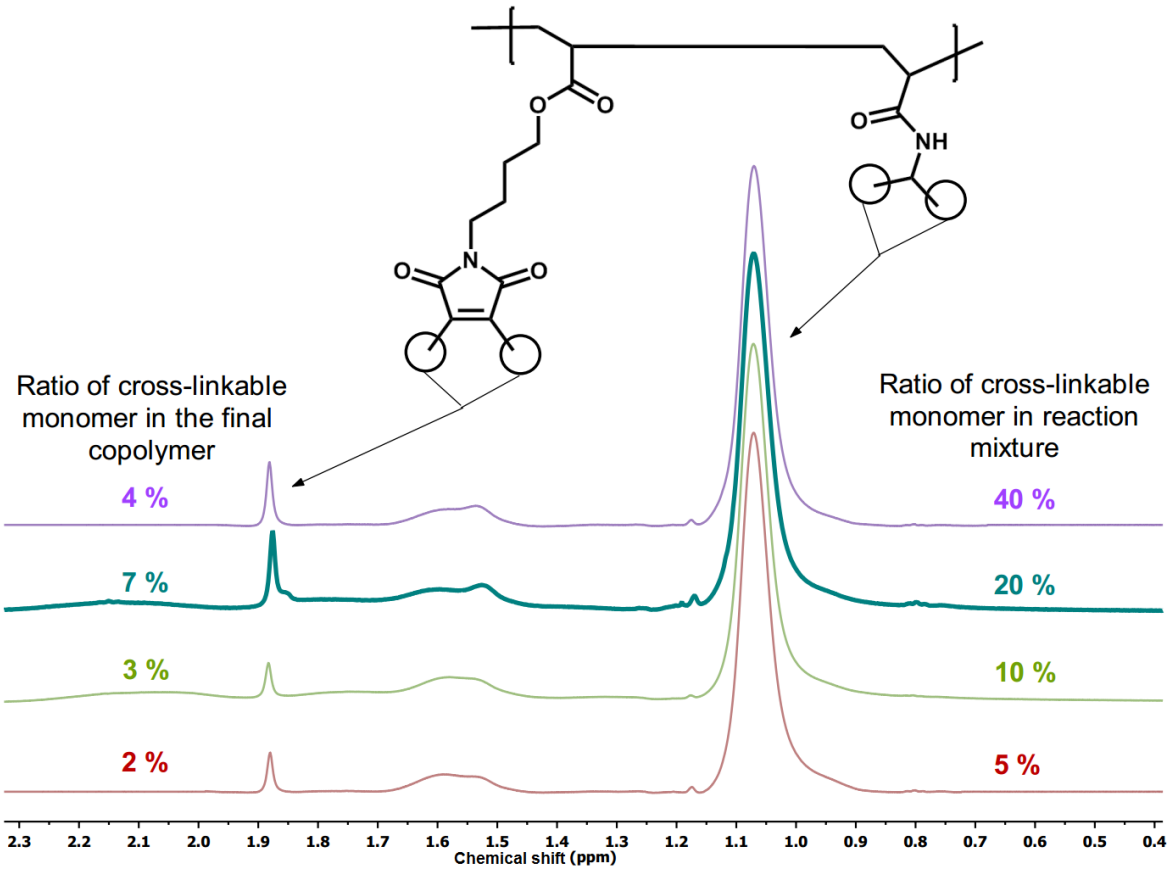

Figure 6.5: *NMR spectra of the copolymer generated by using various amounts of DMMIBA, showing that the copolymer can be formed with incorporations of DMMIBA ranging from 2 to 7 % of the final copolymer.*

6.4. Reactions in MPD buffer with BSA

6.4.1. Optimizing the synthesis of BSA macroinitiator

The aim of this thesis was to generate conjugates of the protein FhuA (explained in detail in **Section 4.1.2** and **Chapter 7**). However, FhuA is not commercially available, difficult to extract and only available in limited quantity. Hence, the reactions were first optimized using BSA, a commercially available cheap protein. The growth of polymers from the spherical protein ferritin via ATRP has previously been reported.[26, 116, 117, 181, 207] First, a functional CRP initiator is attached to the lysine residues of the protein and consecutively grafting-from polymerization carried out from the so called 'macroinitiator'.

However, the reaction conditions had to be adjusted to transfer this approach to the transmembrane protein FhuA, especially to avoid the exposure of FhuA to an organic co-solvent. Even though the reported polymerizations are free of organic solvent, the attachment of the CRP initiator or chain transfer agent (CTA) usually requires an organic co-solvent for solubilization,[156, 160, 162] thus exposing the protein to the solvent, prior to polymerization. In order to avoid that, a water-soluble NHS-ester activated CRP initiator was chosen to be linked to the lysine residues of BSA to form the BSA macroinitiator (BSA MI).[164] Additionally, FhuA being a transmembrane protein, requires MPD molecules to remain correctly folded. Hence, the optimization reactions were carried out in MPD buffer.

BSA MI was prepared at various pH values using *N*-2-bromo-2-methylpropanoyl-*β*-alanine *N'*-oxysuccinimide ester as the functional CRP initiator. MALDI ToF MS allowed precise characterization of BSA MI. The extent of modification was estimated by dividing the difference in molecular weight of unmodified BSA and BSA MI by 220 Da (the mass of one attached initiator unit). It is known that at higher pH, the reactivity of NHS ester towards primary amines is higher, however, so is the rate of hydrolysis.[208] Hence, a

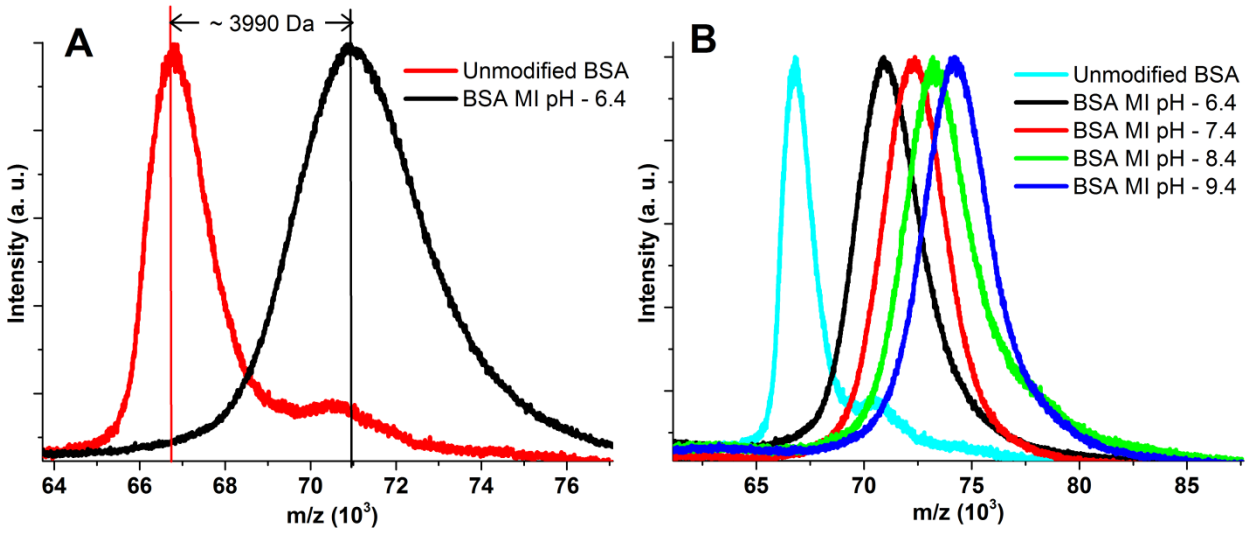

Figure 6.6: *Modification of BSA monitored by MALDI-ToF MS spectra A) BSA and BSA MI showing a modification of ~18 lysine residues. B) BSA and BSA MI showing the effect of pH on modification of the lysine residues: ca. 18, 25, 29 and 34 lysines were modified at pH 6.4, pH 7.4, pH 8.4 and pH 9.4, respectively.*

molar excess of 25 functional CRP initiators to each lysine residue was used to reduce the effect of hydrolysis at higher pH. Out of a total of 61 lysines present on BSA, between ca. 18 to 34 lysines were modified, giving an estimated number of solvent accessible lysines to be ca. 34 per BSA. The higher the pH, the higher was the extent of modification (Figure 6.6B). Hence, keeping the stability of FhuA in mind, the pH of 9.0 was chosen to obtain maximum modification for all the further reactions with BSA and for all reactions with FhuA.

6.4.2. Optimizing grafting-from polymerization for the generation of protein-polymer conjugates

After successfully generating BSA MI, the next step was to grow polymer chains from the CRP initiator units on BSA MI. The approach employed was copper-mediated CRP with Me_6TREN as the ligand. The polymerization was carried out in MPD buffer, without the use of any organic co-solvent. The reaction conditions that were used for homopolymerization of NIPAAm and DMAEMA were also employed for growing polymer chains from BSA MI. BiBA was used as the sacrificial initiator (see next paragraph for more detailed description), as already shown in previously reported literature.[117]

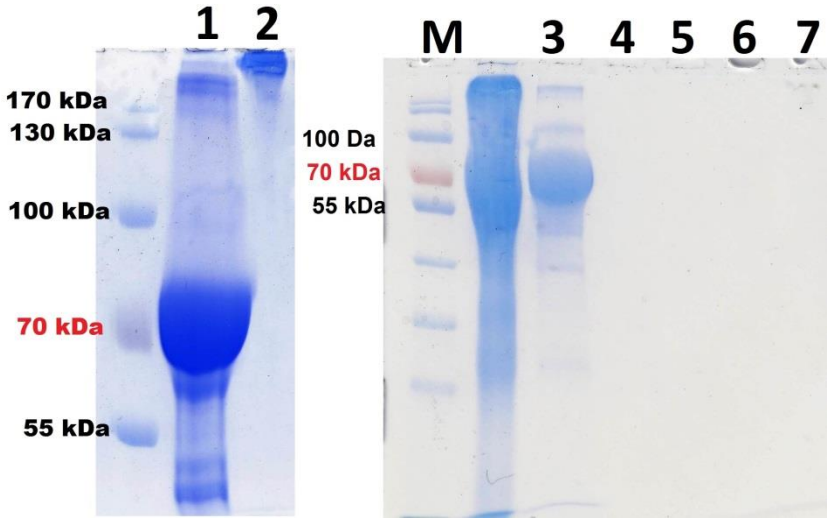

Figure 6.7: *SDS-PAGE profile of BSA (lane 1, lane 3), BSA-PNIPAAm with BiBA as the sacrificial initiator (lane 2) and PNIPAAm (3.625 mg/ml, 6.25 mg/ml, 12.5 mg/ml and 25 mg/ml for lane 4, 5, 6 and 7, respectively)*

Previously it was claimed that the use of sacrificial initiators (usually small molecules; hence having much less steric hindrance than a macroinitiator) was helpful in providing control over the polymerization and overcome the induction period.[209] SDS-PAGE profiles shown in Figure 6.7 show the faded bands typical of protein-polymer conjugates. Additionally, only PNIPAAm was also run in the gel to investigate whether PNIPAAm by itself could give false positive. Up to a concentration of 25 mg/ml, there was no visual confirmation of any stained bands of PNIPAAm (Figure 6.7).

However, the removal of free polymer chains resulting from the used sacrificial initiator is tedious and inefficient. Hence, it is desirable to be able to do the polymerization without using any sacrificial initiator. In recently reported research, it was possible to achieve control over polymerization even without the use of sacrificial initiator.[162] It would be interesting to use this approach to FhuA (and hence optimized using BSA). The resultant conjugates could be easily purified since all unwanted products, being small molecules, could be efficiently removed by dialysis. Furthermore, characterization techniques such as AUC and CD spectroscopy, which are sensitive to presence of free polymer chains, could be employed to protein-polymer conjugates if there were no free polymer chains. However, FhuA is only available in limited amounts due to complicated extraction procedure. Hence, one of the problems in optimizing this approach with low amounts of BSA was with the low amount of water-insoluble reactants (such as CuBr), which were impractical to be weighed (i.e. quantities less than 0.1 mg, the least count of the balance). This problem could be overcome easily by increasing the scale of reaction, while keeping the ratio of all the reactants the same. Increasing the quantity of all the reactants indeed resulted in conjugates with near complete conversion of the monomer (based on analysis by NMR of the unpurified reaction mixture; data not shown). Figure 6.8 (lanes 1, 2, 10 and 11) shows the conjugates successfully generated in this way without the use of any sacrificial initiator (See **Section 7.6.1** for detailed explanation of the staining methods and analysis of conjugates using SDS-PAGE). In order to check whether unmodified BSA can be dragged with the conjugate, the BSA-PNIPAAm conjugate was mixed with unmodified BSA in a 50:50 ratio, and loaded on the SDS-PAGE gel (Figure 6.8, lane 9). It was unequivocally proved that if there is some unmodified BSA, it is clearly visible as a separate distinct band. Hence, it was proved

that the conjugate formation without the sacrificial initiator is also highly efficient, resulting in complete modification of BSA MI.

However, for a protein like FhuA, which is not commercially available, scaling up the whole reaction can be a challenge because of limited quantity of the protein. Hence, another approach was developed to generate the conjugates. The amount of the catalyst (i.e. CuBr as well as Me_6TREN) was increased while keeping the amount of initiator (i.e. BSA MI) and the amount of monomer the same. Instead of the usual ratio of 1 : 121 : 1.3 : 1.9 for initiator : NIPAAm : CuBr : Me_6TREN, the ratio 1 : 121 : 13 : 19 (i.e. 10 times the catalyst while keeping the rest the same) was used. This also resulted in conjugates with complete conversion. Figure 6.8 (lanes 3, 4, 5, 6, 7 and 8) shows the BSA-PNIPAAm conjugates synthesized using this approach. Similarly, BSA-PNIPAAm-r-PDMMIBA and BSA-PDMAEMA-r-DMMIBA conjugates were also generated using 10 times the catalyst ratio (Figure 6.9). The BSA sample in lane 1 also

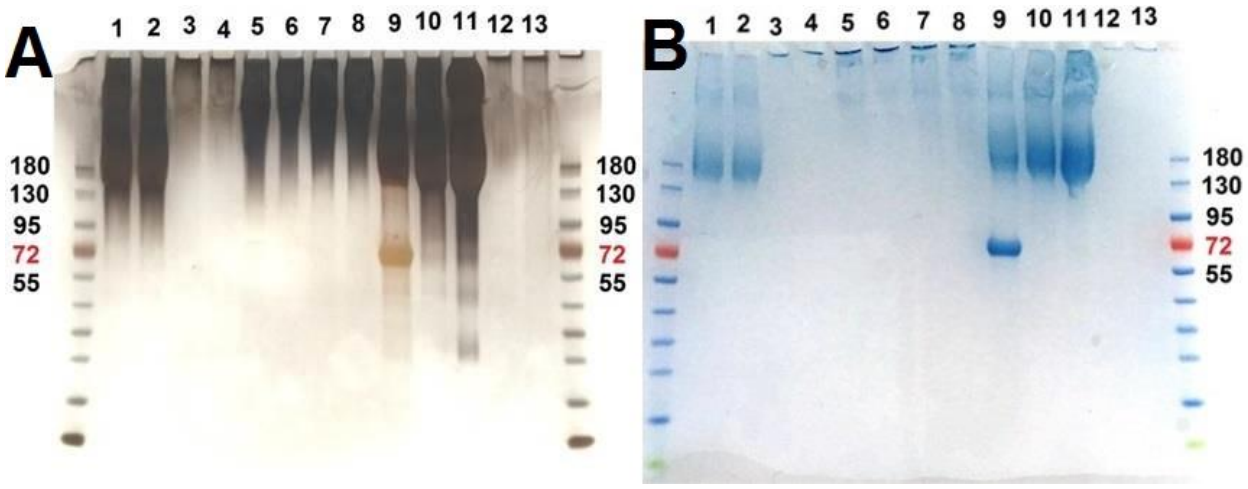

Figure 6.8: *Silver (A) and Coomassie (B) stained SDS-PAGE analysis of conjugation of polymers to BSA without sacrificial initiator at different ratios of reactants. Lane 1/2: BSA-PNIPAAm at 10x total amount of all reactants (see text for details); lane 3/4: BSA-PNIPAAm at 10x catalyst, initiator and monomer amount the same (see text for details); lane 5/6/7/8: BSA-PNIPAAm-PDMIAAm at 10x catalyst, initiator and monomer amount the same; lane 9: A 50:50 mixture of unmodified BSA and BSA-PNIPAAm from lane 1; lane 10/11: BSA-PNIPAAm same as lane 1, two times volume loaded onto gel; lane 12/13: unrelated samples.*

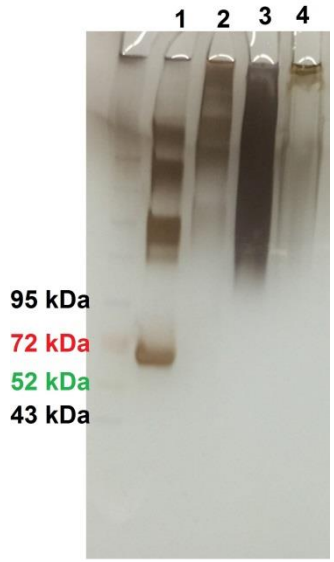

Figure 6.9: *SDS-PAGE of BSA and its conjugates. Lane 1 – BSA, lane 2 – unrelated sample, lane 3 – BSA-PNIPAAm-r-PDMMIBA and lane 4 – BSA-PDMAEMA-r-PDMMIBA. No sacrificial initiator was used in the synthesis of any of these conjugates.*

shows contamination in pure BSA, which has been reported in literature to occur from time to time.[162]

As a result of successful formation of conjugates without any free polymer chains, it was also possible to characterize the conjugates with additional techniques like analytical ultracentrifugation (AUC). AUC is a sensitive technique to estimate the size of particles by putting them under high centrifugal force and analyzing their velocity profiles. In the presence of free polymer chains in the conjugate solution, the velocity profile of the conjugate cannot be accurately measured because of hindered movement of the conjugate through the free polymer chains, resulting in measurement artefacts. Additionally, the absorbance from free polymer chains also creates noise in the velocity profile data. AUC results (Figure 6.10A and Figure 6.10B) clearly show an increase in the hydrodynamic radius of BSA pre and post modification. Unlike other techniques, AUC measures the proteins and conjugates in their natural aqueous environment, hence avoiding any drying or freezing related artefacts. However, the partial specific volume of a particle is needed for accurate diffusion corrected results (Figure 6.10B). Although a simple experiment, accurate determination of partial specific volume of a particle

requires large quantity of the protein or particle. For BSA and BSA-PNIPAAm, the extrapolated values were 1.00082 cm^3/g and 1.00080 cm^3/g respectively. While for BSA, a commercially available protein, it was feasible, for FhuA it was counter-productive. Nonetheless, even non-diffusion corrected results were helpful enough in proving conjugation (Figure 7.9).

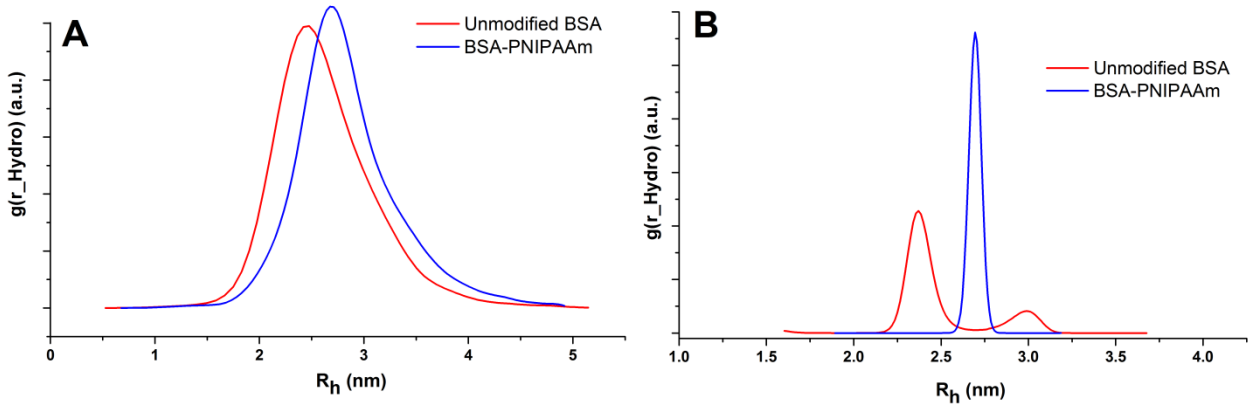

Figure 6.10: *AUC measurements of BSA and BSA-PNIPAAm without (A) and with (B) diffusion correction. These data clearly show a change in size of BSA upon modification. The conjugates without sacrificial initiator were crucial to obtain reliable data for BSA-PNIPAAm.*

6.5. Summary

In conclusion, the reaction conditions were optimized to be applied to the protein FhuA. Hence, all experiments were conducted in MPD buffer and without the use of any additional organic co-solvent. First, the homopolymerization of NIPAAm and DMAEMA and then the copolymerization of NIPAAm with DMIAAm in MPD buffer with BiBA as the initiator were investigated. Copper-mediated CRP with Me_6TREN as the ligand was used. The polymer samples were characterized using MALDI-ToF MS and GPC. The optimized conditions were then employed for grafting-from polymerization using BSA as a model protein. A BSA macroinitiator (MI) was first generated by reacting BSA with a water-soluble functional CRP initiator. The efficiency of coupling of the initiator was investigated using MALDI-ToF MS at various pH and optimum value of pH 9.0 was obtained. Consecutively, grafting-from polymerization with BSA MI was carried out in MPD buffer using the optimized conditions from the homopolymerization and

copolymerization experiments with BiBA as a sacrificial initiator. The formation of conjugates was proved by SDS-PAGE analysis using coomassie as well as silver staining. Furthermore, two approaches to avoid the use of sacrificial initiator were investigated – one to scale up the whole reaction, and second to use 10-times higher amount of the catalyst (i.e. CuBr and Me_6TREN). Both the techniques resulted in successful generation of conjugates with BSA. Conjugates of BSA without the free polymer chains (resulting from sacrificial initiator) enabled analysis using AUC, which unequivocally proved the conjugate synthesis by demonstrating an increase in the hydrodynamic radius of BSA pre and post modification. Based on the optimization experiments explained in this chapter, conjugates of various genetic variants of FhuA (**Chapter 7**) and many other proteins (**Chapter 8**) were synthesized.

7 Synthesis and characterization of conjugates of FhuA

The synthesis and characterization of the protein and its variants, used for the study shown in this chapter, were done by our collaboration partners; Julia Kinzel, Deepak Anand and others in the group of Prof. Schwaneberg at the RWTH Aachen University.

7.1. Introduction

After optimizing the reaction conditions with BiBA and BSA, the focus was moved to modify the protein of interest, ferric hydroxamate uptake protein component A (FhuA). This chapter deals with the syntheses of various "building blocks based on transmembrane proteins" (BBTP) from the transmembrane protein FhuA by grafting three different polymers from its surface. The grafted polymers were poly(*N*-isopropylacrylamide) (PNIPAAm), a copolymer of NIPAAm and 3,4-dimethyl maleic imidobutyl acrylate (DMMIBA) and poly((2-dimethylamino)ethyl methacrylate) (PDMAEMA). The grafting was performed from FhuA WT and three variants, two of which had been genetically optimized to avoid growth of polymer chains inside the FhuA channel. These two variants had up to 11 lysines, uniformly distributed in a rim exclusively on the outer surface of FhuA. This distribution should facilitate the growth of polymer chains as well as avoid possible instability in the protein structure because of its modification. A water-soluble functional CRP initiator was linked to the amine groups of the lysine residues of FhuA and subsequently polymer chains were grafted from the protein surface. Although, non-specific grafting-to on the surface of cells (and hence membrane proteins) has been reported before,[210] to the best of my knowledge, this study was the first example of grafting a polymer from a transmembrane protein.

7.2. Preparation and characterization

7.2.1. Materials

All chemicals used were of analytical reagent grade or higher quality, purchased from Applichem (Darmstadt, Germany), Alfa Aesar (Karlsruhe, Germany) or Sigma-Aldrich Chemie (Taufkirchen, Germany), if not stated otherwise. NIPAAm was purified by two successive recrystallizations from a mixture of *n*-hexane and benzene (4:1 v:v). Before use, DMAEMA was passed through basic alumina twice, to remove the inhibitor. CuBr was purified by stirring in acetic acid overnight. After filtration, it was washed successively with ethanol and diethylether and then dried in vacuum. All other chemicals were used as received without further purification. *N*-2-bromo-2-methylpropanoyl-β-alanine N'-oxysuccinimide ester was synthesized according to reference.[164] The crosslinkable monomer, 3,4-dimethyl maleic imidobutyl acrylate (DMMIBA), was synthesized according to a procedure reported for similar compounds.[105, 110]

MPD buffer is defined as the buffer containing 50 mM MPD, 10 mM sodium phosphate, 1 mM EDTA and 1 mM NaN_3 at pH 7.4, unless otherwise stated.

Rational design, cloning, expression and extraction of FhuA variants: The protein was provided by the group of Prof. Schwaneberg, RWTH Aachen University, and generated using protocol reported in the reference.[14]

Formation of FhuA solution: The lyophilized powder of respective FhuA (containing ca. 66 wt. % SDS) was dissolved in MPD buffer and dialyzed two times (against MPD buffer using dialysis membrane with a MWCO of 12-14 kDa for 24 h). The dialyzed solution was centrifuged at 3200 g for 20 min and passed through a 0.2 µm PVDF filter in order to remove any larger aggregates or bacteria. The concentration of the purified sample was estimated using BCA

assay kit provided by Thermo-Fischer scientific and the samples were stored at 12 °C before further use.

Formation of FhuA macroinitiator (FhuA MI): pH of the respective FhuA solution was increased by exchanging the buffer from MPD buffer to MPD buffer pH 9.0. To do that, three times centrifugation at 3,200 g was performed using a 10 kDa MWCO Amicon Ultra-4 filter unit. Then, 25 equivalents of *N*-2-bromo-2-methylpropanoyl-*β*-alanine *N'*-oxysuccinimide ester per lysine residue of the respective FhuA variant were added to the protein solution at around 5 mg/ml. The reaction was allowed to proceed at 12 °C for 12 h on a shaking platform. Afterwards, the solution was dialyzed twice (against MPD buffer using dialysis membrane with a MWCO of 12-14 kDa for 24 h) and stored at 12 °C before being polymerized. The concentration of the purified sample was estimated using BCA assay kit provided by Thermo-Fischer scientific.

Polymerization from FhuA MI: Each FhuA MI solution was first dialyzed against MPD buffer without NaN_3, since NaN_3 influences the CRP catalyst complex. Monomers (NIPAAm / DMAEMA / DMMIBA) were then added to the respective FhuA MI solution. In case of use of a sacrificial initiator, 2-bromoisobutyric acid (BiBA) was also added. The solution was deoxygenated by purging with nitrogen for 30 min while cooling it in an ice bath. Simultaneously, a solution of CuBr and Me_6TREN in 1 ml Millipore water was degassed likewise. The monomer/(macro)initiator solution was then transferred to the catalyst solution via cannula transfer. The typical final ratio of components for the reaction was initiator (FhuA MI) : monomer : CuBr : Me_6TREN = 1 : 200 : 7 : 10 when using no sacrificial initiator, and initiator (FhuA MI + BiBA) : monomer : CuBr : Me_6TREN = 1 :50 : 1.3 : 1.9 when using sacrificial initiator. The amount of sacrificial initiator was kept the same for each FhuA variant. The excess of BiBA for all the variants was 345 BiBA per FhuA. The reaction was allowed to proceed for 12 h, initially at 0 °C and gradually rising to room temperature as the ice melted after about 2 h. The obtained products were purified first by two times dialysis (against MPD buffer using dialysis membrane with a MWCO of 12-14 kDa for 24 h) to

remove all unreacted monomer and small molecules. Nine times centrifugation at 3,200 g (MPD buffer using a 50 kDa MWCO Amicon Ultra-4 filter unit) was carried out to remove the free polymer, if sacrificial initiator was used; otherwise this step was skipped. Finally, the sample was collected and stored at 15 °C until further characterization. The concentration of the purified sample was estimated using BCA assay kit provided by Thermo-Fischer scientific.

7.2.2. Characterization techniques

SDS-PAGE: To perform gel electrophoresis of FhuA, FhuA MI and FhuA-polymer conjugates together, a 4-15 % gradient polyacrylamide gel was used (90 V, ca. 2.5 h, Mini-PROTEAN® Electrophoresis System-Bio-Rad, München, Germany). Samples were prepared by denaturing the protein using 2-mercaptoethanol at 65 °C for 3 min. Then, 8 µl of each sample was loaded onto the gel. Silver and/or coomassie staining were used to resolve the gel. The staining protocols are described in **Section 6.2.2** in detail.

CD spectroscopy: CD spectra were recorded on Olis SDM 17 at room temperature (Olis, Bogart, USA, software Olis GlobalWorks version 4.7.40) using 0.5 mm path length cuvettes and 0.5 mg/ml protein concentration. The bandwidth of 2 nm, data pitch of 1 nm, scan speed of 20 nm/min and data integration time (DIT) of 1 sec was used for all measurements. An average of three spectra was taken for all measurements. Spectra were smoothed using Savitzky-Golay filter. FhuA MI and FhuA-polymer conjugates were analyzed on J 815 device (Jasco Analytical Instruments, Easton, USA, software Spectra manager-2) at 20 °C using 0.2 mm path length cuvettes and 1 mg/ml protein concentration. The bandwidth of 1 nm, data pitch of 1 nm, scan speed of 50 nm/min and DIT of 4 sec was used for all measurements. An average of three spectra was taken for all measurements, without smoothening.

MALDI-ToF mass spectrometry: Spectra were acquired using a 337 nm laser Bruker UTX MALDI-ToF mass spectrometer (Bruker, Bremen, Germany) with

pulsed ion extraction. The masses were determined in positive ion linear mode. The sample solutions were applied on a ground steel target using the dried droplet technique with $ZipTip_{C4}$ pipette tips (Millipore, Darmstadt, Germany). Super-DHB, a 9:1 mixture of 2,5-dihydroxybenzoic acid (DHB) and 2-hydroxy-5-methoxybenzoic acid, was used as matrix substance in a 50 mg/ml solution in Millipore water:acetonitrile 1:1 with 0.1 % trifluoroacetic acid. Mass calibration was performed with external calibration.

Analytical ultracentrifugation: Ultracentrifugation was performed with an Optima XL-I centrifuge from Beckman Coulter (Krefeld, Germany) equipped with an interference optical detection system and AN60Ti rotor. The protein concentration of the samples was 0.2 mg/ml and the centrifugation speed 31,000 rcf. Three parallel runs for 16 h at 20°C were averaged to get the final spectra. The software XL-I 3.01h, SEDFIT V14.81 (2015) and Mathematica 10 were used for data analysis.

Chromatography: SEC was performed on a Knauer instrument (Berlin, Germany) with a Knauer BioFox 17/100 SEC protein column using UV detection at 210 nm, 254 nm, 280 nm and 300 nm simultaneously. The column was eluted using MPD buffer at a rate of 1 ml/min.

Transmission Electron Microscopy: TEM was performed on a Philips CM-200 device operating at 120 kV. The samples were deposited on nitrogen glow discharged carbon/cellulose acetate film coated grids, washed 2 times with Millipore water, stained using 2 % (w/v) uranyl acetate solution, and analyzed on the same day.

7.3. FhuA stabilization

Membrane proteins are anchored in a phospholipid bilayer by hydrophobic amino acid side chains exposed to their outer barrel surface leading to hydrophobic interactions in the ~2.5 nm thick hydrophobic bilayer in their natural environment.

Transmembrane proteins usually require detergents to keep these hydrophobic patches covered and keep the protein correctly folded after its extraction from cells. The detergent octyl-polyoxyethylene (oPOE)[35, 185, 211] and the block-copolymer polyethylene-polyethyleneglycol (PE-PEG)[212, 213] have been shown to successfully refold FhuA. However, steric hindrance of oPOE/PE-PEG is unfavorable for modification most likely because of shielding of lysine residues and furthermore the high costs of oPOE make them inappropriate as a suitable detergent for FhuA refolding. A water-miscible amphipathic alcohol, 2-methyl-2,4-pentanediol (MPD), was used as an alternative stabilizing agent for FhuA for experiments reported in this thesis. The method, originally developed by Michaux *et al*.,[214] consists of using amphipathic co-solvents to refold SDS-denatured proteins and enable them to regain their active form. Using MPD was not only beneficial for the polymerization process, but also enabled me to perform characterization with dynamic light scattering (DLS) and transmission electron microscopy (TEM). CD spectra proved that FhuA WT and the three variants had predominantly β-sheet structure, as expected, in presence of 50 mM MPD (Figure 7.11).

Later into the project it was realized that all FhuA variants and their conjugates tend to attract bacteria when stored over a week (Figure 7.1A/B). Hence, in order to avoid bacterial growth in the samples, 1mM NaN_3 was included in the MPD buffer (experimental section). However, NaN_3 interferes with the polymerization; possibly disrupting the catalyst complex and giving it a greenish colour, as opposed to the usual blue colour (Figure 7.1C/D). Hence, before the polymerization, NaN_3 was dialyzed out; and after the polymerization, normal MPD buffer with NaN_3 was used for dialysis.

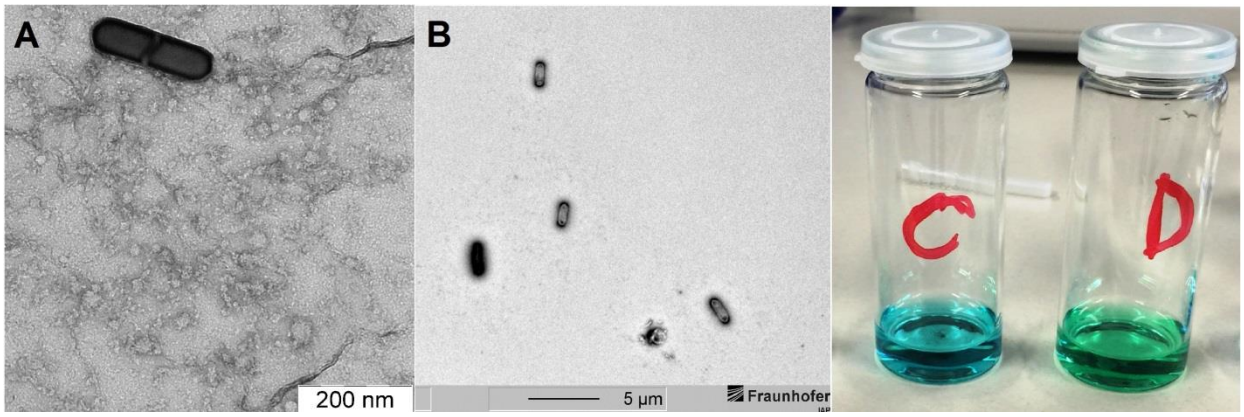

Figure 7.1: *Contamination of a sample of FhuA WT (A) and FhuA WT-PNIPAAm (B). Color of the catalyst complex when in MPD buffer without (C) and with (D) NaN_3.*

7.4. Rational design of FhuA WT and variants

Starting from naturally occurring FhuA WT,[34] the pore-blocking cork domain can be removed by deletion of the amino acids 1-159. The resulting variant FhuA Δ1-159 has already been used for stability studies,[38] transport in artificial membranes[35-37] and formation of catalytically active channels (FhuA ΔCVF^{tev}).[215, 216] BBTP formation was successfully demonstrated for both variants, but their use is not advantageous for any imaginable applications of BBTP. Although FhuA ΔCVF^{tev} has an open pore, the 28 lysine residues are non-uniformly distributed around the whole protein, including some exposed to the channel entrance or interior (Table 7.1). Hence, their modification and polymer growth would probably block the channel. Furthermore, the modification of residues located in the hydrophobic region of FhuA could be hindered by the stabilizing agent, which ensures the proper folding and solubility of the transmembrane protein. Additionally, after linkage of chemical groups to a charged amino acid residue, the salt bridge would be destroyed and the stability decreased (explained in **Section 4.1.1**).

Table 7.1: *Overview of FhuA WT and FhuA variants along with their properties. FhuA deletion variants including two recognitions sites for TEV protease resulting in a desired fragment (blue); K, lysine residue (magenta); TEV, Tobacco Etch Virus.*

Variant	FhuA WT	FhuA ΔCVF^{tev}	FhuA ΔCVF^{tev} K_8^{mid}	FhuA ΔCVF^{tev} K_{11}^{up}
Molecular weight [kDa]	78.9	63.5	64.0	64.2
No. of lysines	36	28	8	11
No. of lysines in salt bridges	36	28	0	0
TEV cleavage sites	0	2	2	2
Lysine(s) on 6 kDa fragment after cleavage	No fragment	K517 K519 K526	K519	K517
Side view	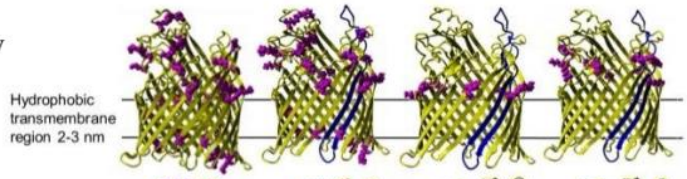			
Top view				

Accommodating all the mentioned factors, two FhuA variants for predefined site-specific modification were designed. Lysine residues (K) are located at defined positions, symmetrically distributed in a plane perpendicular to the protein channel, exclusively on the outer surface of the barrel and above the hydrophobic region (Table 7.1). FhuA ΔCVF^{tev}K_8^{mid} and FhuA ΔCVF^{tev}K_{11}^{up} contain lysine residues evenly distributed in a rim around FhuA and not directly involved in salt bridges. These lysines are expected to be easily accessible, and the resultant FhuA-polymer conjugates more stable. FhuA ΔCVF^{tev} as well as the two new FhuA variants additionally included two recognition sites for the Tobacco Etch Virus protease (TEV protease),[217] in the sequence of FhuA ΔCVF^{tev}, FhuA ΔCVF^{tev}K_8^{mid} and FhuA ΔCVF^{tev}K_{11}^{up}. TEV protease is a highly site-specific enzyme that recognizes the amino acid sequence ENLYFQ|G and cleaves the main chain of the protein after Q.[217] Thus, the respective FhuA variants are cleaved into three fragments (Figure 7.2). FhuA ΔCVF^{tev}K_8^{mid} and

FhuA ΔCVF^{tev}K$_{11}$^{up} were designed in the way that the 6 kDa fragment contains one lysine residue each to facilitate analysis of the lysine modification with mass spectrometry (Table 7.1).

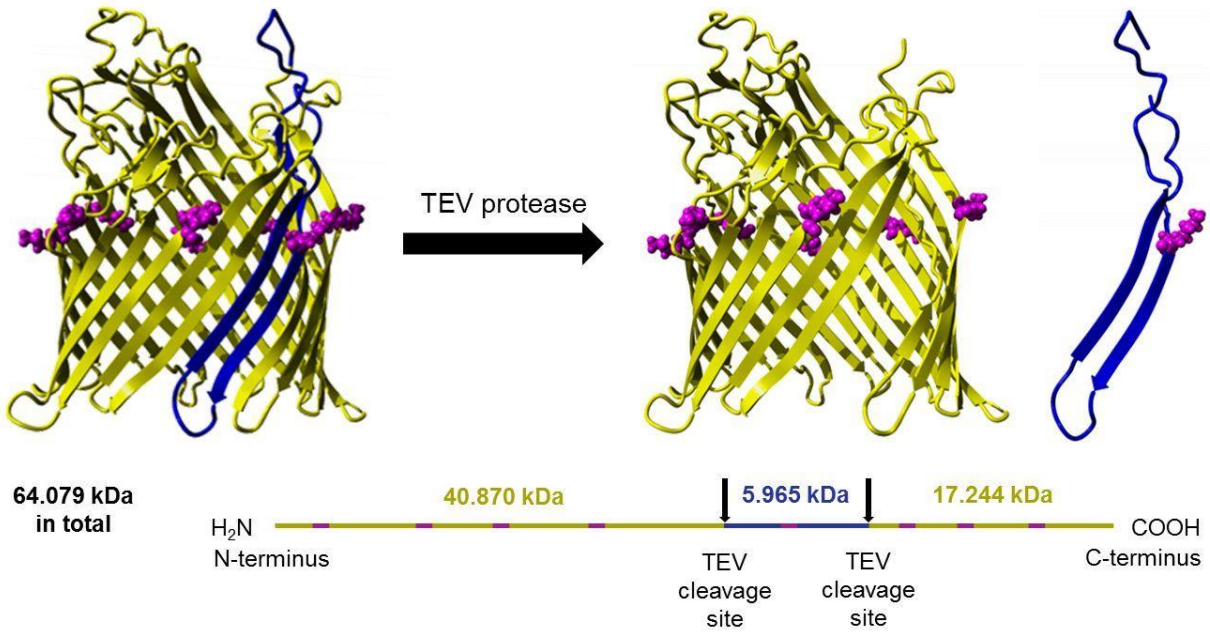

Figure 7.2: *Cleavage of FhuA ΔCVF^{tev}K$_8$^{mid} (shown as an example) through Tobacco Etch Virus (TEV) protease to obtain a 5.965 kDa fragment for mass spectrometry analysis. The small fragment (blue) of the shown FhuA ΔCVF^{tev}K$_8$^{mid} variant contains the lysine residue K519 (ball structure in magenta).*

7.5. Synthesizing FhuA macroinitiator

The macroinitiators for polymerization were generated by the reaction of the respective FhuA variant with *N*-2-bromo-2-methylpropanoyl-*β*-alanine *N*'-oxy-succinimide ester at pH 9.0, as the reactivity of amines towards NHS activated acylating agents is higher at elevated pH.[208] The reaction was carried out at 12 °C in order to maintain the stability of FhuA. However, the rate of hydrolysis of NHS esters also increases at elevated pH and higher temperature conditions (also see **Section 6.4.1** for comparable BSA macroinitiators). A 25 fold stoichiometric excess of the initiator compound per lysine group of the respective FhuA variant

worked well to achieve a high degree of modification. After the reaction, FhuA MI was purified from unconjugated initiator and NHS by dialysis against MPD buffer. SDS-PAGE was performed on a gradient gel. Compared to unmodified FhuA, the macroinitiators show a slight shift to higher molecular weight in all the variants (Figure 7.8). Although the change cannot be exactly quantified, it indicates that some addition has indeed taken place.

Top-down mass spectrometry of membrane proteins (that is analysis of intact membrane proteins) was reported in 1996 by Fearnley and Walker.[218] While analysis of soluble proteins is relatively straight forward[219] (as also shown in **Chapter 6** for BSA), for integral membrane proteins, it remains challenging. Owing to a lot of apolar residues, membrane proteins may have less number of ionizable side chains in comparison to soluble proteins of similar size.[219] Furthermore, transmembrane proteins often have domains strongly H-bonded in their secondary structure, possibly resulting in the proteins being more folded and less charged in the gas phase.[219] These effects are expected to become more pronounced with the increasing size of proteins.

Nonetheless, we were successful in obtaining the mass spectra of intact FhuA WT, FhuA $\Delta CVF^{tev}K_8^{mid}$ and FhuA $\Delta CVF^{tev}K_{11}^{up}$. Unfortunately, spectra were not obtained for all FhuA variants before and after modification. In order to circumvent this problem, FhuA samples were digested using TEV protease (Figure 7.2 and Figure 7.3). The digestion of FhuA with the TEV protease resulted in three fragments, the smallest fragment of which, 6 kDa, can be detected with matrix-assisted laser desorption/ionization time-of-flight (MALDI-ToF) mass spectrometry and gives a hint of the modification. For FhuA $\Delta CVF^{tev}K_8^{mid}$ as an example, the fragment has one lysine residue which appears to be modified after the reaction with the functional CRP initiator (Figure 7.4A). The MALDI-ToF mass spectrum shows an increase of 211 Da, corresponding to the mass of one initiator unit. The intensity of the peak of the unmodified fragment is nearly insignificant, thus supporting the claim that the efficiency of coupling is high.

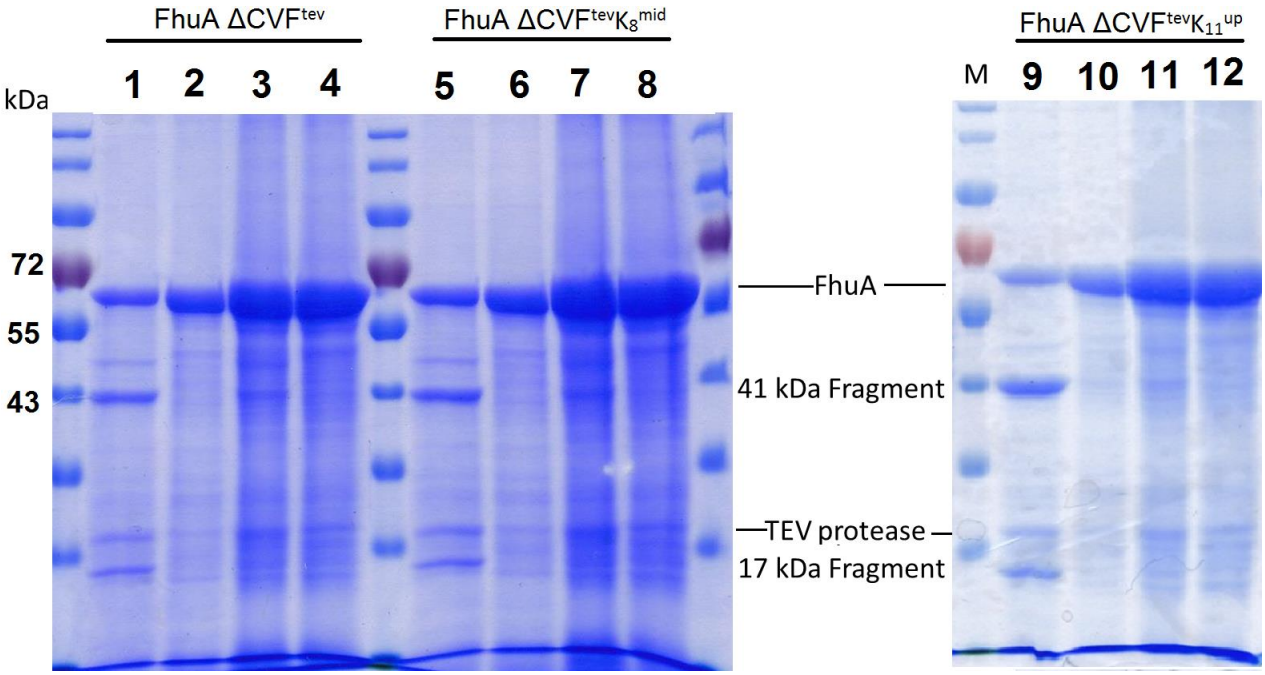

Figure 7.3: *Digestion of FhuA and FhuA MI by TEV protease. Respective FhuA samples with the protease (Lane 1, 5, 9) show the 41 kDa and 17 kDa fragments, unlike FhuA samples without the protease (Lane 2, 6, 10). Digestion for FhuA MI was more difficult to prove. Respective FhuA MI with protease (Lane 3, 7, 11) show a slight band for the 41 kDa fragment, while without protease (Lane 4, 8, 12) they do not show the digestion fragments.*

The structural integrity of FhuA MIs was analysed by CD spectroscopy. The spectra in Figure 7.11 show that all FhuA and their corresponding MI have a minimum around 215 nm,[220] typical for anti-parallel β-barrel proteins like FhuA.[38] This indicates that the attachment of initiator units does not affect the folding of the protein. CD spectra also showed that it is possible to lyophilize and store the macroinitiators in freezer (-20 °C). The samples were simply dialyzed for a day to get the sample in aqueous environment without the loss of its secondary structure (Figure 7.5).

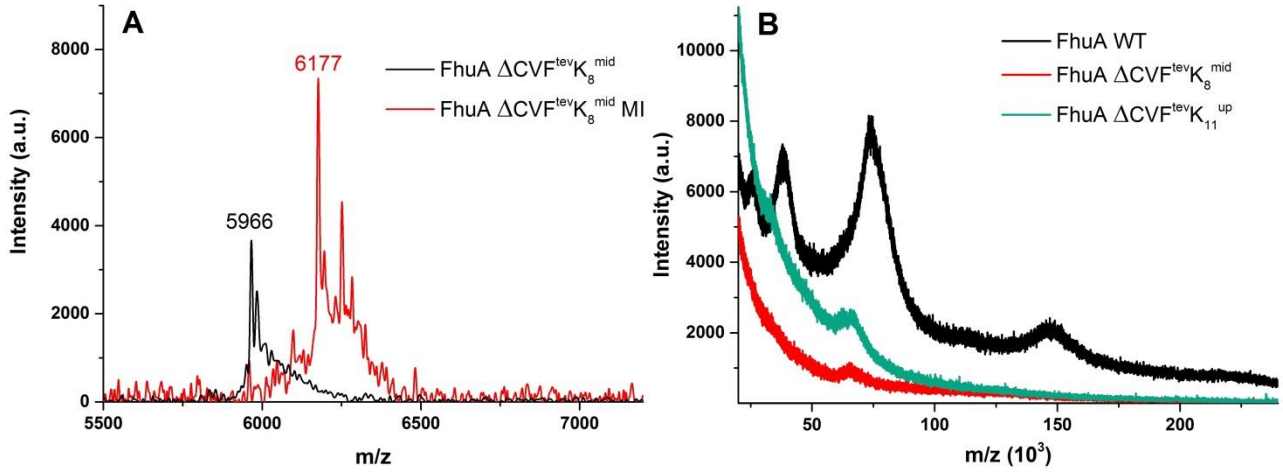

Figure 7.4: *MALDI-ToF mass spectra of FhuA and FhuA MI. A) The 6 kDa fragment of FhuA ΔCVF^{tev}K$_8^{mid}$ after cleavage with protease from Tobacco Etch Virus (TEV). The spectrum shows the fragment before (black) and after modification by initiator (red). The observed mass changes by 211 Da corresponding to the linkage of one initiator unit. B) MALDI-ToF spectra of intact FhuA WT, FhuA ΔCVF^{tev}K$_8^{mid}$ and FhuA ΔCVF^{tev}K$_{11}^{up}$ were also obtained. FhuA WT was detected as 1-, 2- and 3-times charged species as well as a dimer (hence a different m/z). The intensity of the other two variants is too low and only the 1-times charged protein was observed.*

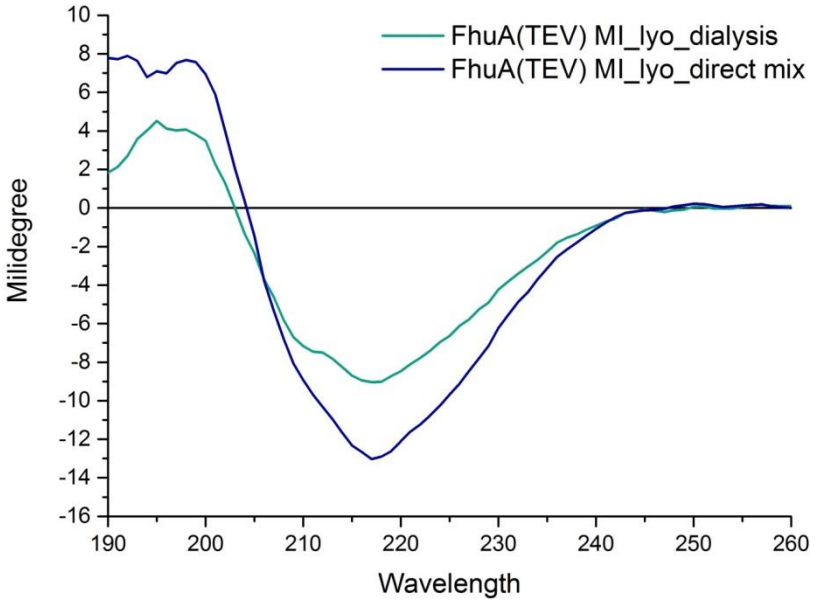

Figure 7.5: *The CD spectra of lyophilized FhuA ΔCVF^{tev} measured directly after dissolving the lyophilized powder in MPD buffer (blue) and after a day of dialysis against MPD buffer (green). The spectra show that the process of lyophilization does not affect the secondary structure of FhuA.*

7.6. Synthesizing conjugates

Three polymer/copolymer combinations were used to generate conjugates, namely PNIPAAm, PNIPAAm-PDMMIBA and PDMAEMA, as shown in Figure 7.6.

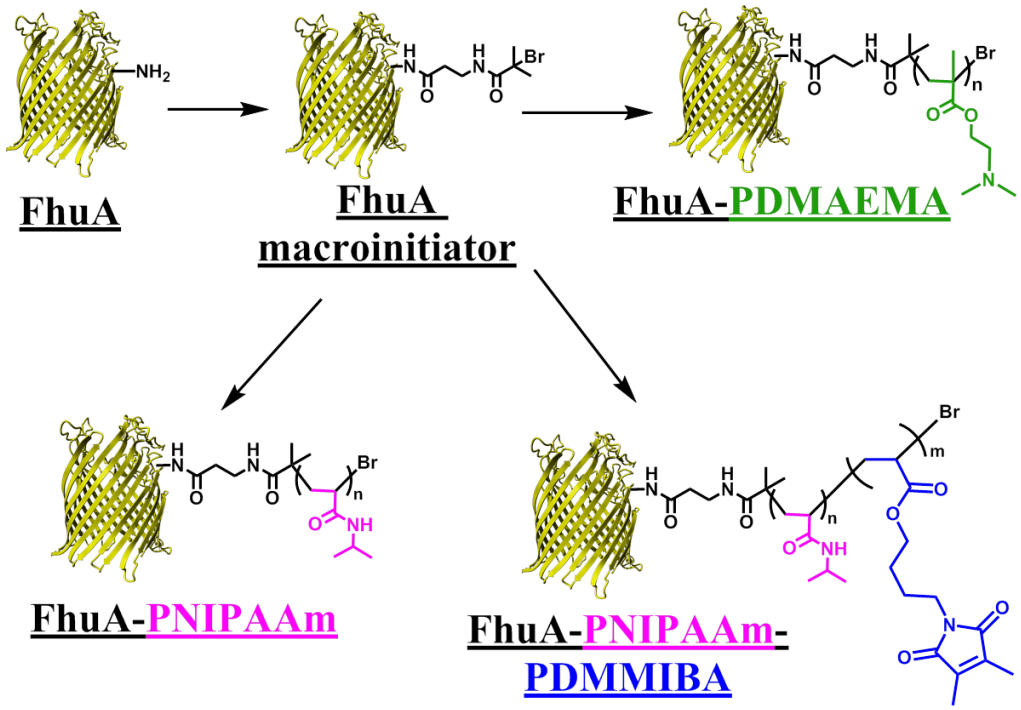

Figure 7.6: *Scheme of synthesis of BBTP with various polymers detailed in this chapter. The respective FhuA variant was modified to generate FhuA macroinitiator, which was further used for the synthesis of conjugates with three polymers as shown. Modification of just one lysine is illustrated as an example.*

7.6.1. Conjugates with PNIPAAm

After characterizing the MI of FhuA WT, FhuA ΔCVF^{tev}, FhuA ΔCVF^{tev}K$_8^{mid}$ and FhuA ΔCVF^{tev}K$_{11}^{up}$, a polymerization was performed from the protein surface under aqueous conditions. The used MPD-containing buffer is different from purely aqueous phosphate buffers. A copper-mediated controlled radical polymerization based on the addition of CuBr and the ligand tris[2-(dimethyl-amino)ethyl]amine (Me$_6$TREN) worked well to obtain FhuA-polymer conjugates. Such polymerizations are described as supplemental activator and reducing

agent atom-transfer radical polymerization (SARA ATRP) or SET-LRP, and a debate about the actual mechanism is going on.[58, 61-63, 162, 206, 221] In order to add a stimulus handle to the BBTP, the monomer *N*-isopropylacrylamide was used for the polymerization from FhuA. PNIPAAm (and hence the generated BBTP) is water-soluble at room temperature and becomes hydrophobic upon raising the temperature above the lower critical solution temperature (LCST). Scheme 7.1 summarizes the formation of FhuA MI and FhuA-PNIPAAm BBTP.

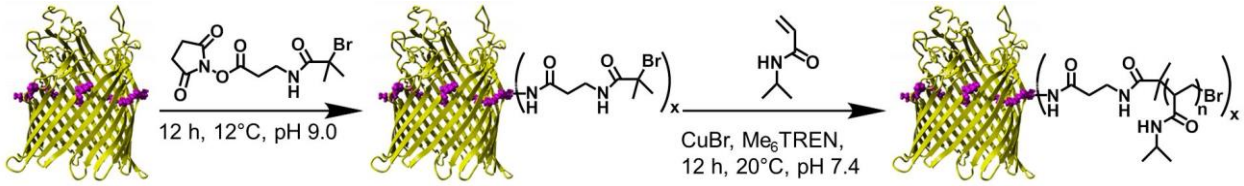

Scheme 7.1: *Formation of FhuA macroinitiator by reacting the functional CRP initiator with the lysine residues of FhuA and subsequent polymerization of NIPAAm under copper-mediated CRP conditions. Here, FhuA ΔCVF^{tev}K$_8^{mid}$ is shown as an example.*

As the rate of polymerization in water is fast, the reaction was started while cooling the solution in an ice bath to avoid early termination, and the temperature was allowed to gradually reach room temperature after around 2 hours. The addition of 2-bromoisobutyric acid (BiBA) as sacrificial initiator resulted in better control over the polymerization. First, small molecules such as the catalyst and unreacted monomer were removed after the reaction by dialysis against MPD buffer for 2 days. Then, the free PNIPAAm created from the sacrificial initiator was removed by extensive centrifugation with MPD buffer against a 50 kDa membrane until no trace of free polymer was visible in the size exclusion chromatography (SEC) spectra (Figure 7.7C). The molecular weight of the polymer chains attached to FhuA was difficult to determine directly. Hence, control experiments, i.e. characterizing the free polymer resulting from the sacrificial initiator and polymerization using only BiBA under identical conditions were used. The MW of these polymer chains was estimated to be around 5000 Da from MALDI-ToF mass spectra (Figure 7.7A and 7.7B).

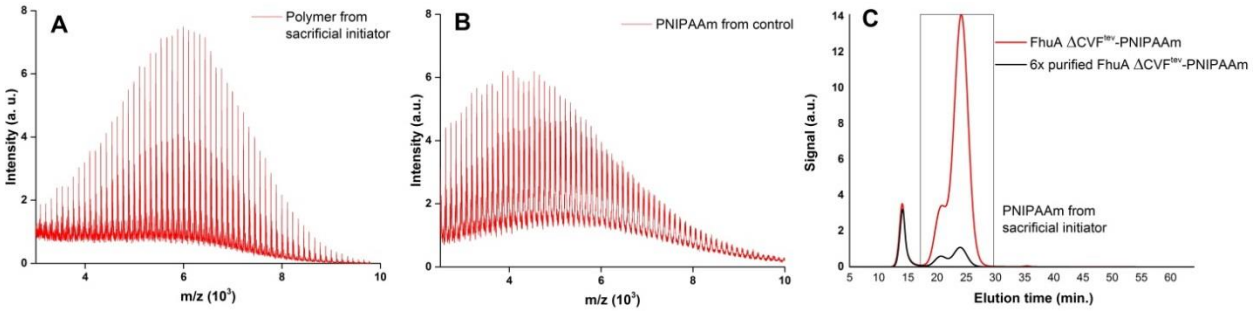

Figure 7.7: *A) MALDI-ToF mass spectrum of unpurified FhuA ΔCVF^{tev}–PNIPAAm, showing the polymer generated from sacrificial initiator B) MALDI-ToF mass spectrum of a control experiment to estimate the MW of free PNIPAAm under similar conditions in absence of FhuA MI. The MW of polymer chains from both (A and B) appears to be around 5000 Da. C) SEC chromatogram of FhuA ΔCVF^{tev}–PNIPAAm conjugate before and after 6 times centrifugation to remove free polymer chains. The purification was continued till the signal from free PNIPAAm was reduced to zero.*

The BBTPs, because of very high molecular weight, could only be visualized by continuous gradient gel electrophoresis (4-15 %). The increased size due to the attachment of uncharged polymer chains hampers their movement into the gel, creating a distinct band characteristic of protein-polymer conjugates. This band was difficult to visualize using coomassie staining (Figure 7.8A), but silver staining (Figure 7.8B) clearly shows a non-distinct band starting from around the size of unmodified FhuA (approximately 79 kDa for FhuA WT and around 64 kDa for FhuA ΔCVF^{tev}, FhuA ΔCVF^{tev}K$_8^{mid}$ and FhuA ΔCVF^{tev}K$_{11}^{up}$) and extending up to much higher molecular weights. One possible explanation of more efficient staining by silver nitrate might be the fact that silver staining is more sensitive than coomassie staining, hence affording efficient staining even at lower protein concentrations. Additionally, silver nitrate has been known to stain just the boundary of the protein band, unlike the coomassie staining. These characteristic bands for the protein-polymer conjugates[117, 222] proved that the polymer chains were covalently linked to FhuA (Figure 7.8B). It is worth noting that in addition to the extended band for conjugates, no unmodified protein is visible in any variant, meaning that the efficiency of initiation and polymerization is high. The smear seen at higher molecular weight is most likely FhuA-PNIPAAm with largest

polymer chain length, which sticks in the stacking gel and cannot smoothly migrate through the running gel (hence occurring at around the same position for all variants).

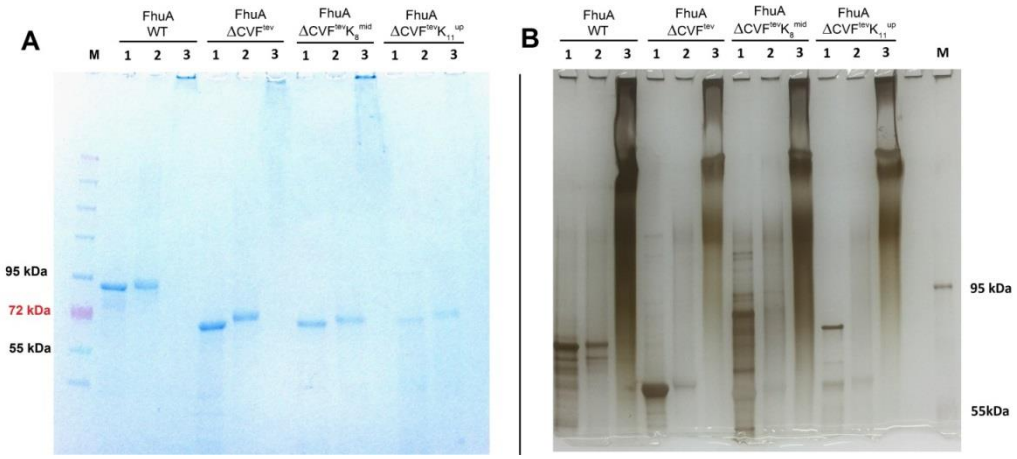

Figure 7.8: *SDS-PAGE of FhuA WT and three FhuA variants: 1) FhuA, 2) FhuA MI and 3) FhuA-PNIPAAm by A) coomassie and B) silver staining. The apparent molecular weight of the FhuA macroinitiators (MI) is slightly higher than unmodified FhuA, indicating attachment of several initiator units. The characteristic extended bands for the conjugates prove covalent attachment of polymer chains to FhuA. Silver staining was much more efficient at visualizing the BBTP, while coomassie was better for unmodified FhuA and FhuA MI.*

Analytical ultracentrifugation (AUC) is a sensitive technique used to analyze the sedimentation coefficient of nanoparticles, based on their rate of sedimentation under high centrifugal forces. The sedimentation coefficient of the particles can be used to distinguish between nanoparticles of different molar masses. The sedimentation coefficient s relates with the molecular weight by the function of $M^{2/3}$.[223] Unmodified FhuA ΔCVF^{tev} has an already rather broad distribution of the sedimentation coefficient because of different amounts of the stabilizing agent around the hydrophobic region (Figure 7.9). The sedimentation coefficient of FhuA ΔCVF^{tev}-PNIPAAm is shifted to higher values and has a much broader distribution as expected for a conjugate. This is in good agreement with the broad bands of the BBTPs observed in the SDS-PAGE compared to the unmodified

protein. AUC raw data were analyzed with a fitting procedure resulting in non-diffusion-corrected distributions (g(s)). The increase in the sedimentation coefficient as well as the broader distribution indicates the successful formation of the BBTP with FhuA with covalently attached polymer chains. Compared to the evidence by SDS-PAGE, the analysis by AUC was provided under non-denaturing conditions.

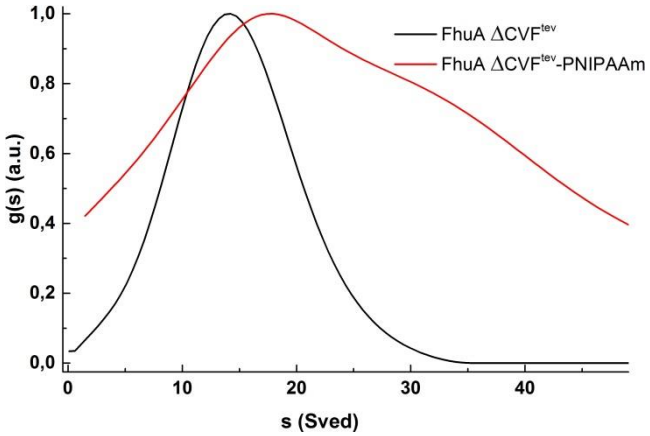

Figure 7.9: *Sedimentation coefficients of unmodified FhuA ΔCVF^{tev} (black) and FhuA ΔCVF^{tev}-PNIPAAm (red) analyzed by AUC. The increase in the sedimentation coefficient and the broader distribution indicate an increase in molecular weight as a result of the attachment of polymer chains on FhuA ΔCVF^{tev}.*

The thermo-responsivity of PNIPAAm additionally allowed us to track the size of the FhuA conjugates as a function of temperature by DLS. Above the LCST, PNIPAAm chains become hydrophobic and aggregate with other BBTP molecules, leading to an apparent increase in the size. This change is reversible and serves as an additional verification of successful polymerization and generation of BBTPs (Figure 7.10A). In addition to analyzing the formation of FhuA conjugates with SDS-PAGE, AUC and DLS, the folding of the transmembrane proteins in the BBTP was investigated by CD spectroscopy. CD spectroscopy is very sensitive to the presence of free PNIPAAm chains as PNIPAAm is highly absorbing in the UV and far UV region. Removal of all free PNIPAAm was critical to obtain spectra in the UV region. The obtained CD spectra follow the normal contour of a characteristic β-barrel protein having a single minimum around 215 nm, thus indicating that FhuA is correctly folded in

the formed conjugates (Figure 7.11).

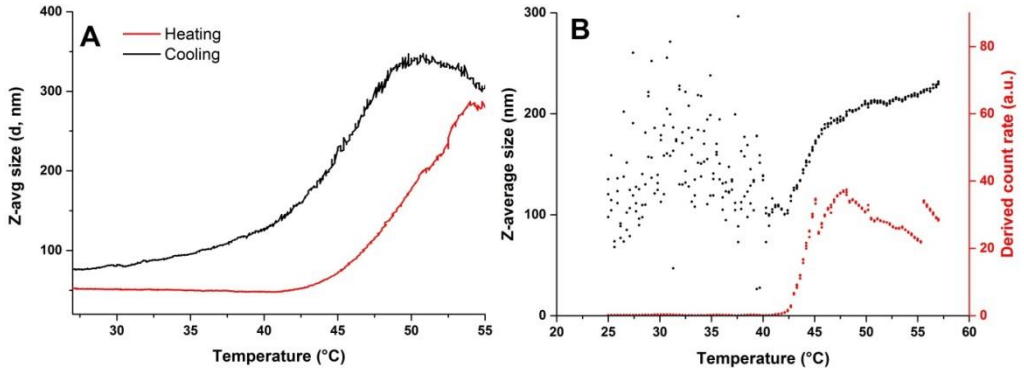

Figure 7.10: *Temperature-responsivity of FhuA ΔCVF^{tev}-PNIPAAm A). The size increases upon heating beyond the lower critical solution temperature of attached PNIPAAm chains, because the polymer chains get water insoluble and aggregate. B) Thermo-responsive behavior of free PNIPAAm in the presence of MPD buffer.*

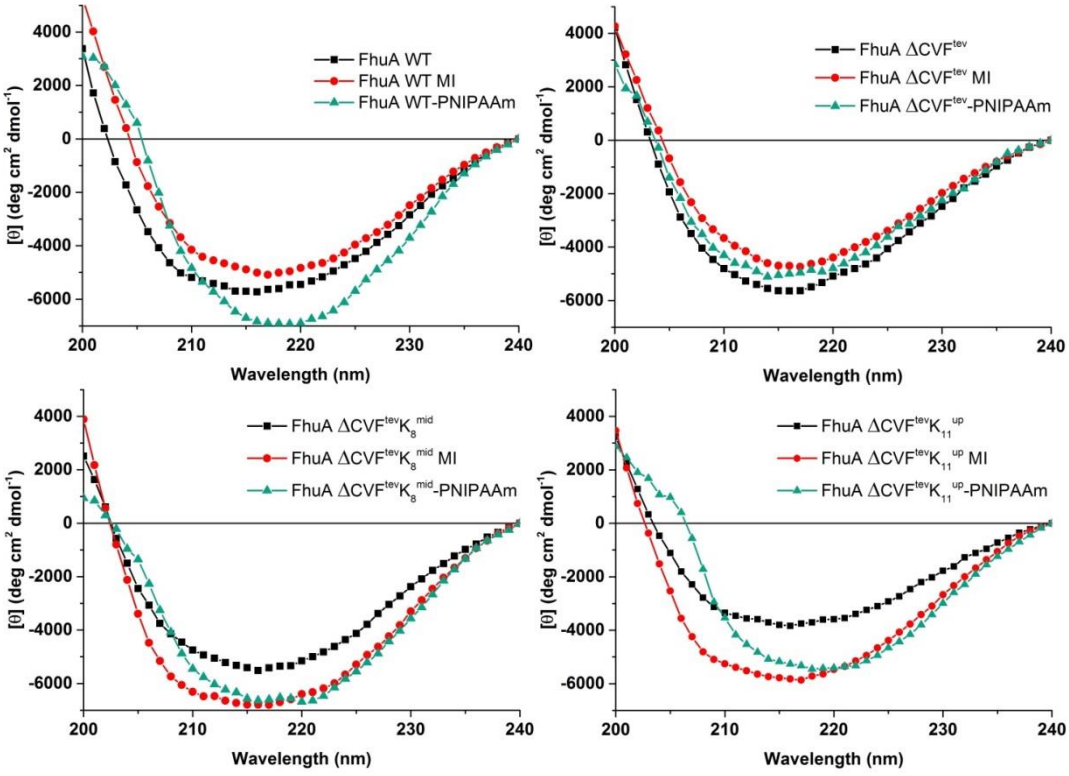

Figure 7.11: *CD spectra of unmodified FhuA, FhuA MI and FhuA-PNIPAAm of all the variants. All samples show a spectrum characteristic for β-barrel proteins, indicating that the formation of the MIs and the process of polymerization do not have a detrimental effect on the structure of the protein.*

Hence, the BBTP could be synthesized without influencing the secondary structure of the transmembrane proteins. In addition to the mentioned characterization of the conjugates, they were also analyzed by transmission electron microscopy (TEM). Their TEM images, in comparison with those of unmodified FhuA, indicate a change in the morphology due to the modification (Figure 7.12). It is challenging to visualize proteins in general and membrane proteins in particular with transmission electron microscopy (TEM). Usually, an appropriate stain is required to generate a clear contrast. To the best of my knowledge, only two references show TEM images of negatively stained FhuA WT after extraction.[224, 225] FhuA ΔCVF^{tev} and FhuA ΔCVF^{tev}-PNIPAAm after removal of free polymer chains were investigated by TEM using negative staining with uranyl acetate (Figure 7.12). Since FhuA is not stained by uranyl acetate, it appears as the white particles in the images. FhuA-PNIPAAm appears larger than FhuA and aggregated in chain-like structures, probably as a result of drying. Nonetheless, the increased size of the protein species can most likely be attributed to the attached polymer chains. The TEM images suggest a change in the morphology because of the modification.

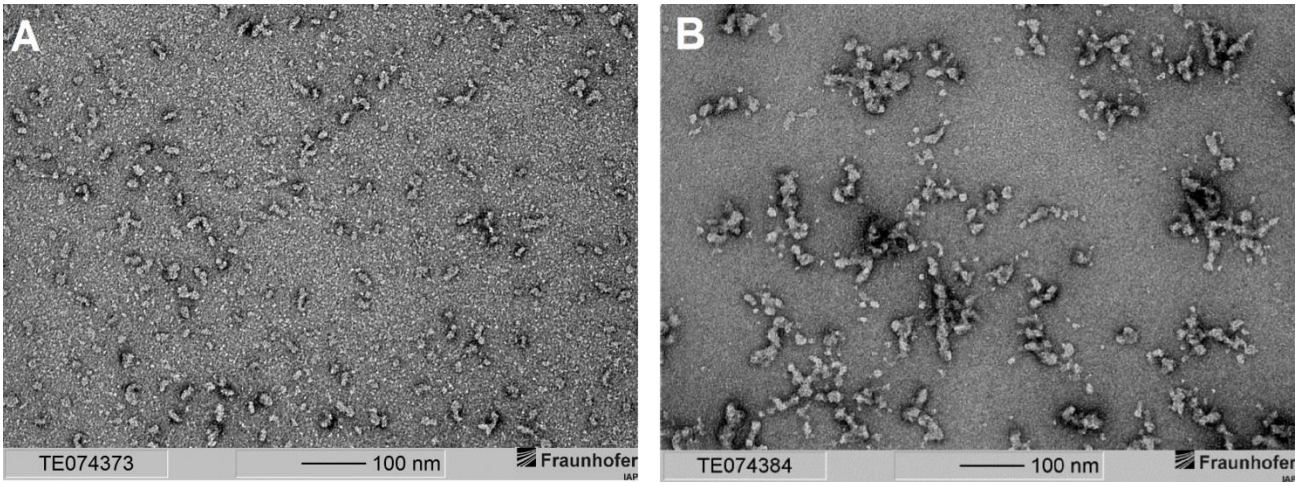

Figure 7.12: *TEM images of A) unmodified FhuA ΔCVF^{tev} and B) FhuA ΔCVF^{tev}-PNIPAAm. The larger FhuA-PNIPAAm chain-like structures indicate a successful growth by the attachment of polymer chains.*

7.6.2. Conjugates with PNIPAAm-PDMMIBA and PDMAEMA

In addition to BBTP with PNIPAAm, more BBTP were synthesized with UV-crosslinkable conomer DMMIBA for applications shown in **chapter 9** and **chapter 10**; namely FhuA ΔCVF^{tev}-PNIPAAm-PDMMIBA and FhuA ΔCVF^{tev}K$_{11}^{up}$-PNIPAAm-PDMMIBA. DMMIBA was used as the random co-monomer, so as to afford crosslinking ability to the resultant BBTP. Based on optimization experiments in **Section 6.3,** 5 mol % DMMIBA and 95 mol % PNIPAAm was used for the generation of crosslinkable polymer chains. The faded bands in the higher MW range of SDS-PAGE profile showed that the conjugates were successfully generated (Figure 7.13).

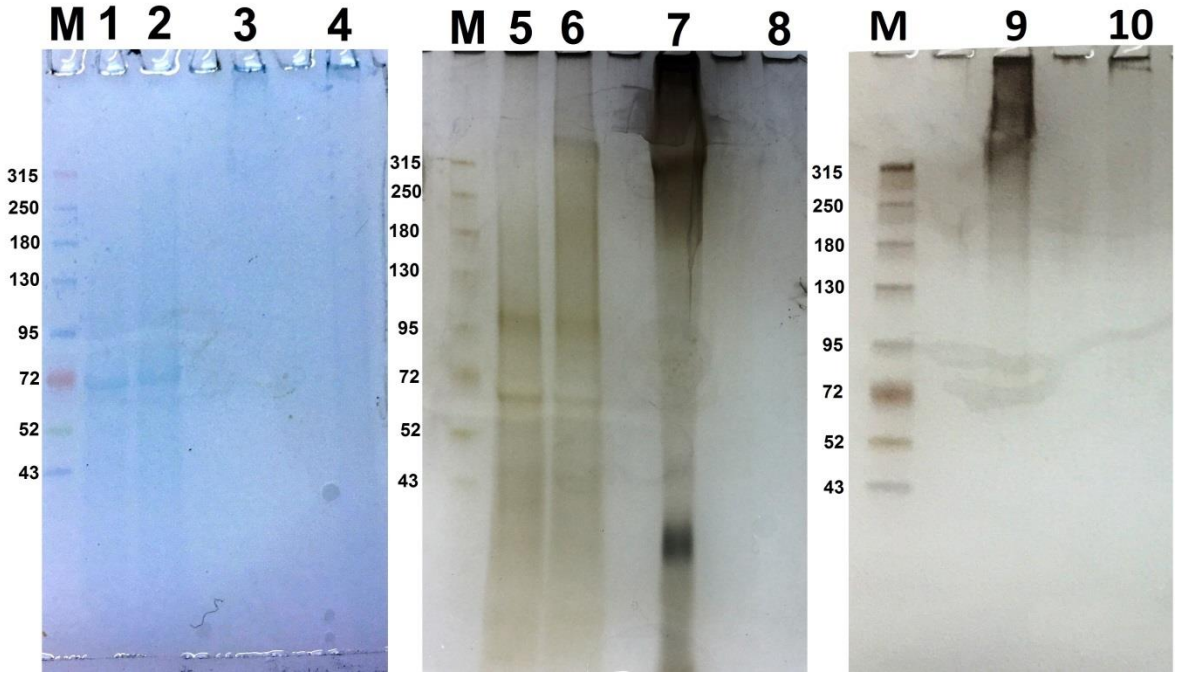

Figure 7.13: *SDS-PAGE of the conjugates with PNIPAAm and PDMAEMA. M: protein marker; Lane 1, 5: unmodified FhuA ΔCVF^{tev}; Lane 2, 6: FhuA ΔCVF^{tev} MI; Lane 3, 7: FhuA ΔCVF^{tev}-PNIPAAm; Lane 4, 8: FhuA ΔCVF^{tev}-PDMAEMA; Lane 9: FhuA ΔCVF^{tev}K$_{11}^{up}$-PNIPAAm-PDMMIBA; Lane 10: FhuA ΔCVF^{tev}-PNIPAAm-PDMMIBA. The faded bands at the top of the stacking gel (lane 3, 4 and 7) prove that conjugates were successfully generated.*

Additionally, BBTP were also synthesized with PDMAEMA, a dual stimuli-responsive polymer. BBTP with PDMAEMA showed responsivity to temperature as well as pH (**Chapter 9**). This responsivity was also shown to affect the macroscopic behavior of the self-assembled systems generated using these BBTP (**Chapter 9**). SDS-PAGE profiles of the BBTP also show the characteristic faded bands in the upper, high MW range (Figure 7.13).

CD spectroscopy was used to monitor the stability of the secondary structure of the protein during the synthesis of the BBTP. Both PNIPAAm and PDMAEMA absorb in the far-UV region, and hence it was not possible to obtain data in the far-UV region. Nonetheless, the spectra show the characteristic single minima of FhuA ΔCVF^{tev} around 215 nm. Hence, two more BBTP with various polymers were generated (Figure 7.14).

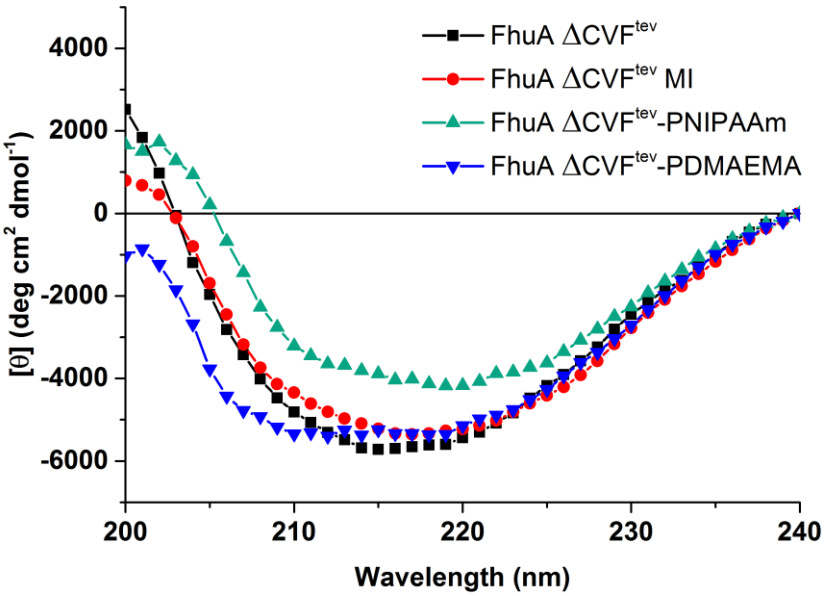

Figure 7.14: *CD spectra of FhuA ΔCVF^{tev}, its MI and conjugates. The data show that the secondary structure remains stable during the course of polymerization.*

7.7. Summary

In this chapter, the successful generation of various BBTP was demonstrated. Four different variants and three different polymers were used to generate these

BBTP. To the best of my knowledge, this is the first report on grafting a polymer from a transmembrane protein. The four genetic variants were – naturally occuring FhuA WT, the open channel FhuA ΔCVF^{tev} and two FhuA variants (FhuA ΔCVF^{tev}K$_8^{mid}$ and FhuA ΔCVF^{tev}K$_{11}^{up}$) which were genetically reengineered to be more efficient in CRP at defined sites. Small amphiphatic compound MPD was chosen to keep FhuA and the variants soluble and correctly folded in aqueous environment as well as avoid interference with characterization techniques such as AUC and TEM. The grafting-from positions of lysines within FhuA variants were chosen to be solely outside of the β-barrel and in a plane perpendicular to the axis of the channel in the variants FhuA ΔCVF^{tev}K$_8^{mid}$ and FhuA ΔCVF^{tev}K$_{11}^{up}$. The latter minimizes the risk of polymerizations within the ß-barrel pore. Notably, the lysines are positioned entirely above the hydrophobic region so that their functionalization does not disturb the stabilizing agent, MPD. More importantly, this arrangement of lysines minimizes the steric hindrance by the stabilizing agent to the linkage of initiator units or the addition of monomer units.

FhuA macroinitiators were formed by reacting the protein and the variants with a water-soluble functional CRP initiator. The conjugates were generated by grafting-from polymerization based on Cu-mediated CRP conditions, with the catalyst system CuBr/Me$_6$TREN which can be classified as SARA ATRP or SET-LRP. The polymers grafted were PNIPAAm, PDMAEMA and a random copolymer of NIPAAm and DMMIBA, a UV-crosslinkable monomer. CD spectroscopy validated that the secondary structure was not influenced during both the reaction steps for any of the conjugates.

The study presented in this chapter engendered the building blocks for the stimuli-responsive and ultra-thin macrostructures prepared in **Chapter 9** and **Chapter 10**. These BBTP could have many potential applications in the healthcare, bio-catalysis and separation industries.

8 Conjugates of enzymes

The idea for the project and the enzymes used for the study shown in this chapter came from our collaboration partners, Dr. Changzhu Wu and Zhiyong Sun at the Technische Universität Dresden.

8.1. Introduction

Despite a lot of potential for using enzymes in organic synthesis, bio-catalysis struggles with the stability of enzymes (see **Section 4.5** for more detailed explanation). Immobilization and conjugation with synthetic polymers often improve pH and temperature resistance of the enzymes, and sometimes augment their reaction specificity,[130-133] hence making them more efficient and more usable for applications in organic synthesis. Recently, Huang *et al.* reported the synthesis of conjugates of three enzymes, glucose amylase, glucose oxidase (GOx) and horseradish peroxidase (HRP) with PNIPAAm. These conjugates were used for the generation of micro-compartments by self-assembly at oil-water interface and consecutive crosslinking to generate a stable system.[179] After replacement of the oil phase with a continuous water phase inside and outside the micro-compartments, they could be used for cascade reactions, although with reduced rate of reaction. The authors attributed the limited accessibility of the active center after crosslinking as one of the primary causes of this reduction in reaction rate. One possible way to eliminate such problems could be to use a non-crosslinked system. Pickering emulsions generated by industrially relevant enzymes could be used for catalyzing the reactions at the interface of polar-apolar media. To test this notion, three enzymes with potential/current industrial relevance, namely *Candida antarctica* lipase B (CalB),[226] benzaldehyde lyase (BAL)[227] and GOx[228] were employed for generation of conjugates with PNIPAAm, and Pickering emulsions generated from them. Using conjugates of the enzymes, instead of the unmodified enzymes provide two benefits: 1) The surface activity of a conjugate is known to be significantly higher than that of the unmodified protein (in this case enzyme),[105, 181] and 2) attaching polymer chains to enzymes can have stabilizing effect on the enzyme (see **Section 4.2.2**). In this chapter, I report the synthesis and characterization of the enzyme macroinitiators and

enzyme-PNIPAAm conjugates.[Ψ] The optimized conditions of **Chapter 6** were also used for the generation of macroinitiators from enzymes and then, the polymerizations were carried out in PBS pH 7.4. Analysis was carried out using MALDI ToF MS and SDS-PAGE.

8.2. Preparation and characterization

8.2.1. Materials

All chemicals used were of analytical reagent grade or higher quality, purchased from Applichem (Darmstadt, Germany), Alfa Aesar (Karlsruhe, Germany) or Sigma-Aldrich Chemie (Taufkirchen, Germany), if not stated otherwise. *N*-2-bromo-2-methylpropanoyl-β-alanine N'-oxysuccinimide ester (functional CRP initiator) was synthesized according to reference.[164] NIPAAm was purified by two successive recrystallizations from a mixture of *n*-hexane and benzene (4:1 v:v). CuBr was purified by stirring in acetic acid overnight. After filtration, it was washed successively with ethanol and diethylether and then dried in vacuum. The enzymes, CalB, BAL and GOx, were provided in the lyophilized form by our collaboration partners. Required amount of the enzyme was dissolved in PBS pH 7.4 and dialyzed one time (against PBS pH 7.4 using dialysis membrane with a MWCO of 12-14 kDa for 24 h) to obtain aqueous solution of the respective enzyme at a final concentration of 4-5 mg/ml. The concentration was measured using the BCA assay kit supplied by Thermo-Fischer scientific.

Formation of enzyme macroinitiator (Enzyme MI): pH of the respective enzyme solution was first increased from pH 7.4 to pH 9.0. To do that, two times dialysis was performed (against PBS pH 9.0 using dialysis membrane with a MWCO of 12-14 kDa for 24 h). Then, 25 equivalents of *N*-2-bromo-2-methylpropanoyl-*β*-alanine *N'*-oxysuccinimide ester per lysine residue of the respective enzyme was added to the enzyme solution at around 4 mg/ml. The reaction was allowed to proceed for 12 h on a shaking platform at 12 °C, 12 °C

[Ψ] *Experiments regarding emulsion generation and determination of enzyme activity were carried out by our collaboration partners.*

and 4 °C for CalB, GOx and BAL respectively. Afterwards, the solution was dialyzed twice (against PBS pH 7.4 using dialysis membrane with a MWCO of 12-14 kDa for 24 h) at RT, RT and 4 °C for CalB, GOx and BAL respectively and stored at 4 °C before being polymerized. The concentrations of the purified samples were estimated using BCA assay kit provided by Thermo-Fischer scientific.

Polymerization from enzyme MI: NIPAAm was added to the respective enzyme MI solution and deoxygenated by purging with nitrogen for 30 min while cooling it in an ice bath. Simultaneously, a solution of CuBr and Me_6TREN in 1 ml Millipore water was degassed likewise. The monomer/(macro)initiator solution was then transferred to the catalyst solution via cannula transfer. The typical final ratio of components for the reaction was initiator (enzyme MI) : monomer : CuBr : Me_6TREN = 1 : 200 : 13 : 19. The amount of monomer was varied (20, 50, 100 or 200 repeat units), keeping the catalyst concentration the same. The reaction was allowed to proceed for 12 h, initially at 0 °C and gradually rising to room temperature as the ice melted after about 2 h. The obtained products were purified first by two times dialysis (against MPD buffer using dialysis membrane with a MWCO of 12-14 kDa for 24 h) at RT, RT and 4 °C for CalB, GOx and BAL respectively. Finally, the sample was collected and stored at 4 °C until further characterization. The concentration of the purified sample was estimated using BCA assay kit provided by Thermo-Fischer scientific.

8.2.2. Characterization techniques

MALDI-ToF mass spectrometry: Spectra were acquired using a 337 nm laser Bruker microflex MALDI-ToF mass spectrometer (Bruker, Bremen, Germany) with pulsed ion extraction. The masses were determined in positive ion linear mode. The masses were determined in positive ion linear mode. The sample solutions were applied on a ground steel target using the dried droplet technique. ZipTipC4 pipette tips (Millipore, Darmstadt, Germany) were used. Super-DHB, a 9:1 mixture of 2,5 dihydroxybenzoic acid (DHB) and 2-hydroxy-5-methoxybenzoic acid, was used as matrix substance in a

50 mg/ml solution in Millipore water:acetonitrile 1:1 with 0.1 % trifluoroacetic acid. Mass calibration was performed with external calibration.

SDS-PAGE: Enzymes and conjugates were analyzed on a 4-15 % gradient polyacrylamide gel (90 V, ca. 2.5 h, Mini-PROTEAN® Electrophoresis System-Bio-Rad, München, Germany). Samples were prepared by denaturing the protein using 2-mercaptoethanol at 65 °C for 3 min. Then, 8 µl of each sample was loaded onto the gel. Silver and/or coomassie staining were used to resolve the gel. The staining protocols are described in **Section 6.2.2** in detail.

8.3. Conjugates of *Candida antarctica* lipase B

Candida antarctica lipase B (CalB), is a monomeric enzyme naturally found in the yeast *Candida antarctica*. It has been used for preparation of amides, chemoselective, regioselective and stereoselective syntheses, kinetic resolution of amines and desymmetrization of prochiral glutarates.[226] Consecutively, it has found many applications as a catalyst in generation of optically active compounds like alcohols and amines.[226] It has a molecular weight of 33 kDa[226] and consists of 19 lysine groups per protein (Figure 8.1). A Pickering emulsion stabilized by CalB might be used for catalyzing reactions in both, the organic as well as the water phase.

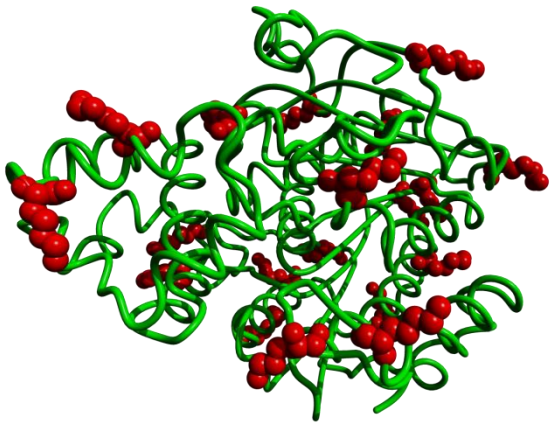

Figure 8.1: *The crystal structure of CalB (PDB ID: 3VEO). The lysine residues are shown in red. CalB has 19 lysine residues per enzyme.*

As shown in Scheme 8.1, first, the approach was to attach a CRP initiator to the lysine residues generating CalB macroinitiator (MI) and then the polymer grafted from the MI via grafting-from polymerization. The conditions for making the MI were similar to those used for BSA and FhuA. MALDI-ToF mass spectra revealed very limited modification (Figure 8.2). Consecutively, the SDS-PAGE of the conjugates synthesized from this batch of macroinitiator indicated minimal amount of generated conjugate (Figure 8.3). As evident, even though, a little bit of CalB-PNIPAAm conjugate could be seen in the SDS-PAGE (Figure 8.3), a lot of unreacted CalB or CalB MI was also visible.

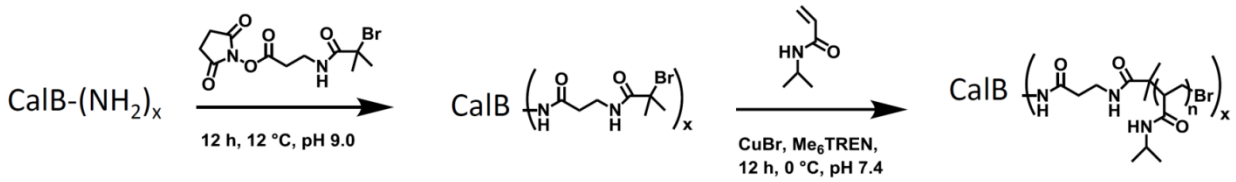

Scheme 8.1: *Scheme of modification of CalB using NHS coupling and grafting-from polymerization.*

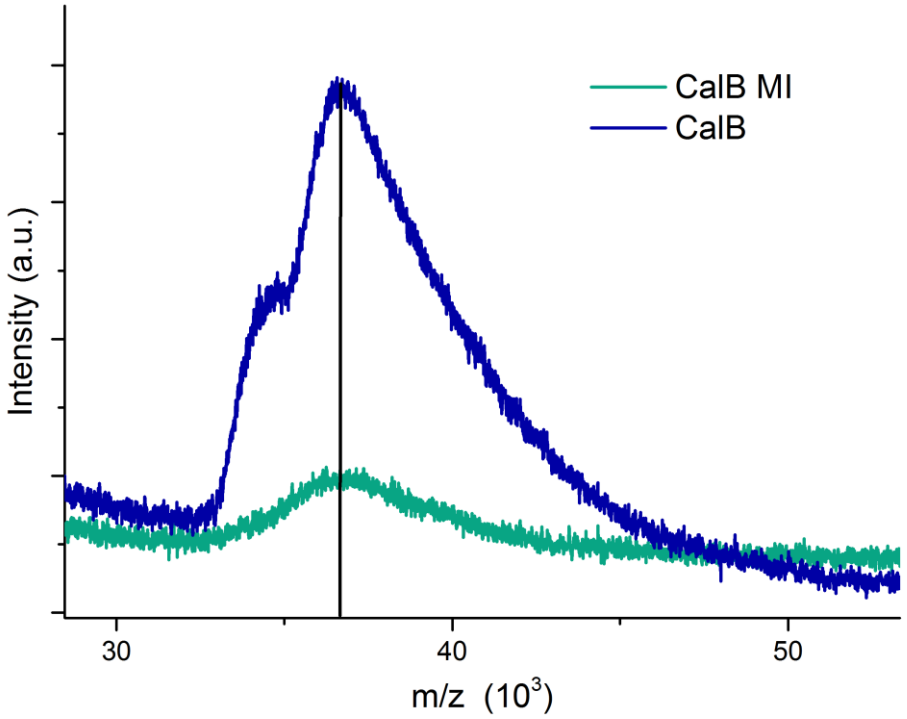

Figure 8.2: *MALDI-ToF mass spectra of CalB and CalB MI. The efficiency of modification was very low, indicating nearly no attachment of the initiator.*

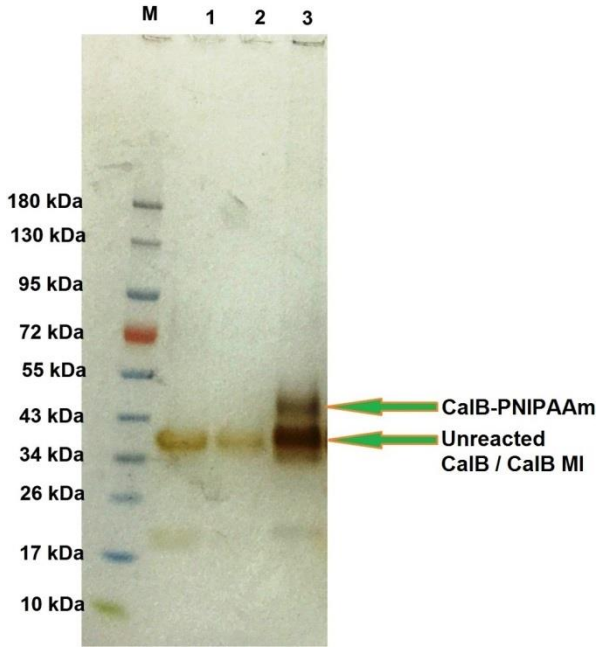

Figure 8.3: *SDS-PAGE of CalB, CalB MI and CalB-PNIPAAm conjugate with silver staining. Lane 1: CalB, lane 2: CalB MI, lane 3: CalB-PNIPAAm. Although a little bit of CalB-PNIPAAm can be seen in lane 3, the amount is much less as compared to the unreacted CalB or CalB MI.*

Since CalB is a lipase, one possible reason for the low macroinitiator formation could be the cleavage of the ester bond in the NHS ester of the functional CRP initiator before being linked to a lysine residue. This would in turn render it ineffective in modifying the enzyme, and no macroinitiator would be generated. When there is no macroinitiator, no conjugate can be generated. The macroinitiator formation was also attempted using the traditional EDC coupling[208] (Scheme 8.2) with the *in situ* generation of a water soluble NHS ester and its consequent reaction with the enzyme. The hope was that the *in situ* generated ester may have a higher reactivity towards the lysine residues as compared to the lysis by the enzyme. However, this also did not result in attachment of the initiator to the lysine residues of the enzyme, evidenced by nearly no increase in mass in the MALDI-ToF MS spectra in Figure 8.4. SDS-PAGE (data not shown) also agreed with this inference. Minimal amount of macroinitiator was visible in comparison to unreacted CalB. To solve this problem, instead of NHS coupling, another one of popular linking chemistries such as cysteine-maleimide coupling or diazonium coupling at the tyrosine

residues could be used.[45] However, since it does not fit to the primary aim of this thesis, this direction was not pursued.

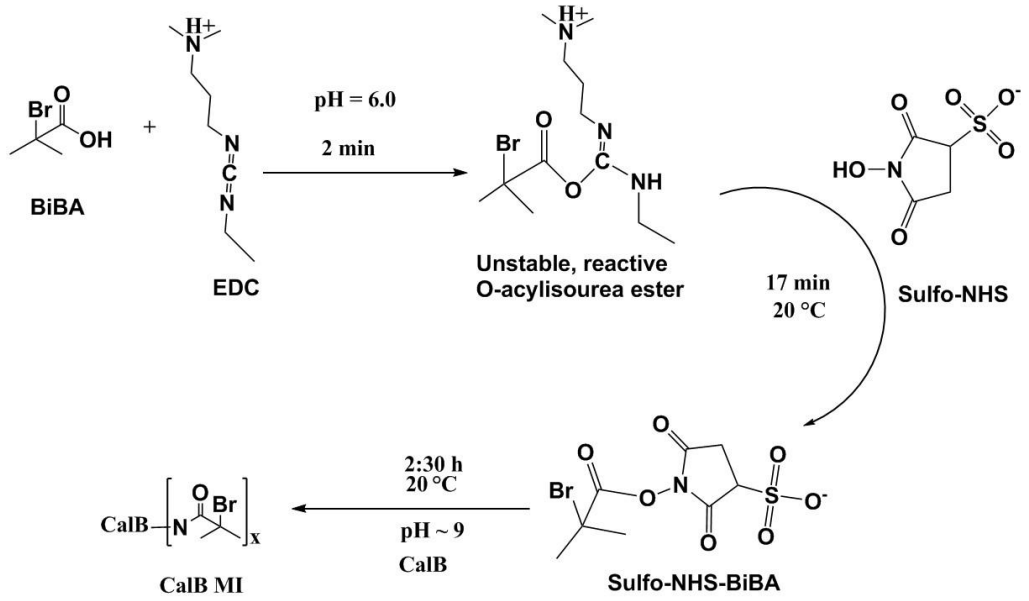

Scheme 8.2: *Synthesis of CalB MI by EDC coupling route with the in situ generation of initiator-NHS ester.*

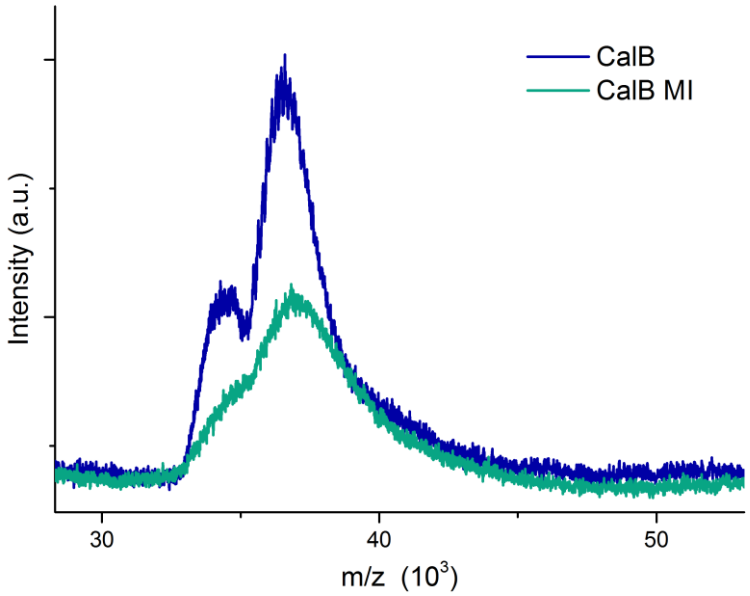

Figure 8.4: *MALDI-ToF mass spectra of CalB and CalB MI by EDC coupling route. The efficiency of modification was still very low, indicated by nearly no attachment of the initiator.*

8.4. Conjugates of benzaldehyde lyase

Benzaldehyde lyase (BAL) is a homotetrameric enzyme, with each subunit having a molecular weight of 58,919 Da.[227] It catalyzes the cleavage and formation of *R*-Benzoin.[227] Each subunit has 11 lysine residues (see Figure 8.5). Since the four subunits of the enzyme are only held together in association by non-covalent interactions, it is sensitive to vigorous reaction conditions, such as high temperature, pH and mechanical stress. Accordingly, care was taken to expose the enzyme to as little vigorous conditions as possible, during the whole modification procedure. Hence, the modification to make the macroinitiator, the polymerization reaction and the dialyses were conducted in the refrigerator at 4 °C. The buffers for dialyses were pre-cooled to 4 °C. Very mild stirring was used for modifications and the samples were always stored at 4 °C.

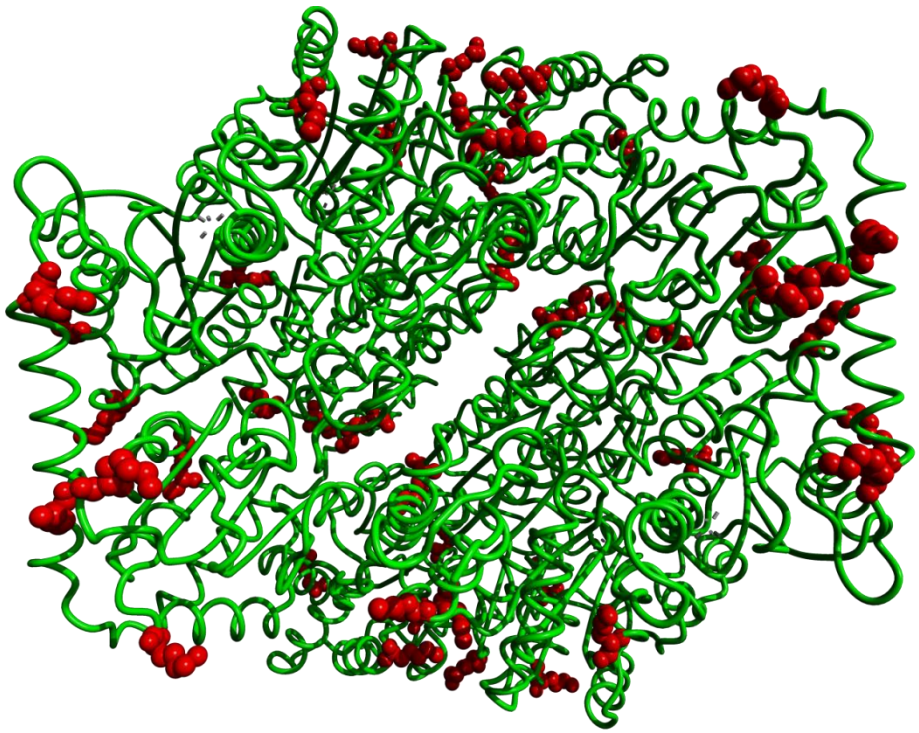

Figure 8.5: *The crystal structure of tetrameric BAL (PDB ID – 2ag0). The lysine residues are shown in red. Each subunit of the four has 11 lysine residues.*

The protocol shown in Scheme 8.3 was employed to first generate BAL MI and consecutively grafting-from polymerization carried out without the use of any sacrificial initiator.

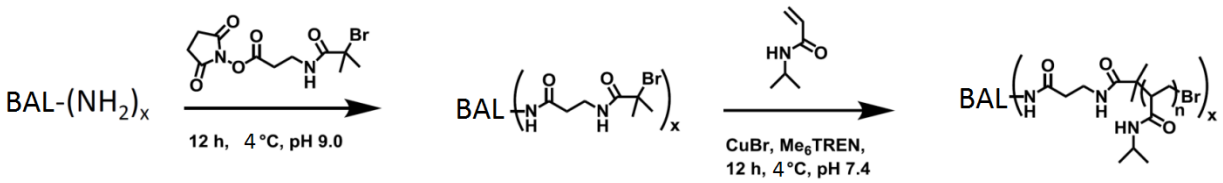

Scheme 8.3: *Scheme of modification of BAL using NHS coupling and grafting-from polymerization.*

MALDI-ToF MS spectra (Figure 8.6) show an increase of ca. 1800 Da in the mass of the BAL subunit upon conversion to macroinitiator. This mass divided by the mass of one initiator unit, 220 Da, indicates that out of a total of 11 lysines per subunit, nearly 8-9 lysines were modified with the initiator. Afterwards, the macroinitiator was used for the generation of conjugates with PNIPAAm using grafting-from CRP with CuBr and Me_6TREN as the catalyst system.

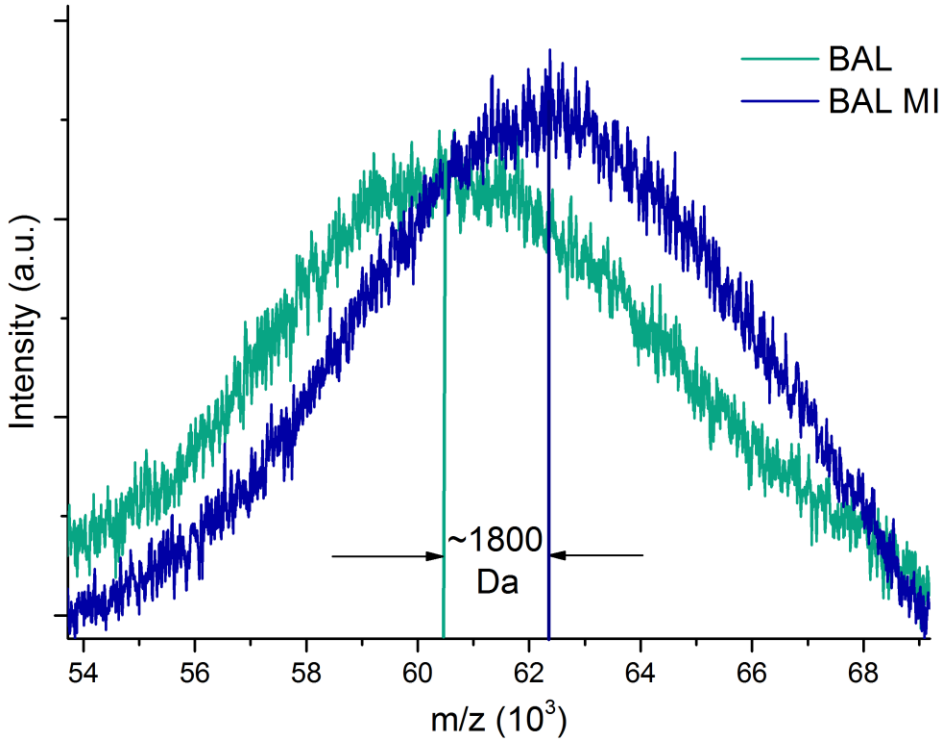

Figure 8.6: *MALDI-ToF mass spectra of BAL and BAL MI. The efficiency of modification was high indicated by nearly 8-9 initiator units attached to each subunit.*

The conditions optimized in Chapter 6 were employed to grow PNIPAAm chains from the enzyme. SDS-PAGE profile (Figure 8.7) shows that the BAL, and consecutively BAL MI, was with small amounts of contaminant proteins (seen as bands with larger MW in lane 1/4 and 2/5). Furthermore, the faded band (lane 3) proved that the polymer chains were indeed covalently linked to the protein.

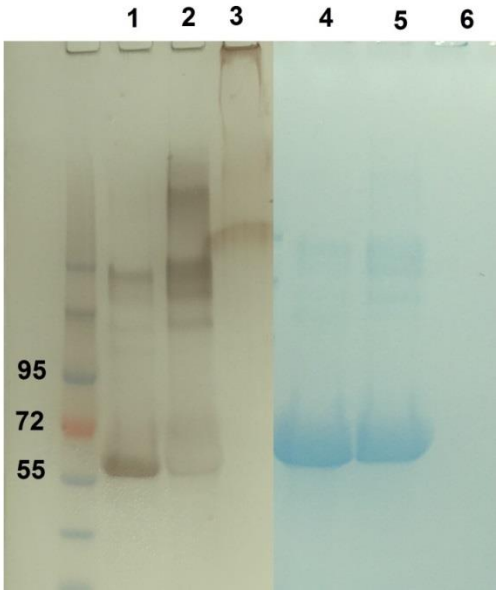

Figure 8.7: SDS-PAGE of BAL (lane 1/4), BAL MI (lane 2/5) and BAL-PNIPAAM (lane 3/6) conjugates with silver (left) and coomassie (right) staining. Lane 3 clearly shows the formation of BAL-PNIPAAm conjugates.

Conjugates with varying polymer chain lengths were also synthesized. With expected degree of polymerization (DP) of 50, 100 and 200, conjugates were generated and characterized. The faded band of the conjugates in SDS-PAGE profiles (Figure 8.8) of BAL-PNIPAAm conjugates with a DP of 200 (lane 7) was in the higher MW region of the gel. While it was not possible to quantify the change of MW based on the faded bands, it does prove that at higher DP (200), the conjugates have lower electrophoretic mobility than at lower DP (50 or 100). This observation may be attributed to the increased resistance to the conjugate as a result of longer polymer chains attached to the enzyme.

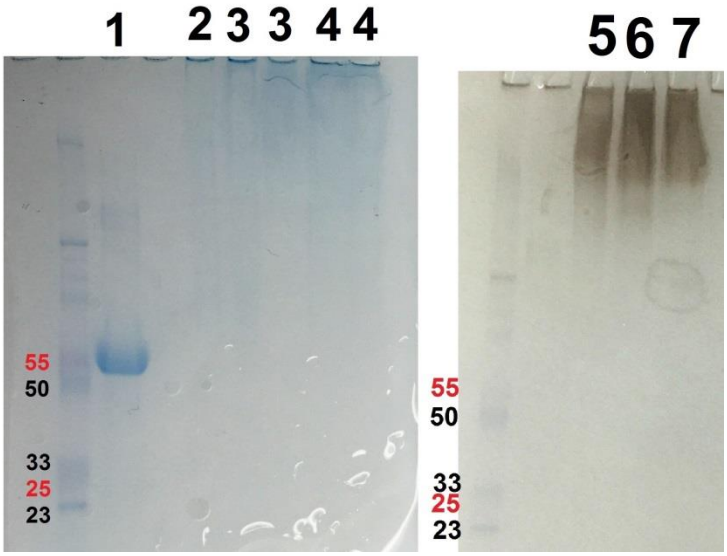

Figure 8.8: *Comparison of BAL-PNIPAAm with different degree of polymerizations (DP) with silver (left) and coomassie (right) staining. Lane 1: BAL MI; lane 2/5: BAL-PNIPAAm, DP 50; lane 3, 6: BAL-PNIPAAm, DP 100; lane 4, 7: BAL-PNIPAAm, DP 200.*

8.5. Conjugates of glucose oxidase

Glucose oxidase (GOx) is a dimeric enzyme which is produced naturally in some fungi and insects where its catalytic product, hydrogen peroxide, acts as an anti-bacterial and anti-fungal agent.[228] GOx catalyzes the oxidation of beta-D-glucose to D-gluconolactone and hydrogen peroxide. Each subunit, having a molecular weight of 77 kDa (PDB ID – 3qvr), contains 15 lysine residues (Figure 8.9). Of the three enzymes being discussed here, GOx has found most industrial applications ranging from an additive in food processing and oxygen scavenger in food preservation on one hand to glucose sensor/assay and in gluconic acid production.[228] Assembling GOx at the interface of oil-water might be an interesting proposition to assess its catalyzing skills in organic as well as aqueous media.

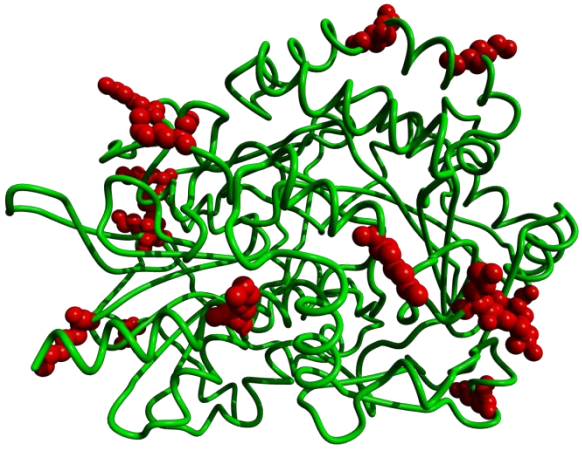

Figure 8.9: *Crystal structure of one subunit of glucose oxidase (PDB ID – 3qvr). The lysine residues are shown in red. Each subunit contains 15 lysine residues.*

GOx was reacted with a functional CRP initiator to give GOx MI, as shown in Scheme 8.4. The optimized reaction conditions from Chapter 6 were used. Consecutively, grafting-from CRP was carried out from GOx MI using CuBr and Me_6TREN as the catalyst system in PBS pH 7.4 to give GOx-PNIPAAm conjugates.

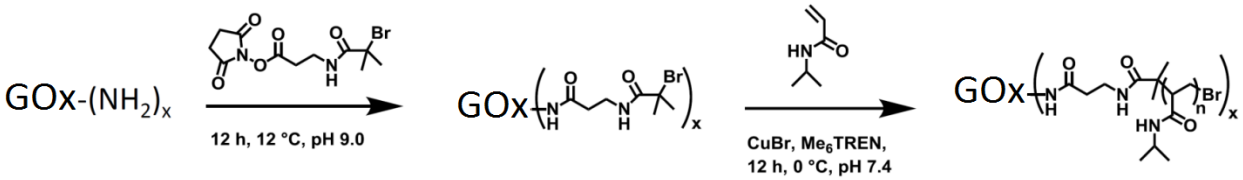

Scheme 8.4: *Scheme of modification of GOx using NHS coupling and grafting-from polymerization.*

Comparison of MALDI-ToF mass spectra of subunits of GOx and GOx MI show that the modification was successful (Figure 8.10). A molecular weight difference of ca. 1600 Da indicates that nearly 7-8 lysines out of 15 were modified with the CRP initiator. Hence, the number of solvent accessible and modifiable lysines on GOx may be estimated to be 7-8.

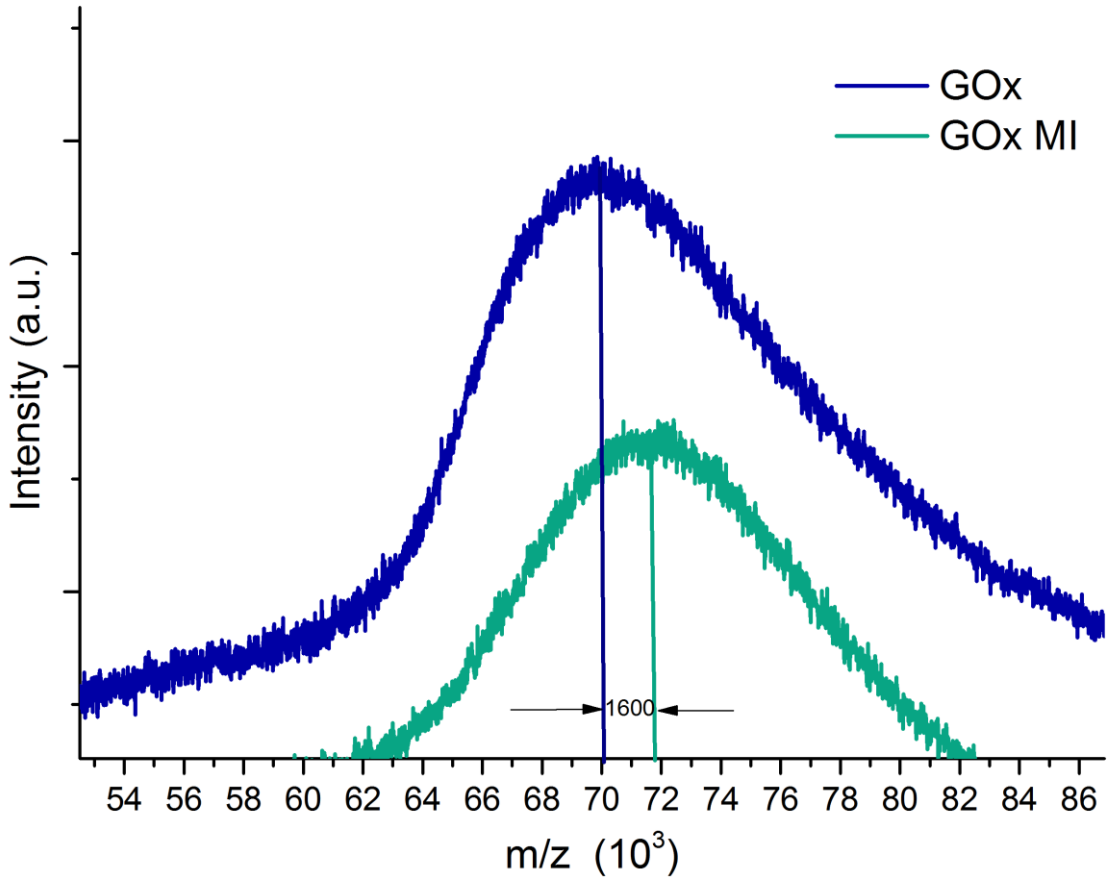

Figure 8.10: *MALDI-ToF mass spectra of GOx and GOx MI. The efficiency of modification was high indicated by nearly 7-8 initiator units attached to each subunit.*

GOx-PNIPAAm conjugates were synthesized with different degrees of polymerization (DP) – 20, 50, 100, 200. SDS-PAGE profiles (Figure 8.11) prove that for DP of 20, although conjugates were generated (faded band at higher MW), the conjugation was not complete. There was unmodified GOx MI in the sample (lane 3/9) of conjugates. For DP 50 and above, there was no unreacted GOx MI visible. This indicated conversion of all the GOx MI to GOx-PNIPAAm. The profiles also indicate increasing MW range when going from DP of 50 to 100/200. Hence, increasing the monomer content showed an increase in MW of the resultant conjugate, as expected. However, this difference is not quantifiable. Perhaps, other analytical techniques such as AUC or field flow fractionation might be employed to better characterize and compare these conjugates.

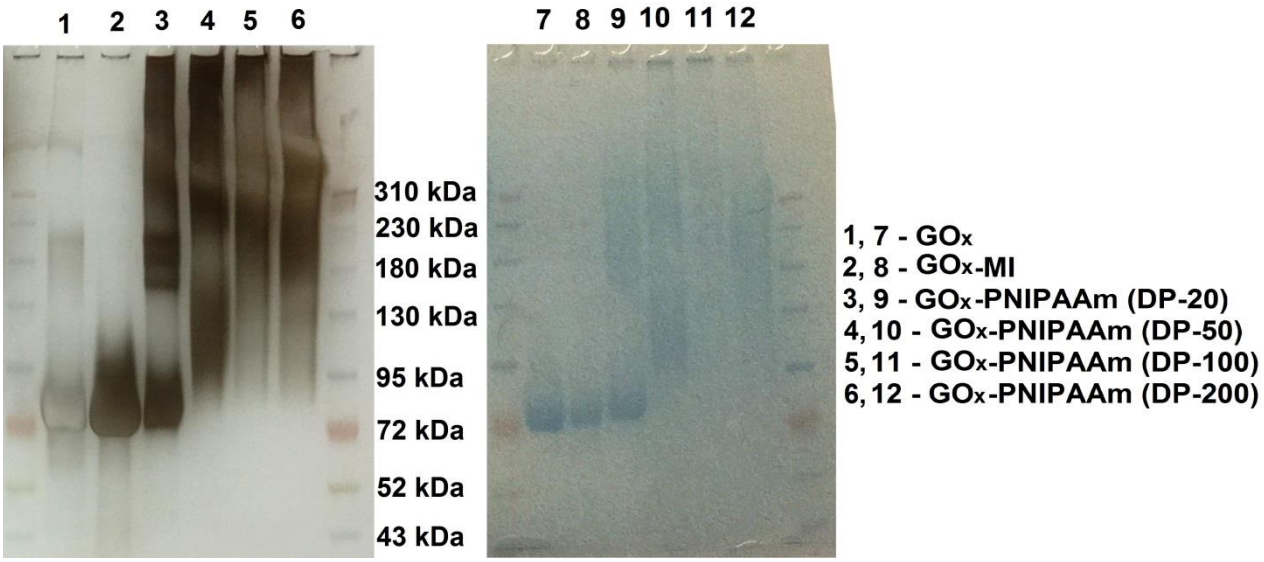

Figure 8.11: *SDS-PAGE of GOx, GOx MI and GOx-PNIPAAm with different degree of polymerizations analyzed by silver (left) and coomassie (right) staining. Lane 1, 7: GOx; lane 2, 8: GOx MI; lane 3, 9: GOx-PNIPAAm, DP 20; lane 4, 10: GOx-PNIPAAm, DP 50; lane 5, 11: GOx-PNIPAAm, DP 100; lane 6, 12: GOx-PNIPAAm, DP 200.*

8.6. Summary and outlook

In conclusion, conjugates of three enzymes with potential/current industrial relevance, namely *Candida antarctica* lipase B, benzaldehyde lyase and glucose oxidase with PNIPAAm were generated. The enzymes were first converted to macroinitiator (MI) by targeting their lysine residues with a functional CRP initiator. MI formation was proved by analyzing the MALDI-ToF MS spectra of unmodified enzyme and the enzyme MI. While CalB could not be modified using NHS chemistry, 8-9 lysine residues on BAL and 7-8 lysine residues on GOx were modified with the CRP initiator. CalB, being a lipase, probably inactivates the NHS ester by cleaving the ester bond and hence no initiator can be attached to the enzyme. Conjugates of BAL and GOx with PNIPAAm were successfully generated using copper-mediated CRP and analyzed using SDS-PAGE. These samples were then sent over to our collaboration partners for analyzing the post-modification activity of the enzymes, Pickering emulsion generation (similar to those reported in **Chapter 9** for FhuA) and further tests.

9 From nano-sized building blocks to micro-structures

9.1. Introduction

After successfully generating conjugates of FhuA or the building blocks based on transmembrane proteins (BBTP), described in **Chapter 7**, the next task was to understand the characteristics of these building blocks and generate higher order structures from them. This chapter focuses on the properties of the BBTP, specifically the conjugates of PDMAEMA, PNIPAAm and PNIPAAm/PDMMIBA with FhuA ΔCVF^{tev} (chosen as a model FhuA variant). Their temperature- and pH-responsivity as well as interfacial activity were investigated. Consecutively, because of high interfacial activity, formation of highly stable Pickering emulsions (from self-assembled BBTP) was demonstrated. Finally, the generation of stable micro-compartments as a result of crosslinked polymer chains was also shown.

9.2. Preparation and characterization

9.2.1. Materials

All chemicals were of analytical grade or higher and obtained from Sigma Aldrich, unless otherwise stated. Conjugates were synthesized as detailed in **Chapter 7**.

9.2.2. Emulsion formation

1 ml of the respective conjugate solution was taken at a concentration of 1.4 mg/ml and 100 µl of trifluorotoluene (with 0.1 mg/ml Nile red) was added to it. Then it was shaken with hand for 1 min to generate the emulsion. For making the hollow capsules, FhuA ΔCVF^{tev}-PNIPAAm-PDMMIBA was used to create emulsion as mentioned above

and then exposed to UV (Panacol UV-F 400F, 450 W) at RT for 30 min. For checking their stability, 50 % to 90 % ethanol (final concentration) was added to the emulsion.

9.2.3. Characterization techniques

UV Visible spectroscopy: UV-Vis measurements were performed for a 125 µl sample at 1 mg/ml on an Agilent Cary 5000 device equipped with a Varian Peltier-controlled temperature stage. The absorbance was measured at 600 nm, while varying the temperature at the rate of 1 °C/min. An average of 30 values was taken as the final value for absorption as well as temperature. For performing the pH dependent measurements, respective solution was dialyzed against buffer of desired pH and the measurement carried out as explained above. For pH 6 MES buffer, for pH 7/8 PBS buffer and for pH 8.5/9 Tris buffer at 10 mM concentration were used. The absorption of 2 and above was tapped at 2 and normalized from (0, 1).

Pendant drop tensiometry: Tensiometry measurements were performed on a Dataphysics OCA 15 EC device equipped with a CCD video camera having a resolution of 752 x 582 pixels. Interfacial tension was estimated by fitting Young Laplace equation to the image of the droplet in inverted view. The droplet was of respective protein solution or buffer and the ambient phase was perfluorodecalin. Dynamic tracking was used to collect data every two seconds for a droplet of volume 10 µl and the resulting value of interfacial tension plotted against time.

Fluorescence microscopy: The measurements were performed on a Leica DMi8 device using a RHOD filter (Excitation wavelength range 541 nm to 551 nm, cutoff wavelength 560 nm and emission wavelength range 565 nm to 605 nm). 20 µl of respective sample was dropped on a clean glass slide and directly measured. 40 µl ethanol was added to estimate the effect of ethanol on the stability of the capsules.

Cryo-SEM: The measurements were performed on a Jeol 6330F instrument, operating at 5 kV and 12 µA of current. Samples were frozen with liquid nitrogen and sublimated

3 min at -75 °C to expose the sample structure. Samples were sputtered with platinum (4 nm) to avoid charges and immediately measured.

Scanning force microscopy: The measurements were performed on a Bruker Dimension FastScan instrument (Bruker, Bremen, Germany). Silicon tip on a Silicon Nitride cantilever [Fastscan-A probe with a force constant of 18 N/m (f_0 = 1400 kHz)] were used for tapping mode measurements in air at a scan rate of 0.506 Hz and 512 samples/line. Emulsions were first washed with ample Millipore water (by adding the water, then shaking and allowing the emulsion to settle down and finally decanting the top; repeated 3 times) to remove the salts and unreacted conjugate and then 20 µl of the crosslinked emulsion droplets put on ethanol-cleaned silicon wafer and allowed to dry overnight before the measurement.

9.3. Behavior of the BBTP

9.3.1. Thermo- and pH-responsivity of the BBTP

FhuA ΔCVF^{tev}-PNIPAAm and FhuA ΔCVF^{tev}-PDMAEMA were analyzed for their thermo-responsivity by monitoring the absorbance of visible light at 600 nm while varying the temperature from 26 °C to 90 °C (Figure 9.1). The wavelength of 600 nm was chosen owing to the absence of any specific absorption at this wavelength as well as its frequent use in literature.[229-231] BBTP with PNIPAAm showed a sharp lower critical solution temperature (LCST) around 33 °C, similar to PNIPAAm as well as for protein-PNIPAAm conjugates.[116] Since PDMAEMA shows responsivity to pH as well as temperature,[103] the BBTP with PDMAEMA were additionally tested at different pH to also check the effect of pH on the thermo-responsive behavior of the BBTP. The BBTP with PDMAEMA at pH 6 and pH 7 showed no thermo-responsive behavior. However, at pH 8, a cloud point of 84 °C was recorded (estimated by the intersection point of the two tangents as reported in literature[103]). Relatively small change in the pH from pH 8 to pH 8.5 resulted in a drastic shift in the cloud point to 57 °C. Similarly, a substantially lower, and more abrupt, transition was observed for pH 9.0 at 34 °C. These findings can

be attributed to the deprotonation of the amine groups under alkaline conditions and correspond to the experimental behavior observed for PDMAEMA alone.[103] These data for the BBTP with PNIPAAm and BBTP with PDMAEMA understandably imply that the thermo- and pH-responsive behavior of the BBTP are strongly influenced by the properties of the polymer. However, above 65 °C, the cloud point might also be significantly affected by the possibly irreversible changes to the secondary structure of FhuA due to its limited stability in that temperature regime.[232, 233]

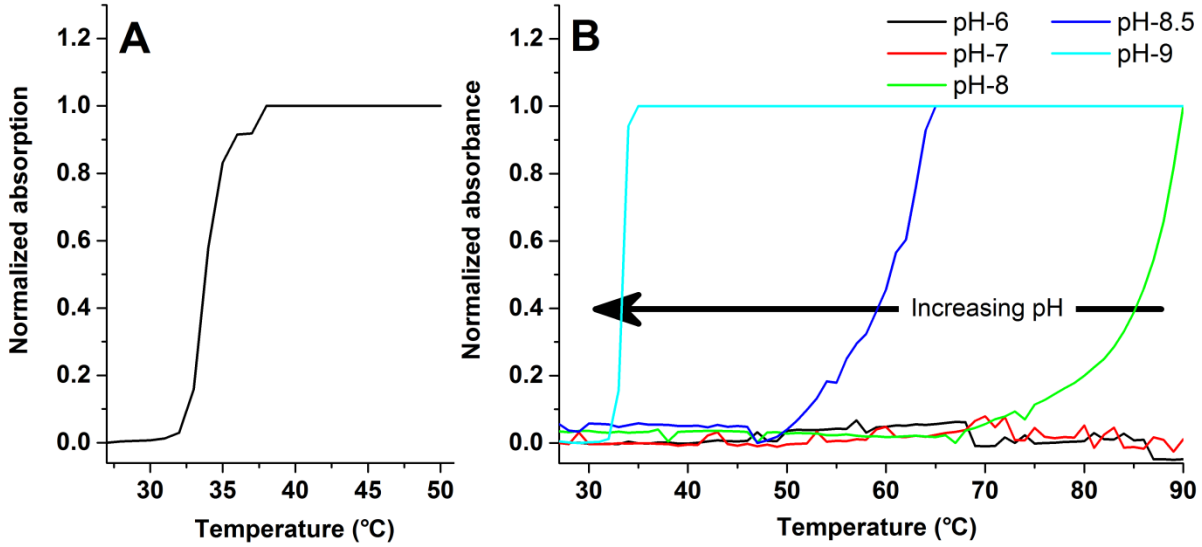

Figure 9.1: *Absorption of the BBTP at 600 nm measured by temperature-dependent UV-Vis spectroscopy. FhuA ΔCVF^{tev}-PNIPAAm (A) showing a LCST of around 33 °C and FhuA ΔCVF^{tev}-PDMAEMA (B) showing a decrease in the LCST upon increase in the pH of the solution. Arrow is added as a guide to show the trend.*

9.3.2. Interfacial activity of the BBTP

Pendant drop tensiometry, considered to be amongst the simplest, yet the most robust techniques to measure interfacial tension has been employed for accessing the interfacial activity of various biomacromolecules.[234] Dynamic interfacial tension experiments were carried out with unmodified FhuA ΔCVF^{tev}, FhuA ΔCVF^{tev}-PNIPAAm and FhuA ΔCVF^{tev}-PDMAEMA conjugates in order to understand the dynamics of stabilization of oil-water interface by the unmodified protein as well as BBTP. Perfluorodecalin (PFD) was kept as the ambient oil phase owing to its chemical and

biological resistance and much higher density as compared to water. As shown in the reference,[181] a high stabilization behavior by protein-polymer conjugates was also observed for semi-fluorinated, aromatic as well as linear hydrocarbon oil phase. MPD buffer by itself showed a little interfacial activity (Figure 9.2A). This was expected in light of the fact that MPD is a small amphipathic diol, whose primary purpose is to stabilize the transmembrane hydrophobic region of FhuA ΔCVF^{tev}. Unmodified FhuA ΔCVF^{tev} showed substantially higher interfacial activity than MPD buffer (Figure 9.2A). Within 2000 seconds, in the presence of the unmodified protein ($c = 5 \cdot 10^{-3}$ mg/ml), the interfacial tension dropped to 27 mN/m. At higher concentrations, the reduction in the interfacial tension was too fast; resulting in the fall of the droplet within a few seconds and the measurement could not be continued. Interestingly, the interfacial activity of FhuA ΔCVF^{tev} is substantially higher than for previously studied globular proteins like ferritin, ß-casein, lysozyme and hydrophobin under respective concentration of the protein.[181, 235-238] Owing to its inherent amphiphilicity as a result of being a transmembrane protein, the higher tendency of FhuA ΔCVF^{tev} to go to the water-oil interface, in comparison to the soluble globular proteins, was the anticipated behavior. However, it is interesting that the dynamics are even faster than for an amphiphilic protein like hydrophobin, which is well-known for its interfacial activity.[235, 236, 239]

The interfacial tension measurements of BBTP with PNIPAAm showed faster dynamics of interfacial stabilization as compared to the unmodified FhuA ΔCVF^{tev} (Figure 9.2B). Although, the final value of the interfacial tension was nearly the same for BBTP as well as the unmodified FhuA ΔCVF^{tev} (~27 mN/m), the dynamics of stabilization are certainly much faster with BBTP. For instance, at a concentration of $5 \cdot 10^{-3}$ mg/ml, the time required to reach the stable value of 27 mN/m was 260 seconds for FhuA ΔCVF^{tev}-PNIPAAm as compared to 2000 seconds of unmodified FhuA ΔCVF^{tev} at the same concentration and pH.

BBTP of FhuA ΔCVF^{tev}-PDMAEMA showed even faster interfacial stabilization than the unmodified FhuA ΔCVF^{tev} as well as FhuA ΔCVF^{tev}-PNIPAAm (Figure 9.2C). For instance, at a concentration of $5 \cdot 10^{-3}$ mg/ml, the stable value of ~27 mN/m was reached already within 200 seconds for FhuA ΔCVF^{tev}-PDMAEMA as compared to

nearly 2000 seconds for unmodified FhuA ΔCVF^{tev} and 260 seconds for FhuA ΔCVF^{tev}-PNIPAAm at the same concentration. That is nearly 10 times faster as compared to unmodified FhuA ΔCVF^{tev} and 1.3 times faster than FhuA ΔCVF^{tev}-PNIPAAm. Additionally, it was possible to go down to $1 \cdot 10^{-6}$ mg/ml, and still the BBTP were substantially more interfacially active than the MPD buffer.

Since, PDMAEMA also shows pH-responsivity, BBTP with PDMAEMA were additionally tested at pH 10 (Figure 9.2D) in order to check the effects of pH on the interfacial activity of the BBTP. Remarkably, the dynamics of the interfacial stabilization were sped up substantially. For instance, at the concentration of $5 \cdot 10^{-3}$ mg/ml, the droplet was stabilized to the value of 27 mN/m within 65 seconds at pH 10, as compared to 200 seconds at pH 7.4. That is, the speed of interfacial stabilization is increased by more than two times of its initial value. This result is important as it gives us an *in situ* handle to tune the interfacial activity, the solubility of the BBTP as well as the final structures generated from the BBTP, simply by changing the pH of the water phase. This drastic change can be attributed to the well documented hydrophobicity of PDMAEMA chains as a result of complete deprotonation at higher pH.[103, 240] Hence, at pH 10, the PDMAEMA chains of the BBTP are hydrophobic and as a result, BBTP show a higher tendency to stabilize the oil/water interface as compared to pH 7.4. Interestingly, the MPD buffer also showed slight interfacial activity at elevated pH.

These results show that the attached polymer chains make the BBTP more interfacially active by at least one order of magnitude vis-à-vis the unmodified transmembrane protein. Free polymers like PNIPAAm have already been shown to be interfacially active and conjugates even more so.[181] It was not surprising to observe that the choice of polymer influences the interfacial behavior of the resulting conjugates.

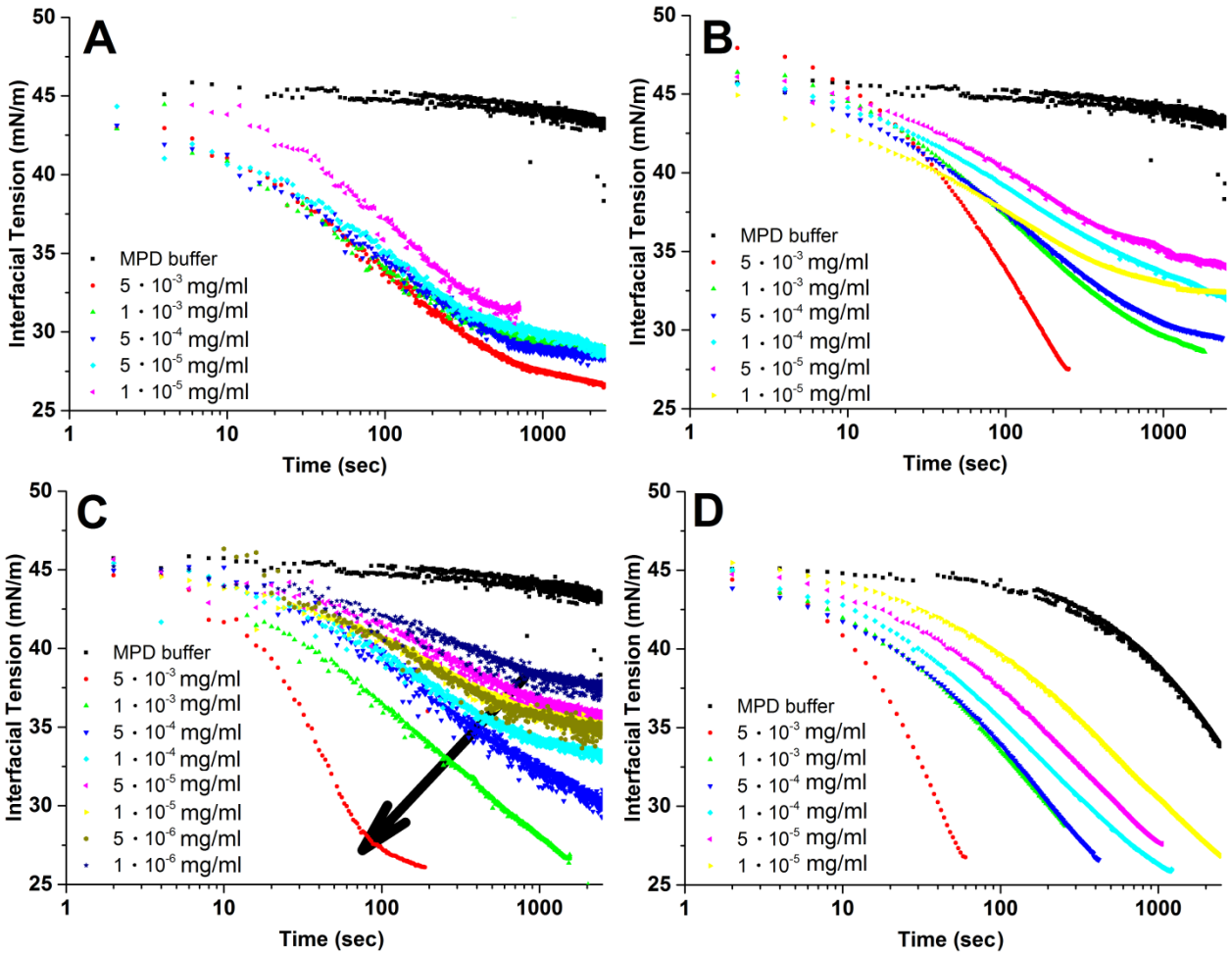

Figure 9.2: *Interfacial tension with respect to time for A) unmodified FhuA ΔCVF^{tev}, B) FhuA ΔCVF^{tev}-PNIPAAm, C) FhuA ΔCVF^{tev}-PDMAEMA at pH 7.4 and D) FhuA ΔCVF^{tev}-PDMAEMA at pH 10. All the conjugates show faster interfacial stabilization as compared to unmodified FhuA ΔCVF^{tev}.*

9.4. Emulsions and micro-compartments

Pickering emulsions stabilized by BBTP were generated by adding Nile red dissolved in PFD to the respective BBTP solution and shaking with hand for a minute. The resulting oil in water (o/w) emulsions were consecutively characterized. Owing to their fast interfacial dynamics, it was expected that the conjugates would be able to stabilize the oil/water interface, and hence rendering the resulting emulsions more stable. That was indeed the case as the emulsions stabilized from FhuA ΔCVF^{tev}-PDMAEMA displayed

exceptional long-term stability (Figure 9.4A). Immediately after formation of the emulsion, there was a distribution of large and small droplets (Figure 9.4B). Under the effect of gravity, the larger droplets settled after a day, resulting in a more uniform emulsion, which stayed stable for well over 40 days (Figure 9.4C).

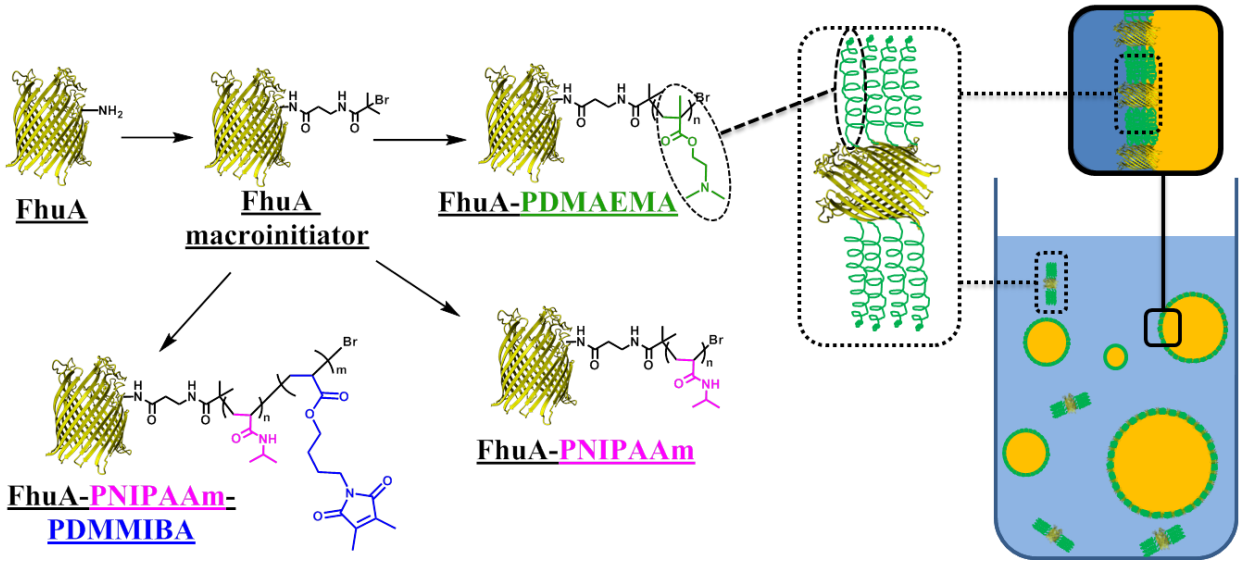

Figure 9.3: *Scheme of various BBTP of FhuA ΔCVF^{tev} used in this chapter. The generated BBTP were utilized for stabilization of Pickering emulsions, owing to their high interfacial activity.*

In **section 7.6**, it was demonstrated by circular dichroism (CD) spectroscopy that the secondary structure of the protein remains intact under the used polymerization conditions. Unfortunately, CD spectroscopy wasn't suitable for estimating the stability of FhuA at oil-water interface due to excessive scattering by the larger emulsion droplets (data not shown). However, being a transmembrane protein, FhuA embedded in its natural lipid bilayer environment is always at the interface of hydrophilic and hydrophobic environments. Moreover, it has been previously reported that site-specific attachment of polymer chains to a protein may improve its stability.[241-243] In light of all these arguments, it can be expected that the structure of FhuA remains stable at the oil/water interface. Furthermore, owing to this intrinsically well-defined hydrophobic/hydrophilic structure of FhuA, the orientation of conjugates shown in Figure 9.3 is the most likely one, whereby, the hydrophobic part of the protein is

expected to go into the apolar phase, while the hydrophilic barrel and loops remain in the water phase.

Emulsions stabilized by FhuA ΔCVF^{tev}-PNIPAAm conjugates were visibly less stable and larger in droplet size than those stabilized by FhuA ΔCVF^{tev}-PDMAEMA (Figure 9.4A and Figure 9.5). Cryo-SEM images (Figure 9.6) show the morphology of frozen emulsion droplets generated from both FhuA ΔCVF^{tev}-PDMAEMA and FhuA ΔCVF^{tev}-PNIPAAm. The hollow capsules seen in the Figure 9.6 were a result of breaking of a frozen droplet, allowing the measurement of the thickness of the stabilizing layer. The thickness of the BBTP layer stabilizing the emulsion was estimated by using ImageJ. This was roughly 18 nm for non-crosslinked FhuA ΔCVF^{tev}-PNIPAAm and roughly 38 nm for non-crosslinked FhuA ΔCVF^{tev}-PDMAEMA. It is also interesting to observe that these results are in tune with the results of interfacial activity, i.e. for same concentration of conjugate solutions used, the thickness of stabilizing layer was more for

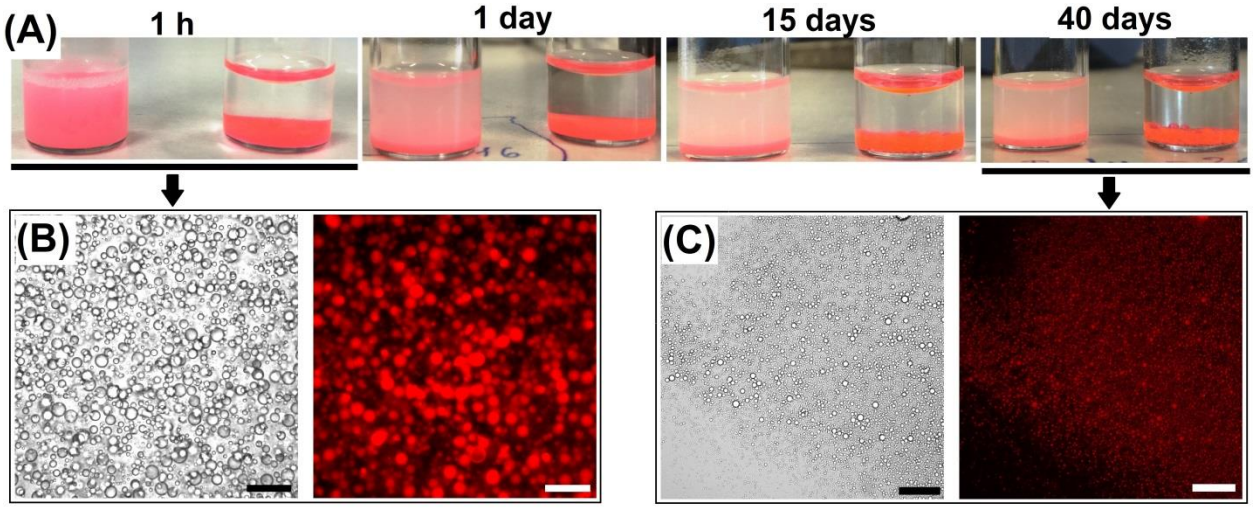

Figure 9.4: *A) Visual inspection of emulsions with Nile red in trifluorotoluene as the oil phase with FhuA ΔCVF^{tev}-PDMAEMA solution as the water phase (left) and MPD buffer as the water phase (right) after different times. B) and C) Bright field (left) and fluorescence (right) microscopy images of emulsions stabilized by FhuA ΔCVF^{tev}-PDMAEMA immediately after creation (B) and 40 days after creation (C). The bigger emulsion droplets settle down after a day as a result of being heavier, resulting in a rather more uniform (and smaller) droplet size (C). Scale bar for all images is 100 µm.*

emulsions stabilized by FhuA ΔCVF^{tev}-PDMAEMA. Likewise, the emulsions made from FhuA ΔCVF^{tev}-PDMAEMA were visibly more stable than those from FhuA ΔCVF^{tev}-PNIPAAm immediately upon creation (Figure 9.5), as well as in the long-term (Figure 9.4A). That means apparently innocuous differences in the dynamic interfacial activity have a direct and significant consequence on the properties of the resulting emulsions, such as their long-term stability. This also means that by reducing the concentration of FhuA ΔCVF^{tev}-PDMAEMA, we might get even thinner stabilizing layers of conjugates, all the while producing stable emulsions.

In order to generate capsules from the BBTP stabilized emulsion droplets, FhuA ΔCVF^{tev}-PNIPAAm conjugates synthesized with DMMIBA (**Section 7.7**), was used for the generation of a Pickering emulsion and exposed to UV for crosslinking the polymer chains, resulting in capsules with the oil phase inside. Figure 9.7A shows the scanning force microscopy image of a dried crosslinked micro-compartment, with the average height of the two collapsed membranes ca. 22 nm (Figure 9.7 and Figure 9.8). Each membrane was thus only 11 nm thick, which when compared to the length of the unmodified FhuA ΔCVF^{tev} barrel (ca. 7-8 nm) indicates that it was a monolayer. The value of 11 nm in the dried state fits well to the evaluated thickness of 18 nm from the cryo-SEM measurement which demonstrates the frozen swollen state. In any case, the measurements provided us a range of (14 ± 4) nm for the thickness of the membrane of BBTP with PNIPAAm, which was efficient enough to stabilize the emulsion droplets of

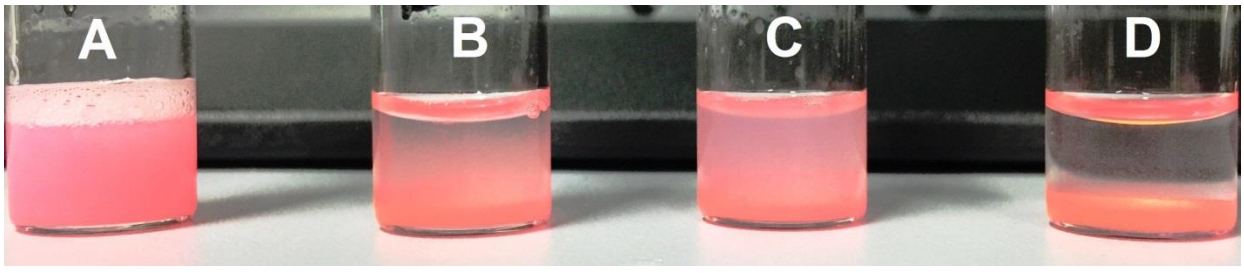

Figure 9.5: *Pickering emulsions stabilized by FhuA ΔCVF^{tev}-PDMAEMA (A 1.4 mg/ml, B 0.026 mg/ml) and FhuA ΔCVF^{tev}-PNIPAAm (C 1.4 mg/ml, D 0.026 mg/ml) immediately after shaking. FhuA ΔCVF^{tev}-PDMAEMA stabilized emulsions were visibly more stable than FhuA ΔCVF^{tev}-PNIPAAm stabilized emulsions.*

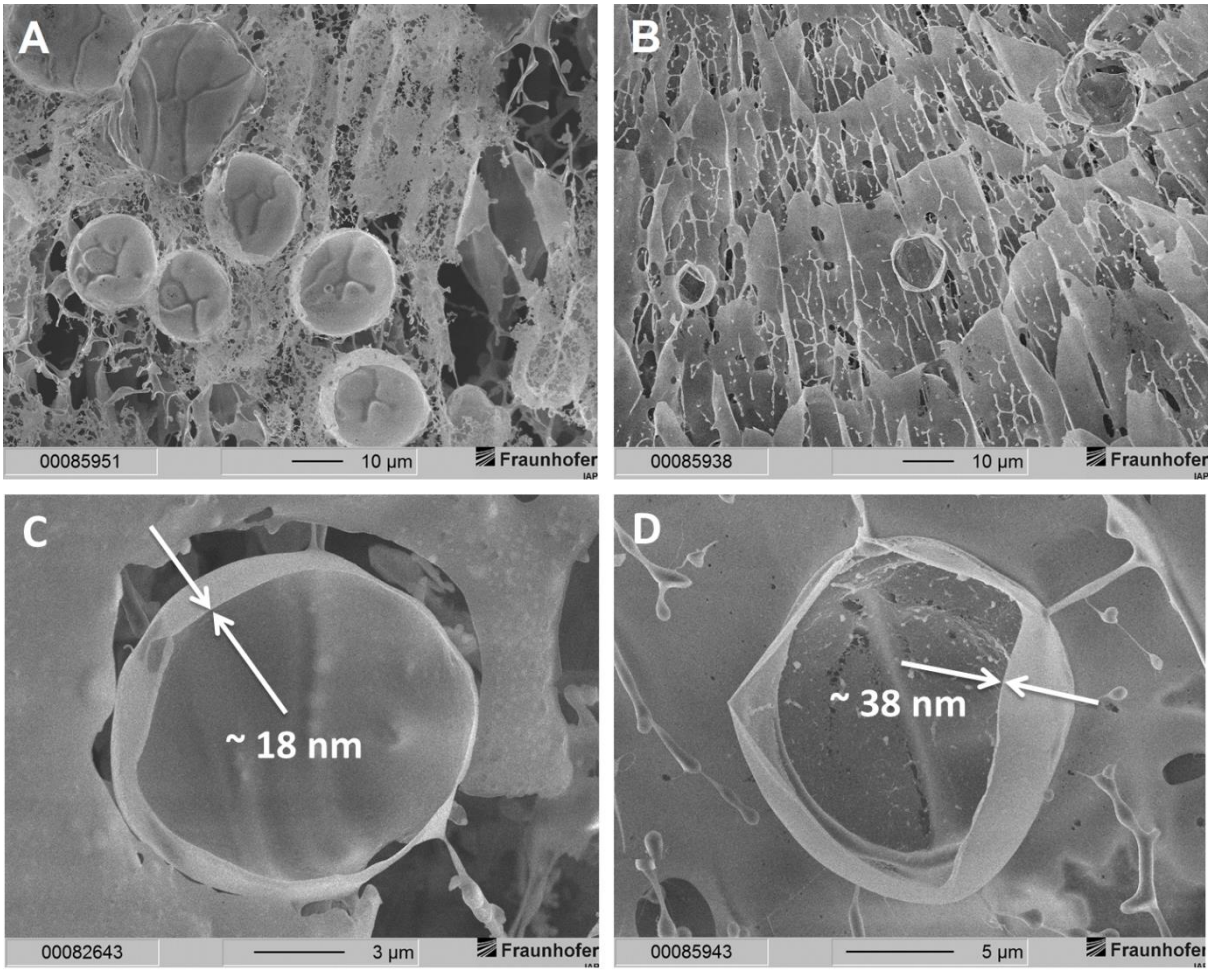

Figure 9.6: *Cryo-SEM images of FhuA ΔCVF^{tev}-PNIPAAm (A and C) and FhuA ΔCVF^{tev}-PDMAEMA (B and D) showing frozen Pickering emulsion droplets. The emulsions of FhuA ΔCVF^{tev}-PDMAEMA had a rough morphology as compared to FhuA ΔCVF^{tev}-PNIPAAm, which had more smooth and textured morphology. The thickness of broken capsule of emulsion stabilized by FhuA ΔCVF^{tev}-PNIPAAm (C) and FhuA ΔCVF^{tev}-PDMAEMA (D) was estimated to be around 18 nm and 38 nm, respectively.*

Micro-meter scale (5 to 90 µm in diameter), that is a droplet at least three orders of magnitude larger than itself. Upon addition of ethanol, the capsules swelled (but not disintegrated) and the oil phase (with Nile Red) leeched out, evidenced by the reduction in fluorescence of Nile red (Figure 9.7C). This behavior has previously been reported.[117] Also, by visual inspection (Figure 9.9), it was clear that the emulsion without crosslinking (no UV exposure) was destroyed to give a clear solution upon addition of ethanol, while

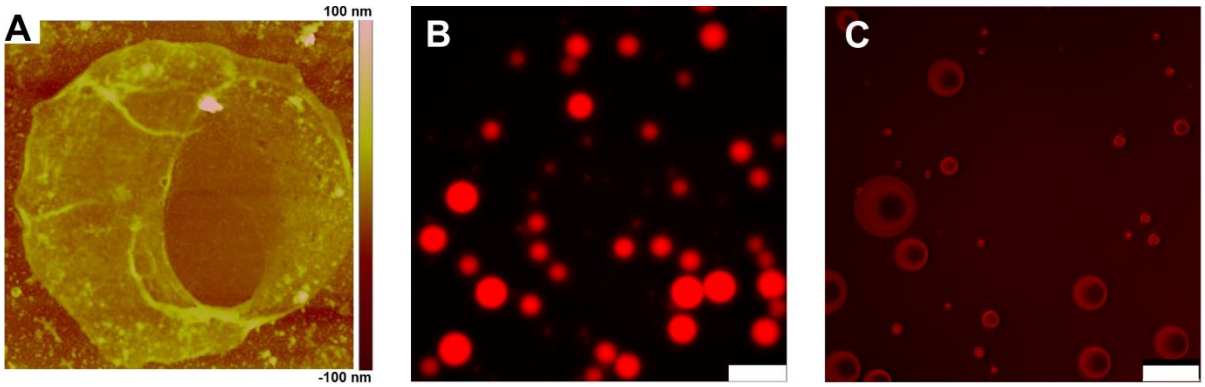

Figure 9.7: *A) Scanning force microscopy image of a dried micro-compartment. The thickness of the dried membrane is ca. 11 nm, indicating a monolayer stabilized system. Area of the image is 11 µm by 11 µm. B) Fluorescence microscopy images of Pickering emulsions with Nile red in trifluorotoluene as the oil phase stabilized by FhuA ΔCVF^{tev}-PNIPAAm. C) Upon adding ethanol, the crosslinked capsules of FhuA ΔCVF^{tev}-PNIPAAm-PDMMIBA swell, and the intensity of Nile red decreases, but they are not destroyed, indicating successful crosslinking by UV irradiation. Scale bar is 100 µm*

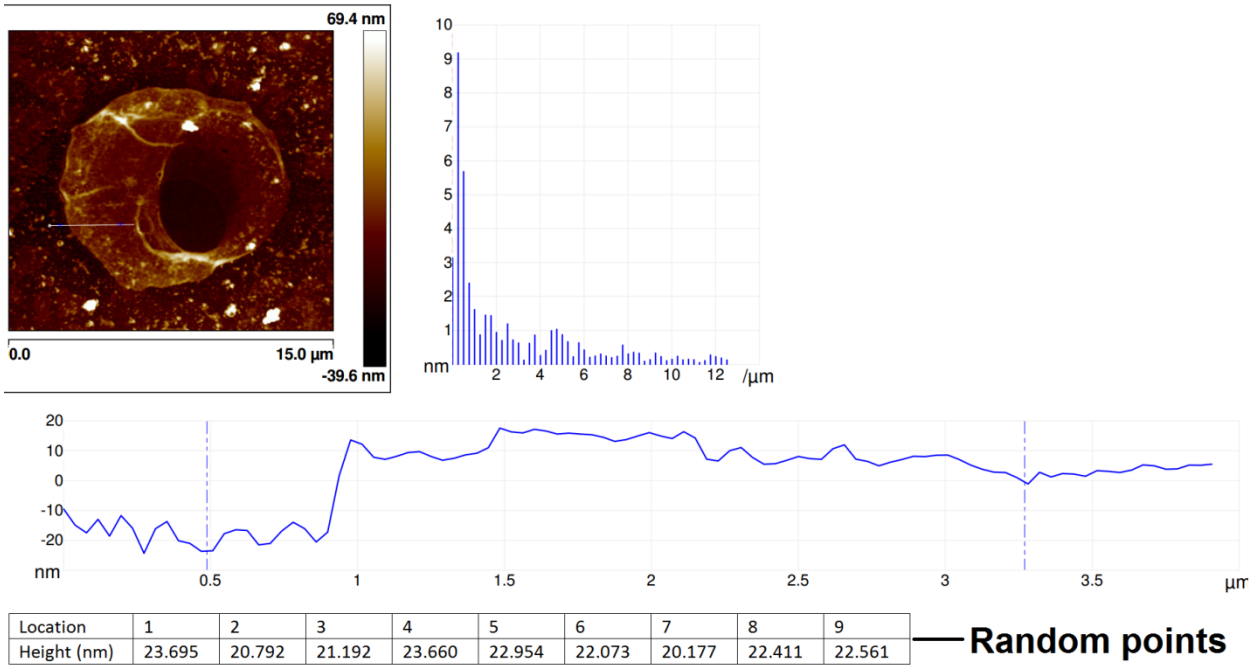

Location	1	2	3	4	5	6	7	8	9
Height (nm)	23.695	20.792	21.192	23.660	22.954	22.073	20.177	22.411	22.561

Random points

Figure 9.8: *The thickness of the membrane was calculated by averaging the vertical distance between two points, one on the dried droplet and one on the silicon wafer. Measurement was carried out at 9 random positions to get an average value.*

the crosslinked emulsion was stable. These results imply that first, the crosslinking was successful and second, BBTP stabilized emulsions can be used as a template for the generation of hollow compartments in the micro-meter range.

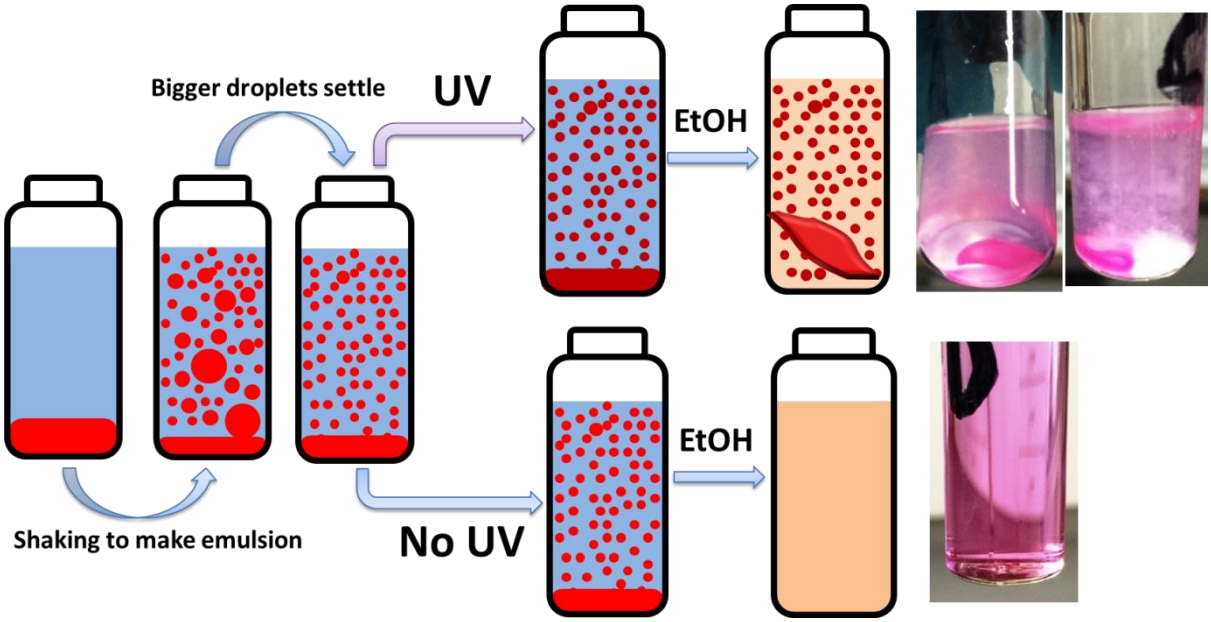

Figure 9.9: *The effect of ethanol on the stability of emulsion. The crosslinked (UV exposed) emulsion maintains integrity after the addition of ethanol, while the one without crosslinking destroys to give a clear solution.*

9.5. Summary

The self-assembly dynamics at oil-water interface as well as pH- and thermo-responsive properties of the BBTP were studied in detail using dynamic interfacial tension measurements and temperature dependent UV-Vis measurements. Unmodified FhuA ΔCVF^{tev} itself showed much higher interfacial activity than previously studied soluble proteins like ferritin, ß-casein and lysozyme, which proves that membrane proteins are very strong amphiphiles. Interestingly, the dynamics of interfacial stabilization were even faster than hydrophobin – a well-known amphiphilic protein. The BBTP, both FhuA ΔCVF^{tev}-PNIPAAm and FhuA ΔCVF^{tev}-PDMAEMA, exhibited at least 10 times faster interfacial dynamics as compared to unmodified FhuA ΔCVF^{tev}; with FhuA ΔCVF^{tev}-PDMAEMA at pH 10 being nearly 20 times faster. The high interfacial activity of the BBTP facilitated the generation of highly stable Pickering emulsions. The

non-crosslinked Pickering emulsions of FhuA ΔCVF^{tev}-PDMAEMA conjugates showed exceptional long-term stability of over 40 days. Finally, more stable capsules of these Pickering emulsions were also generated by UV-crosslinking the polymer chains of FhuA ΔCVF^{tev}-PNIPAAm-PDMMIBA. Visual inspection, dissolution experiments and optical/fluorescence microscopy were used to prove successful crosslinking. SFM and cryo-SEM analysis additionally indicated that the thickness as low as 11.1 ± 0.6 nm, corresponding to at most two layers of the BBTP, was capable of stabilizing the emulsion droplets. It is remarkable in light of the fact that such a thin membrane can stabilize an emulsion droplet two to three orders of magnitude larger than itself and still remain intact. The experiments shown in this chapter were the next logical step to the BBTP generation; synthesis of larger order structures (micro-meter range) using the building blocks synthesized in previous chapters. Very similar structures would be synthesized with the conjugates of enzymes (**Chapter 8**), for potential applications in heterogeneous catalysis and healthcare. Furthermore, these experiments and results formed the foundation of protocol used for the generation of ultra-thin membranes detailed in **Chapter 10**.

10 Stable stimuli-responsive nano-thin membranes

10.1. Introduction

After successfully generating micro-structures from the nano-scale building blocks, described in **Chapter 9**, the aim was to go from micro-structure to even larger structures; going from spherical geometry to planar. Informed with the knowledge of interfacial activity behavior of BBTP with FhuA ΔCVF^{tev} (**Chapter 9**), it was expected that BBTP with other variants would also quickly self-assemble at oil-water and air-water interface. In this chapter, BBTP with FhuA WT, FhuA ΔCVF^{tev}K$_8^{mid}$ and FhuA ΔCVF^{tev}K$_{11}^{up}$ and copolymer of NIPAAm and 3,4-dimethyl maleic imidobutyl acrylate (DMMIBA) or 2-(dimethyl maleinimido)-*N*-ethyl-acrylamide (DMIAAm) were self-assembled at these interfaces. Crosslinking the self-assembled conjugates by exposure to the UV generated stable large scale planar membranes. Nano-thin membranes were generated at oil-water interface and water dropping tests conducted on them to investigate their mechanical stability. Membranes were further generated at air-water interface and characterized after drying on silicon wafers. Scanning force microscopy (SFM) was used to assess the morphology and thickness of these membranes. Finally, water flux and permeation experiments through membranes self-assembled and crosslinked on polyether sulfone supports were carried out. Since, PNIPAAm is a thermo-responsive polymer, the membrane permeation and flux data were collected by carrying out the measurements at RT as well as 40 °C, below and above the LCST of PNIPAAm. Only initial flux and permeation measurements are reported in this chapter. In the following research, these measurements will be optimized and membrane selectivity towards nano-sized permeates would be investigated.

10.2. Preparation and characterization

10.2.1. Materials

All chemicals used were of analytical reagent grade or higher quality, purchased from Applichem (Darmstadt, Germany), Alfa Aesar (Karlsruhe, Germany) or Sigma-Aldrich Chemie (Taufkirchen, Germany), if not stated otherwise. The synthesis of BBTP or conjugates of FhuA variants was carried out without using any sacrificial initiator as explained in **Section 7.2.1**. Millipore water was used for all flux and permeation tests. Boron doped p-type 625 µm thick silicon wafers were purchased from CrysTec GmbH, Berlin. Circular PES membranes with diameter of 47 mm and pore size 0.2 µm were purchased from PALL Life Sciences (New York, USA). Glass fiber filters, type MN 85/70 BF with a diameter of 45 mm, were purchased from Carl Roth GmbH (Karlsruhe, Germany).
For this chapter, MPD buffer is defined as the buffer containing 50 mM MPD, 10 mM sodium phosphate, 1 mM EDTA and 1 mM NaN_3 at pH 7.4.

10.2.2. Self-assembly and membrane generation

Membranes on silicon wafers: Silicon wafers were cut in 1 cm by 1 cm size and stored in ethanol before use. When preparing membranes for SFM, the silicon wafers were dried with pressurized air and then cleaned with CO_2 snow-jet. To impart hydrophilicity, the wafers were etched with O_2 plasma for 5 minutes at 0.2 mbar pressure. 120 µl of conjugate solution diluted with Millipore water to the respective concentration ($2.6 \cdot 10^{-1}$ mg/ml, $2.6 \cdot 10^{-2}$ mg/ml or $2.6 \cdot 10^{-3}$ mg/ml.), was put on the wafers and either dried overnight (for non-crosslinked samples) or put under the UV light on a TEFLON block atop an ice bath for 1 h for drying-mediated self-assembly and crosslinking (Figure 10.1). After the crosslinking, the silicon wafer was put under air overnight and SFM scans performed the following morning.

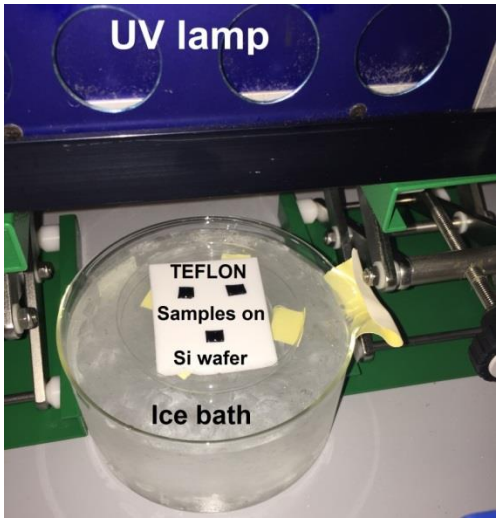

Figure 10.1: *UV-crosslinking table partially submerged in an ice bath.*

Membranes at oil-water interface: The polar-apolar interfacial membrane tests were conducted using 500 µl of MPD buffer or respective BBTP (conjugate) solution at a protein concentration of $2.6 \cdot 10^{-1}$ mg/ml (diluted from stock solution with MDP buffer) and 2000 µl of toluene. The samples were put in 3 ml vials, which after a 30 min stabilization period were exposed to UV for 3 h in an ice bath. After the interfacial self-assembly and simultaneous crosslinking, 10 % (v/v) blue-black LAMY ink (in water) was dropped on the membrane using a 1 ml syringe, and the process was recorded on video using an iPhone camera for either two min or until the two phases (10 % dye and underlying water phase) mixed – depending on which was reached first.

Membranes on PES support: PES support was put on a Teflon block with the shiny side down. 3 ml of respective BBTP (conjugate) solution at a protein concentration of $5.2 \cdot 10^{-2}$ mg/ml (diluted from stock solution with water) was then carefully poured over the support. After leaving the block undisturbed for BBTP to self-assemble at air-water interface for 1 h, it was put atop ice bath with ice water touching the Teflon block from the bottom, in a condition shown in Figure 10.1. This assembly was then exposed to UV light for ca. 1 h 50 min (until the filter is just dry) and allowed to crosslink as water evaporated. After that, the dry BBTP membrane atop PES support was used for water flux and permeation experiments.

10.2.3. Characterization techniques and equipment used

Plasma etching: 30 GUNJET from spraying systems co. (Wheaton, USA) with a heating plate at 200 °C was used to clean silicon wafers of any dirt first. Then, PlasmaFlecto etcher from plasma technology, Herrenberg, Germany assisted with DEVILBISS 5 liter oxygen concentrator, from Devilbiss healthcare, USA was used for plasma etching the silicon wafers.

SFM: The measurements were performed on a Bruker Dimension FastScan instrument (Bruker, Bremen, Germany). Silicon tip on a Silicon Nitride cantilever [Fastscan-A probe with a force constant of 18 N/m (f_0 = 1400 kHz)] were used for tapping mode measurements in air at a scan rate of 0.506 Hz and 512 samples/line. A scratch was made using a needle at multiple places on the dried membrane to measure the thickness of the membrane.

UV-crosslinking: UV crosslinking was carried out with Panacol UV-F 400F, operating at 450 W.

Flux and permeation measurements: The flux and permeation measurements were conducted on a custom made device, assembled in house. The scheme for the device is shown in Figure 10.2. The flow rate was calculated by recording the rate of increase of mass on the balance.

For flux measurements, after an equilibration time of 4 min, increase in mass over the balance was recorded every 30 sec for 7 min at a given transmembrane pressure [varied by the height of the water level (ΔH) and hence the hydrostatic pressure]. After these set of recordings, the pressure was varied, flow allowed to equilibrate for 4 min and the next set of data recorded as described above. Average flux over 7 minutes was then plotted against corresponding transmembrane pressure. The transmembrane pressure was sequentially increased from 4.6 mbar to 48.9 mbar (called trace measurement) and then sequentially decreased (called retrace measurement). The flux

at a given pressure was calculated using the formula $Flux = \frac{1}{\rho A}\frac{dw}{dt}$ where, ρ is the density of water, A is the area of the generated membrane and $(\frac{dw}{dt})$ is the rate of increase of mass as recorded on the balance.

For permeation measurements, the water level was kept fixed at the height difference (ΔH) of 10 cm using an AL-300 syringe pump from World Precision Instruments (Sarasota, USA) to generate a constant hydrostatic pressure of ca. 9.8 mbar across the

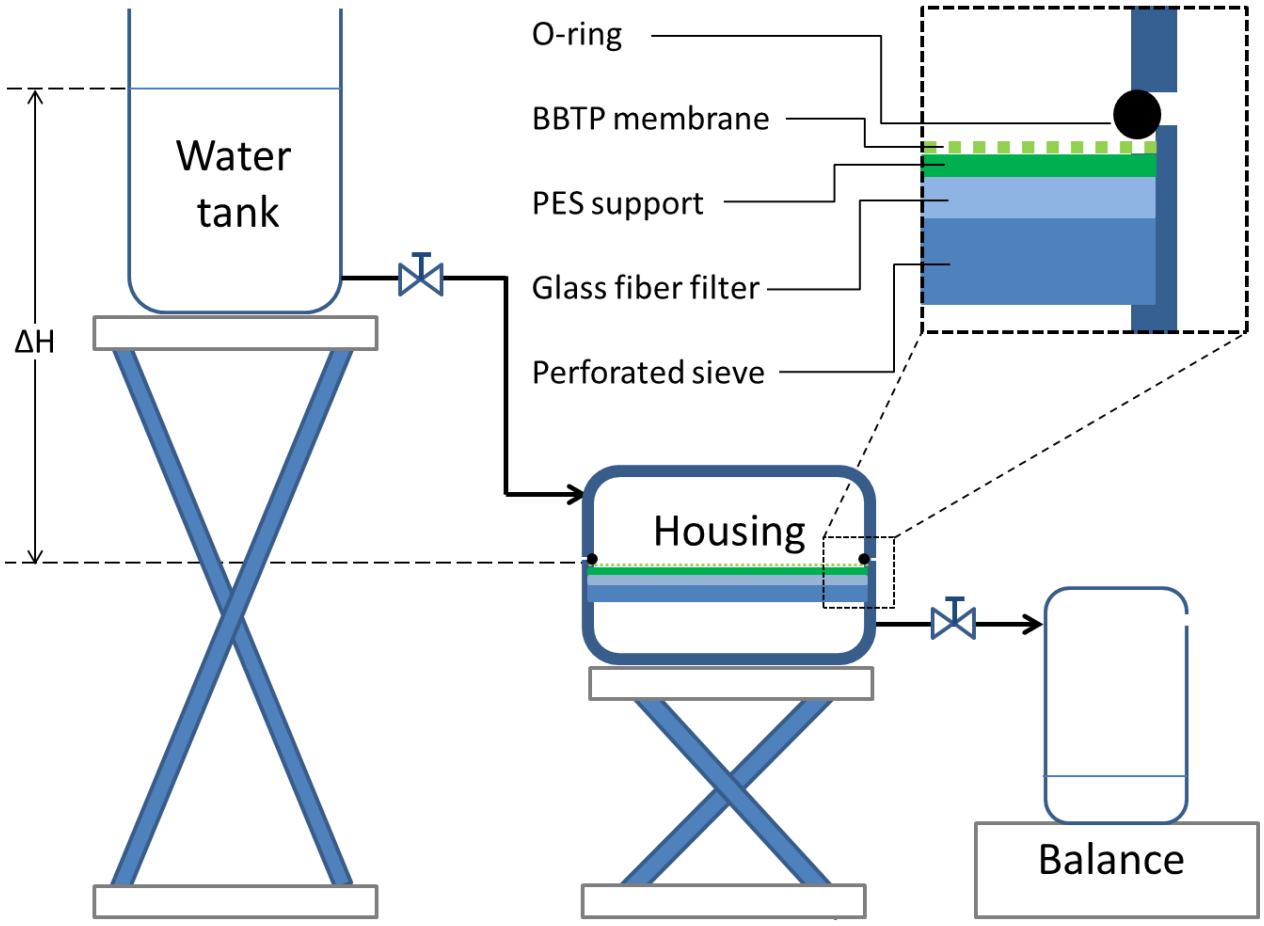

Figure 10.2: *The scheme representing the in house assembled flux and permeation measurement device. The BBTP membrane with PES support was kept on a glass filter, which itself was on top of a perforated hard plastic sieve. The setup was sealed using an O-ring. The flow through could be measured using the weighing balance. The transmembrane pressure could be varied adjusting the height of the top of water level in the water tank with respect to the membrane.*

membrane. After an initial equilibration time of 5 min, the increase in mass on the balance was recorded every 5 min for 120 min, and avg. permeation over an interval of each 5 min was plotted against time. To carry out permeation experiments at 40 °C, the whole assembly, i.e. the water and the water tank, housing and balance, was first equilibrated to 40 °C in an incubator (Heratherm IMH180 from Thermo-Scientific) for 2 h. After this, the device was assembled and protocol detailed above was followed in an identical fashion. The permeation at a given pressure was calculated using the formula $Permeation = \frac{1}{\rho AP}\frac{dw}{dt}$ where, ρ is the density of water, A is the area of the generated membrane, P is the transmembrane pressure and ($\frac{dw}{dt}$) is the rate of increase of mass as recorded on the balance.

10.3. Membrane synthesis and optimization

After analyzing the interfacial behavior of the BBTP in **Chapter 9**, the next step was to generate planar membranes from BBTP, exploiting this interfacial behavior. FhuA ΔCVF^{tev}K$_{11}{}^{up}$-PNIPAAm-PDMMIBA and FhuA ΔCVF^{tev}K$_8{}^{mid}$-PNIPAAm-PDMIAAm conjugates were synthesized as described in **Chapter 6** / **Chapter 7** and utilized for the generation and characterization of membranes. These two variants were used because they were specifically designed for polymerization, and have a passive diffusion channel. Figure 10.3 shows the general scheme of generation of membranes from BBTP. The conjugates were allowed to self-assemble at the air-water interface and then exposed to the UV light to crosslink the polymer chains as the water evaporated. The result was a crosslinked polymer matrix with FhuA embedded inside it.

In order to characterize and study the properties of the membranes from BBTP, three different concentrations of the protein were investigated. After preparing the silicon wafers as explained in the **Section 10.2.2**, respective solution was put on them and the polymer chains of the self-assembled BBTP crosslinked at the air-water interface by exposure to UV light (Figure 10.4D, Figure 10.4E and Figure 10.4F). Negative controls, with no exposure to the UV light, were also prepared simultaneously (Figure 10.4A, Figure 10.4B and Figure 10.4C). Optical microscopy was utilized to analyze the

morphology of the generated membranes. At concentrations $2.6 \cdot 10^{-1}$ mg/ml (Figure 10.4D) and $2.6 \cdot 10^{-2}$ mg/ml (Figure 10.4E), the morphology of the membranes exposed to the UV light was strikingly different than those without. The presence of wrinkles indicates that the crosslinking was finished before complete drying of the membrane. Over time, as the water evaporated, the effective area of the membrane reduced, resulting in wrinkles. At concentration of $2.6 \cdot 10^{-3}$ mg/ml (Figure 10.4F), however, the wrinkled membrane was not visible. On the other hand, at the same concentrations without UV-crosslinking, the conjugates seemed just to aggregate into lumps (Figure 10.4A, Figure 10.4B and Figure 10.4C).

Furthermore, making a scratch on the generated membrane resulted in exposure of the underlying silicon wafer (Figure 10.5B). Consecutively, the thickness of the membrane was estimated by scanning perpendicular to the scratch with the SFM and estimating the height the membrane layer from the surface of the silica wafer. The value of ca. 20 nm, for a concentration of $2.6 \cdot 10^{-2}$ mg/ml, indicates that nano-thin macroscopic membranes could be generated from self-assembled BBTP.

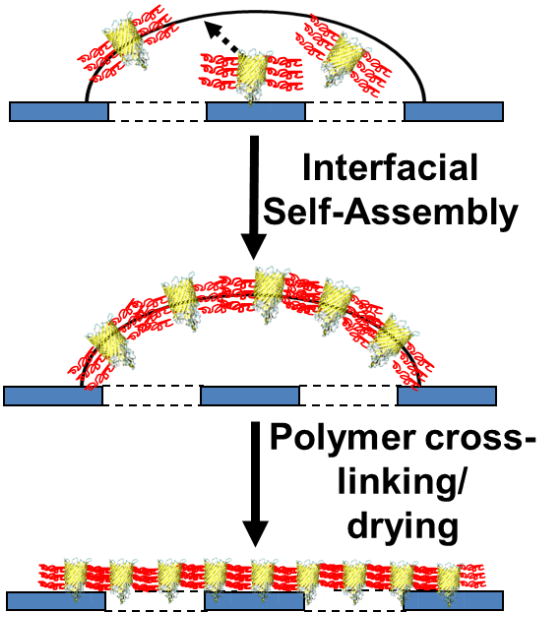

Figure 10.3: *The general approach of membrane formation. In **Chapter 9** it was discovered that BBTP were highly interfacially active. Hence, this behavior was exploited for their self-assembly at the air-water interface and consecutive crosslinking by exposure to UV light in order to generate nano-thin membranes.*

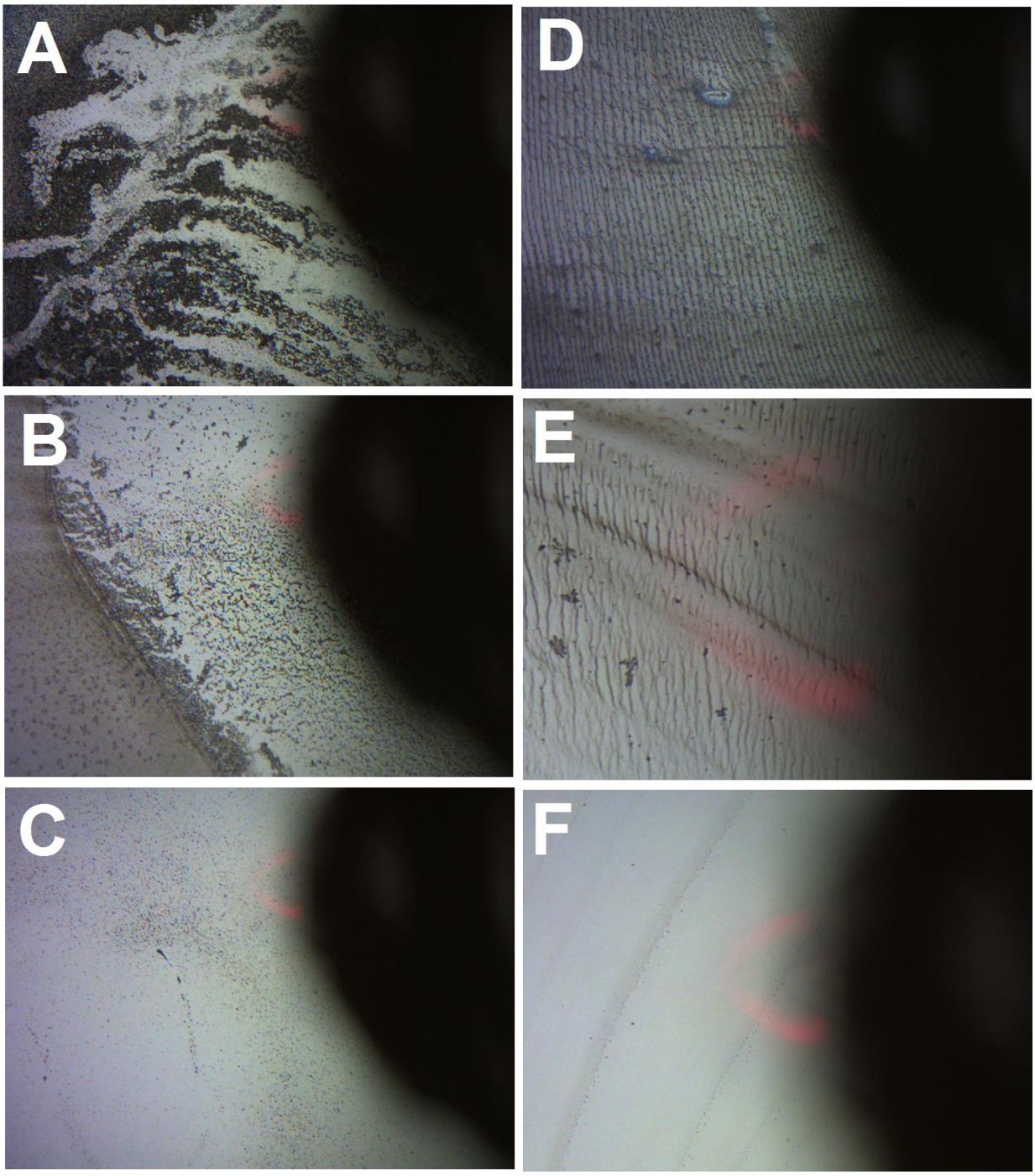

Figure 10.4: *Optical images of membranes made from FhuA ΔCVF^{tev}K$_{11}$^{up}-PNIPAAm-PDMMIBA on a silicon wafer. A, B and C were allowed to dry without any exposure to UV light, while D, E and F were exposed to the UV light, resulting in a crosslinked membrane. Concentration of protein in the conjugate sample (BCA assay) used were A/D = 2.6 · 10^{-1} mg/ml, B/E = 2.6 · 10^{-2} mg/ml and C/F = 2.6 · 10^{-3} mg/ml.*

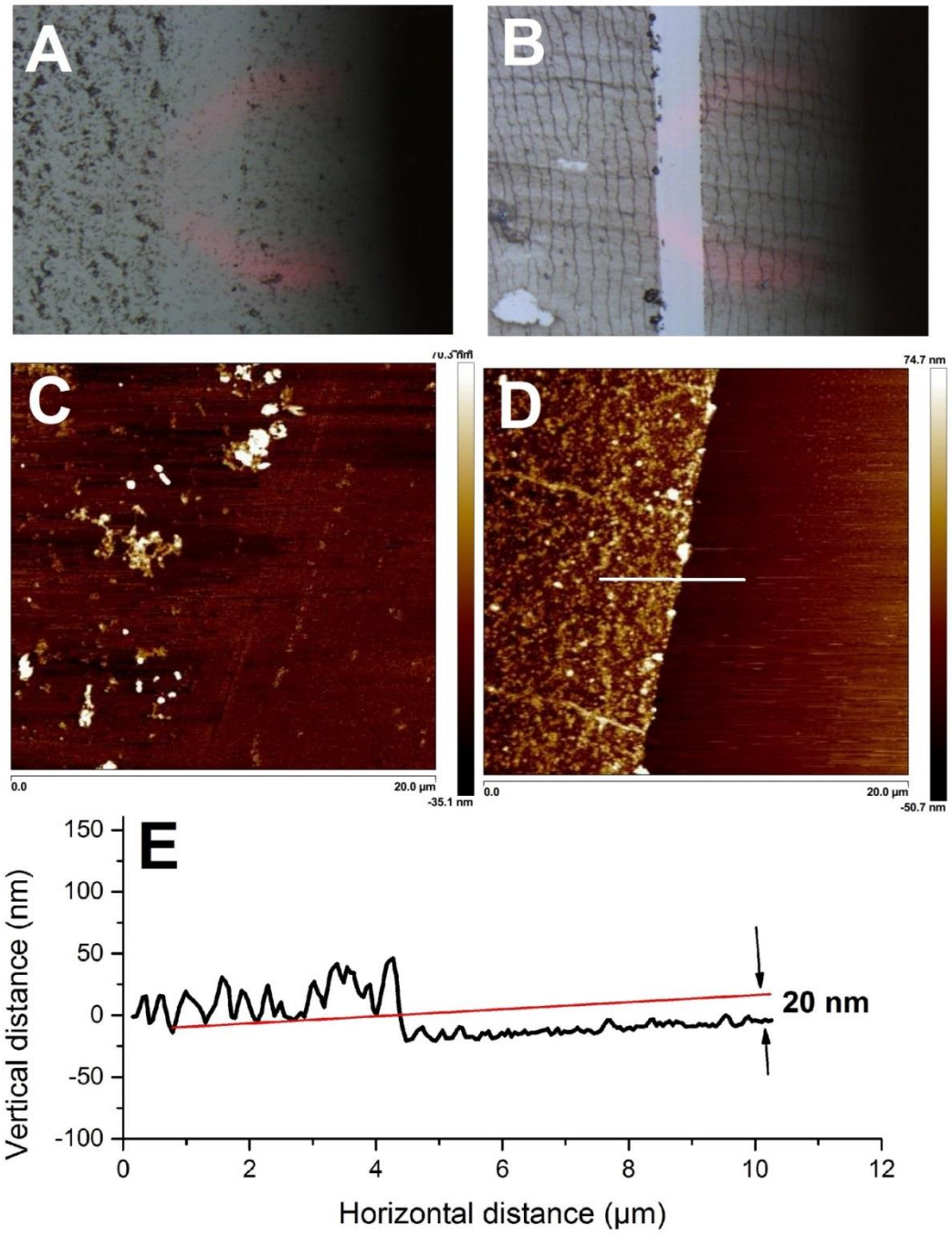

Figure 10.5: *SFM analysis of membrane formed from FhuA ΔCVF^{tev}K$_{11}$^{up}-PNIPAAm-PDMMIBA (conc. 2.6 · 10^{-2} mg/ml) on a silicon wafer. A scratch was made on samples without UV-crosslinking (A) and with UV-crosslinking (B). SFM scan of the sample not exposed to UV light (C) shows some aggregates while the crosslinked one (D), shows membrane like structure on the left half and the underlying Si wafer on the right half. The thickness of the membrane (measured from height of the scratch in D) was estimated (E) to be around ca. 20 nm.*

In order to investigate the mechanical stability of the nano-thin membranes, self-assembled membranes were also synthesized at the toluene-water interface (Figure 10.6). Toluene was poured on top of a $2.6 \cdot 10^{-1}$ mg/ml solution of FhuA Δ CVF^{tev}K$_8^{mid}$-PNIPAAm-PDMIAAm (water phase) and the conjugates allowed to self-assemble and crosslinked by exposure to the UV light. MPD buffer, without any BBTP (water phase) was used as the negative control. When a drop of dye-colored water (10 % aqueous solution of Lamy ink for fountain pens) was released in the toluene phase, it sedimented and sat on the membrane without mixing for up to 30 s. When the same was done with MPD buffer (Figure 10.6B), the two water phases mixed instantaneously. This experiment showed that a drop of dye-colored water was sitting on top of bulk water phase, separated only by the nano-thin membrane generated from the crosslinked FhuA conjugates. Needless to say, even though ultra-thin, these membranes also showed mechanical stability. However, the reproducibility of these

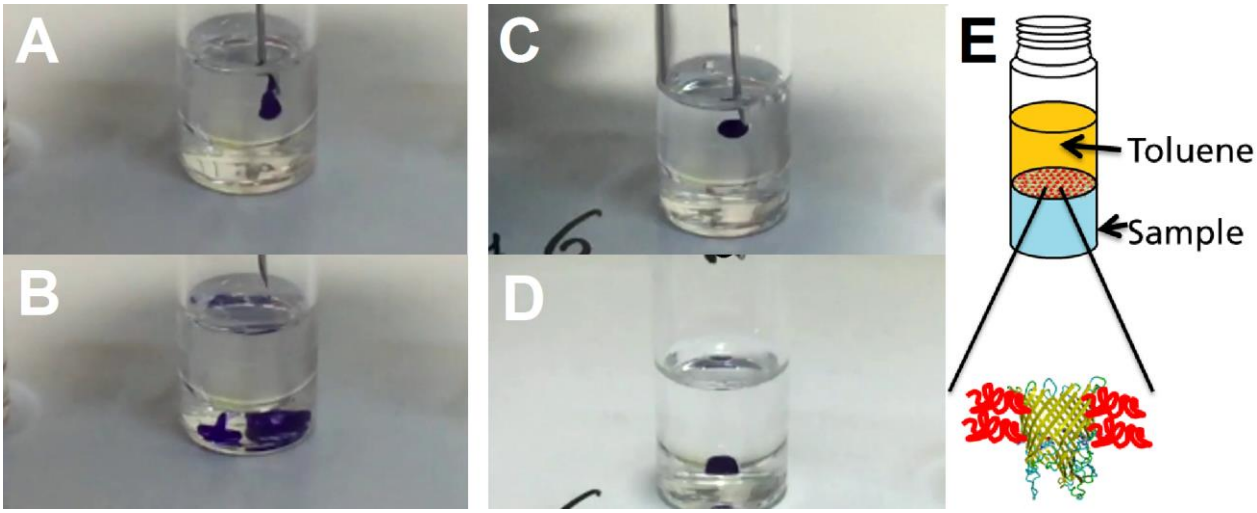

Figure 10.6: *A toluene-water interface with MPD buffer as the water phase results in instantaneous mixing of dye-colored water droplet added from the top (A & B). On the other hand FhuA ΔCVF^{tev}K$_8^{mid}$-PNIPAAm-PDMIAAm solution as the water phase and exposure to UV light halted the dye-colored water droplet (C and D). In essence this means a water droplet sat on bulk water phase separated by the self-assembled membrane from BBTP. Both A/B and C/D were exposed to identical UV light. E schematically shows the self-assembled and crosslinked membrane at the toluene-water interface.*

experiments, including the effect of the concentration of the conjugate solution on the thickness and stability of the generated membrane still needs to be analyzed, and will be done in research following this thesis.

10.4. Flux and permeation measurements

After morphological and mechanical analysis of nano-thin membranes on silicon wafers and oil-water interfaces, the flow of water through them was characterized. In order to demonstrate the applicability of the membrane formation approach, the size of membrane was increased to cover an area of ca. 17.35 cm^2. In order to provide strength to the nano-thick BBTP membrane of such large area, polyether sulfone (PES) filters were used as mechanical support (see experimental section for details). The BBTP solutions were kept on the PES support, allowed to self-assemble and then crosslinked. Membranes were always prepared fresh and immediately tested.

Flux through a membrane is defined as flow of the analyte per unit area of the membrane. Flux depends on the transmembrane pressure, which is defined as the pressure difference across the membrane being analyzed. The higher the transmembrane pressure, higher is the flux. The setup shown in Figure 10.2 was employed for the measurements. This setup proved efficient in easy control of the hydrostatic pressure (and hence transmembrane pressure) by changing the height of the storage tank. However, it must be noted that equating the hydrostatic pressure and transmembrane pressure is an approximation, which may be subject to deviations from the actual transmembrane pressure. In order to calculate actual transmembrane pressure, two pressure sensors, one on each side of the membrane would be required. When assembling the setup, the housing was first filled up with water, leaving no air bubbles inside and the connection then fixed. The values from a weighing balance were used to record the mass of permeated water every 30 s. The volume (and hence the flow rate and consecutively flux) was then calculated using the density of water at 25 °C. Figure 10.7 shows the flux at RT through just the PES support as well as membrane from FhuA WT-PNIPAAm-PDMMIBA generated atop the PES support. As expected, the

flux increases with increasing transmembrane pressure. The flux through the PES support with the BBTP membrane is slightly lower than just the PES support because of the resistance provided by the self-assembled membrane. This only slight difference in flux may be attributed to the ultra-low thickness (as demonstrated in the previous section) and hydrophilicity of the membrane matrix. At a constant transmembrane pressure, if the membrane breaks at some point during the measurement, a sudden increase in flux would be observed. Hence, the measurements were always carried in duplicates, once successively increasing the transmembrane pressure (trace) and then successively reducing the transmembrane pressure (retrace). Since, the trace and retrace were close enough, it can be inferred that the membrane did not break during the measurement and was mechanically robust up to a transmembrane pressure of at least 48.9 mbar.

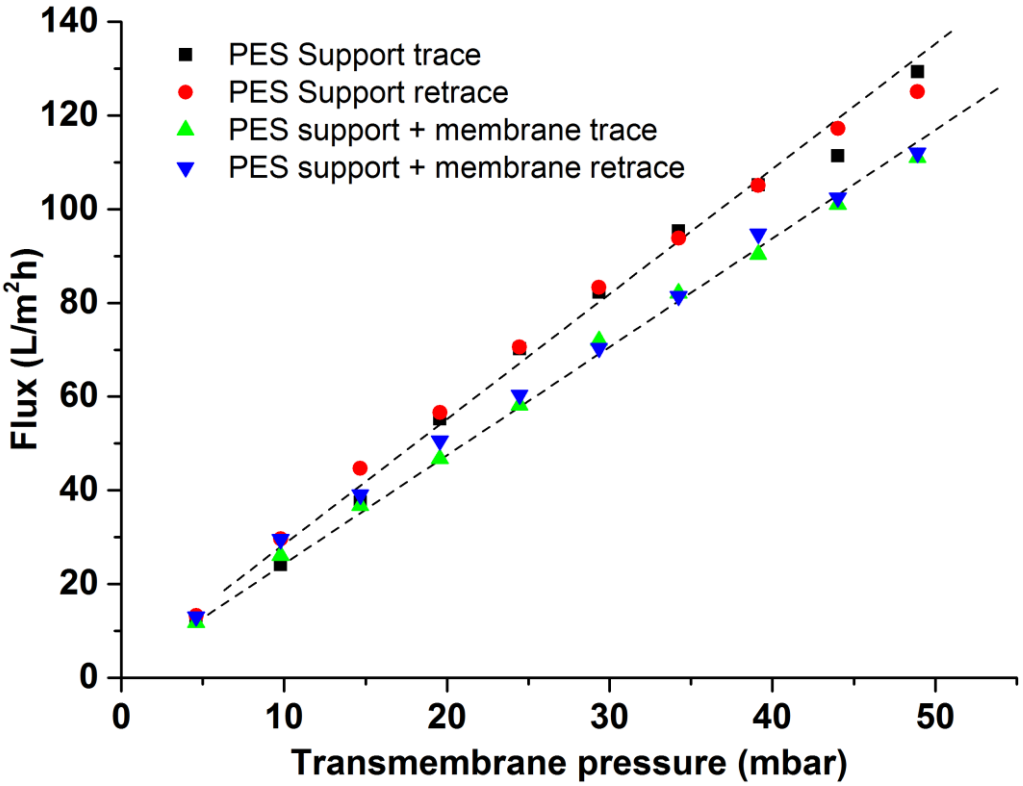

Figure 10.7: *Flux of water through only the PES support and PES support with membranes made from FhuA WT-PNIPAAm-PDMMIBA at RT. In the presence of the membranes made from BBTP, the value of flux is lower, because of slight resistance provided by the membrane.*

On the other hand, membrane fouling and accumulation usually reduce the flux at a constant transmembrane pressure.[244] Consecutively, when using a membrane over longer periods of time, it is quite often required to increase the transmembrane pressure to maintain a constant flux. For many micro-filtration systems, significant changes in transmembrane pressure are required.[245] Hence, flow of water through the membranes was also analyzed using permeation, which is defined as flux per unit transmembrane pressure. The transmembrane pressure was kept constant and permeation plotted over a period of 2 hours (Figure 10.8). The setup shown in Figure 10.2 was used for all measurements at RT as well as 40 °C. The tests were carried out on PES supported self-assembled membranes made from FhuA WT-PNIPAAm-PDMMIBA and FhuA $\Delta CVF^{tev}K_{11}^{up}$-PNIPAAm-PDMMIBA. At room temperature, the PNIPAAm chains are hydrophilic and the water can also go through the crosslinked polymer matrix. However, the crosslinked PNIPAAm matrix is expected to undergo volume phase transition at ~32 °C, resulting in the matrix becoming hydrophobic. Consecutively, at 40 °C this aspect of the hydrophobic polymer matrix is reflected by a decrease in the permeation because of increased resistance to flow of water. Membranes synthesized by BBTP of both FhuA WT as well as FhuA $\Delta CVF^{tev}K_{11}^{up}$ exhibited substantial reduction in permeation when conducting the experiments at 40 °C, proving that the thermo-responsivity of PNIPAAm can be used to alter the membrane flow characteristics. Furthermore, membranes synthesized by BBTP of FhuA WT had lower permeation both at RT as well as 40 °C than those synthesized by BBTP of FhuA $\Delta CVF^{tev}K_{11}^{up}$. This result matches the expected behavior since FhuA WT has a narrower channel area (because of the pore blocking cork domain) as compared to FhuA $\Delta CVF^{tev}K_{11}^{up}$, which has an open channel (Table 7.1). Consecutively, the membranes with the conjugate of FhuA $\Delta CVF^{tev}K_{11}^{up}$ have higher permeation even at 40 °C than for the membranes with the conjugates of FhuA WT at RT. Furthermore, the reduction in permeation at higher temperature for membranes with conjugates of FhuA WT is around 2000 L/m^{2}h bar while that for membranes with the conjugates of FhuA $\Delta CVF^{tev}K_{11}^{up}$ is around 2700 L/m^{2}h bar. However, it must be noted that these measurements, flux as well as permeation, are only preliminary results and will be rerun and their reproducibility analyzed in future experiments.

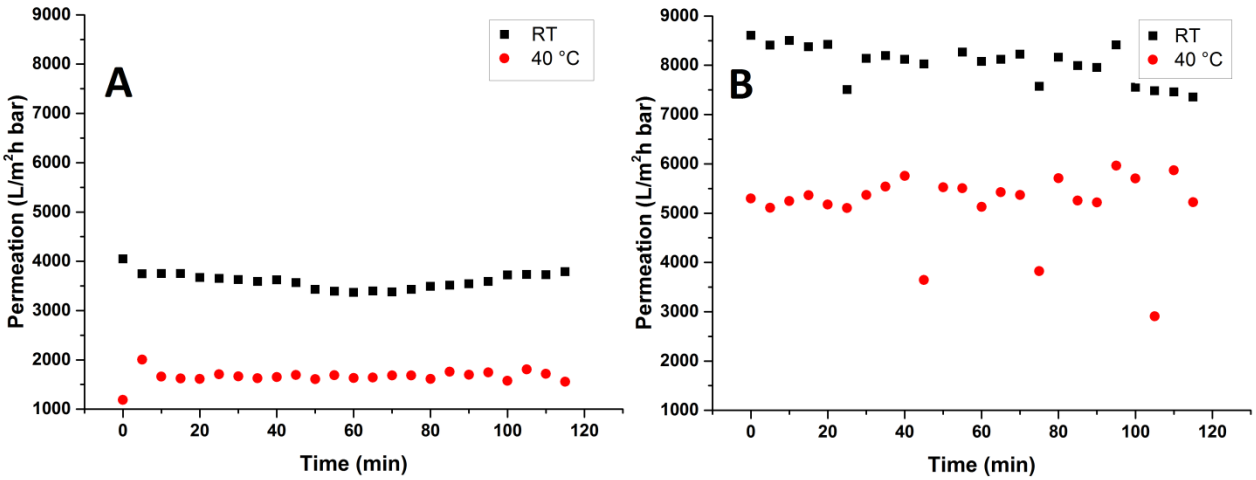

Figure 10.8: *Permeation of water at RT and 40 °C through membranes made from FhuA WT-PNIPAAm-PDMMIBA (A) and FhuA ΔCVF^{tev}K$_{11}^{up}$-PNIPAAm-PDMMIBA (B).*

10.5. Summary and outlook

In conclusion, nano-thin membranes were generated from self-assembled conjugates of the transmembrane protein FhuA. BBTP from FhuA WT, FhuA ΔCVF^{tev}K$_8^{mid}$ and FhuA ΔCVF^{tev}K$_{11}^{up}$ and copolymer of NIPAAm and DMMIBA or DMIAAm were self-assembled and crosslinked at oil-water and air-water interfaces to generate membranes up to ca. 17.35 cm^2 in area. SFM analysis revealed thickness of ca. 20 nm for membrane prepared from FhuA ΔCVF^{tev}K$_{11}^{up}$-PNIPAAm-PDMMIBA (conc. 2.6 · 10^{-2} mg/ml). Despite ultra-low thickness in the nanometer range, the nearly 1 cm^2 sized membranes generated at the interface of toluene-water were mechanically robust enough to sustain a drop of water atop the bulk water phase, while a drop atop the negative control with only MPD buffer resulted in instantaneous mixing of the drop into the water phase. Flux of water through the PES filter supported membranes from FhuA WT-PNIPAAm-PDMMIBA was investigated. The presence of the membranes only slightly reduced the flux of water because of their ultra-low thickness and the hydrophilicity of the polymer matrix. The membranes were shown to be stable up to a transmembrane pressure of at least 48.9 mbar. In order to analyze the long-term (* 2 h) flow, permeation experiments were also done. Because FhuA WT has a channel blocking cork domain which FhuA ΔCVF^{tev}K$_{11}^{up}$ doesn't, the permeation through the

membranes from FhuA WT conjugates was substantially and consistently lower than those made from FhuA $\Delta CVF^{tev}K_{11}{}^{up}$ conjugates. The membranes also exhibited thermo-responsivity; substantially reduced permeation was observed at 40 °C compared to at RT for the membranes generated from FhuA $\Delta CVF^{tev}K_{11}{}^{up}$-PNIPAAm-PDMMIBA and FhuA WT-PNIPAAm-PDMMIBA. All these results are particularly significant in two respects: 1) They show a new method of preparation of mechanically stable nano-thin membranes that are as large as 17.35 cm^2 in area, and 2) The thermo-responsivity of the polymer matrix can be exploited to control the flow characteristics of the membranes. The scale of the generated membranes is much larger than competing techniques such as spreading of polymersomes on solid supports. Furthermore, the number of incorporated membrane proteins per unit area for the approach presented in this thesis is expected to substantially higher than in the spreading of polymersomes.

Tests of membranes with pH- as well as thermo-responsive PDMAEMA as the polymer matrix are underway. The most significant advantage of using PDMAEMA would be the possibility of making the polymer matrix hydrophobic at RT by increasing the pH, hence avoiding the requirement of heating up the whole setup. Furthermore, experiments to investigate the orientation and stability of FhuA at these interfaces are planned to be carried out next. Moreover, new genetic variants of FhuA with a chiral region in the channel are currently being developed by our collaboration partners, the group of Prof. Schwaneberg. When successfully generated, they would be tested for their capability of show selective permeability towards one enantiomer of an amino acid (D or L) from a racemic mixture of D and L enantiomers. Such membranes, the so to speak chiral membranes, hold a great potential as alternatives to conventional approaches towards resolution of racemic mixtures. The techniques described in this thesis in detail could be employed directly or with little optimization to generate chiral membranes.

The approaches shown in this chapter in particular, and in this thesis in general, open up possibilities of new and promising micro-scale systems such as micro-compartments and micro-reactors with transmembrane proteins acting as the pores. These systems have many potential applications in gene and drug delivery, biocatalysis and heterogeneous catalysis. Most importantly, nano-thin nano-porous large scale

membranes have a huge potential as membranes for functional separation. With many successful strides in this direction, perhaps one day we might be able to generate sophisticated nano-filtration devices that can act as artificial kidneys !

11 Bibliography

1. J. Zhao, X. Zhao, Z. Jiang, Z. Li, X. Fan, J. Zhu, H. Wu, Y. Su, D. Yang, F. Pan and J. Shi, *Prog. Polym. Sci.*, 2014, **39**, 1668-1720.
2. S. W. Kowalczyk, T. R. Blosser and C. Dekker, *Trends Biotechnol.*, 2011, **29**, 607-614.
3. I. Tokarev and S. Minko, *Adv. Mater.*, 2009, **21**, 241-247.
4. B. Alberts, A. Johnson, J. Lewis, D. Morgan, M. Raff, K. Roberts and P. Walter, *Molecular Biology of the Cell*, Garland Science, 2014.
5. C. I. Branden and J. Tooze, *Introduction to Protein Structure*, Garland Pub., Second edn., 1999.
6. H. Sui, B.-G. Han, J. K. Lee, P. Walian and B. K. Jap, *Nature*, 2001, **414**, 872-878.
7. G. M. Preston, T. P. Carroll, W. B. Guggino and P. Agre, *Science*, 1992, **256**, 385-387.
8. A.-K. Meinild, D. A. Klaerke and T. Zeuthen, *J. Biol. Chem.*, 1998, **273**, 32446-32451.
9. D. A. Doyle, J. M. Cabral, R. A. Pfuetzner, A. Kuo, J. M. Gulbis, S. L. Cohen, B. T. Chait and R. MacKinnon, *Science*, 1998, **280**, 69-77.
10. P. Carter, *Biochem. J.*, 1986, **237**, 1-7.
11. S. N. Ho, H. D. Hunt, R. M. Horton, J. K. Pullen and L. R. Pease, *Gene*, 1989, **77**, 51-59.
12. R. Chen, *Trends Biotechnol.*, 2001, **19**, 13-14.
13. W. P. Stemmer, *Proc. Natl. Acad. Sci. U. S. A.*, 1994, **91**, 10747-10751.
14. H. Charan, J. Kinzel, U. Glebe, D. Anand, T. M. Garakani, L. Zhu, M. Bocola, U. Schwaneberg and A. Böker, *Biomaterials*, 2016, **107**, 115-123.
15. H. Caner, E. Groner, L. Levy and I. Agranat, *Drug Discovery Today*, 2004, **9**, 105-110.
16. -. _NA_(DOI:10.1002/chir.530040513), *Chirality*, 1992, **4**, 338-340.
17. R. Xie, L.-Y. Chu and J.-G. Deng, *Chem. Soc. Rev.*, 2008, **37**, 1243-1263.

18. C. Meng, Y. Sheng, Q. Chen, H. Tan and H. Liu, *J. Membr. Sci.*, 2017, **526**, 25-31.
19. M. M. Pérez-Madrigal, L. J. del Valle, E. Armelin, C. Michaux, G. Roussel, E. A. Perpète and C. Alemán, *ACS Appl. Mater. Interfaces*, 2015, **7**, 1632-1643.
20. Y. Zhao, C. Qiu, X. Li, A. Vararattanavech, W. Shen, J. Torres, C. Hélix-Nielsen, R. Wang, X. Hu, A. G. Fane and C. Y. Tang, *J. Membr. Sci.*, 2012, **423–424**, 422-428.
21. S. Ihle, O. Onaca, P. Rigler, B. Hauer, F. Rodriguez-Ropero, M. Fioroni and U. Schwaneberg, *Soft Matter*, 2011, **7**, 532-539.
22. C. G. Palivan, R. Goers, A. Najer, X. Zhang, A. Car and W. Meier, *Chem. Soc. Rev.*, 2016, **45**, 377-411.
23. H. Wang, T.-S. Chung, Y. W. Tong, W. Meier, Z. Chen, M. Hong, K. Jeyaseelan and A. Armugam, *Soft Matter*, 2011, **7**, 7274-7280.
24. P. H. H. Duong, T.-S. Chung, K. Jeyaseelan, A. Armugam, Z. Chen, J. Yang and M. Hong, *J. Membr. Sci.*, 2012, **409–410**, 34-43.
25. H. Wang, T.-S. Chung, Y. W. Tong, K. Jeyaseelan, A. Armugam, Z. Chen, M. Hong and W. Meier, *Small*, 2012, **8**, 1185-1190.
26. P. van Rijn, M. Tutus, C. Kathrein, N. C. Mougin, H. Park, C. Hein, M. P. Schürings and A. Böker, *Adv. Funct. Mater.*, 2014, **24**, 6762-6770.
27. L. Wu, U. Glebe and A. Böker, *Polym. Chem.*, 2015, **6**, 5143-5184.
28. A. C. Obermeyer and B. D. Olsen, *ACS Macro Lett.*, 2015, **4**, 101-110.
29. S. Kumar and R. Nussinov, *ChemBioChem*, 2002, **3**, 604-617.
30. M. Al-Haggar, A. Madej-Pilarczyk, L. Kozlowski, J. M. Bujnicki, S. Yahia, D. Abdel-Hadi, A. Shams, N. Ahmad, S. Hamed and M. Puzianowska-Kuznicka, *Eur. J. Hum. Genet.*, 2012, **20**, 1134-1140.
31. R. Koebnik, K. P. Locher and P. Van Gelder, *Mol. Microbiol.*, 2000, **37**, 239-253.
32. Y.-x. Shen, P. O. Saboe, I. T. Sines, M. Erbakan and M. Kumar, *J. Membr. Sci.*, 2014, **454**, 359-381.
33. A. D. Ferguson, E. Hofmann, J. W. Coulton, K. Diederichs and W. Welte, *Science*, 1998, **282**, 2215-2220.
34. K. P. Locher, B. Rees, R. Koebnik, A. Mitschler, L. Moulinier, J. P. Rosenbusch and D. Moras, *Cell*, 1998, **95**, 771-778.

35. A. Güven, M. Fioroni, B. Hauer and U. Schwaneberg, *J. Nanobiotechnol.*, 2010, **8**, 1-9.
36. O. Onaca, P. Sarkar, D. Roccatano, T. Friedrich, B. Hauer, M. Grzelakowski, A. Güven, M. Fioroni and U. Schwaneberg, *Angew. Chem. Int. Ed.*, 2008, **47**, 7029-7031.
37. A. Güven, T. Dworeck, M. Fioroni and U. Schwaneberg, *Adv. Eng. Mater.*, 2011, **13**, B324-B329.
38. S.-J. Tenne and U. Schwaneberg, *Int. J. Mol. Sci.*, 2012, **13**, 2459-2471.
39. N. Muhammad, T. Dworeck, M. Fioroni and U. Schwaneberg, *J. Nanobiotechnol.*, 2011, **9**, 8-8.
40. M. Krewinkel, T. Dworeck and M. Fioroni, *J. Nanobiotechnol.*, 2011, **9**, 1-8.
41. A. J. Wolfe, M. M. Mohammad, A. K. Thakur and L. Movileanu, *Biochim. Biophys. Acta*, 2016, **1858**, 19-29.
42. B. Jung and P. Theato, in *Bio-synthetic Polymer Conjugates*, ed. H. Schlaad, Springer Berlin Heidelberg, 2013, vol. 253, ch. 169, pp. 37-70.
43. S. Moelbert, E. Emberly and C. Tang, *Protein Sci.*, 2004, **13**, 752-762.
44. U. Glebe, B. S. de Miranda, P. van Rijn and A. Böker, in *Bio-Synthetic Hybrid Materials and Bionano-particles : A Biological Chemical Approach Towards Material Science* eds. A. Böker and P. van Rijn, Royal Society of Chemistry, 2015, ch. 1, pp. 1-29.
45. L. A. Canalle, D. W. P. M. Lowik and J. C. M. van Hest, *Chem. Soc. Rev.*, 2010, **39**, 329-353.
46. P. van Rijn and A. Böker, *J. Mater. Chem.*, 2011, **21**, 16735-16747.
47. D. Jenkins Aubrey, G. Jones Richard and G. Moad, *Pure Appl. Chem.*, 2009, **82**, 483.
48. K. Matyjaszewski, *Macromolecules*, 2012, **45**, 4015-4039.
49. K. Matyjaszewski and J. Xia, *Chem. Rev.*, 2001, **101**, 2921-2990.
50. H. Fischer, *Chem. Rev.*, 2001, **101**, 3581-3610.
51. W. Jakubowski, K. Min and K. Matyjaszewski, *Macromolecules*, 2006, **39**, 39-45.
52. K. Min, H. Gao and K. Matyjaszewski, *J. Am. Chem. Soc.*, 2005, **127**, 3825-3830.
53. G. Hizal, U. Tunca, S. Aras and H. Mert, *J. Polym. Sci., Part A: Polym. Chem.*, 2006, **44**, 77-87.

54. N. V. Tsarevsky and K. Matyjaszewski, *Chem. Rev.*, 2007, **107**, 2270-2299.
55. K. Matyjaszewski, W. Jakubowski, K. Min, W. Tang, J. Huang, W. A. Braunecker and N. V. Tsarevsky, *Proc. Natl. Acad. Sci. U. S. A.*, 2006, **103**, 15309-15314.
56. V. Percec, T. Guliashvili, J. S. Ladislaw, A. Wistrand, A. Stjerndahl, M. J. Sienkowska, M. J. Monteiro and S. Sahoo, *J. Am. Chem. Soc.*, 2006, **128**, 14156-14165.
57. K. Matyjaszewski, N. V. Tsarevsky, W. A. Braunecker, H. Dong, J. Huang, W. Jakubowski, Y. Kwak, R. Nicolay, W. Tang and J. A. Yoon, *Macromolecules*, 2007, **40**, 7795-7806.
58. D. Konkolewicz, Y. Wang, P. Krys, M. Zhong, A. A. Isse, A. Gennaro and K. Matyjaszewski, *Polym. Chem.*, 2014, **5**, 4396-4417.
59. Y. Gao, T. Zhao and W. Wang, *RSC Adv.*, 2014, **4**, 61687-61690.
60. N. Zhang, S. R. Samanta, B. M. Rosen and V. Percec, *Chem. Rev.*, 2014, **114**, 5848-5958.
61. F. Alsubaie, A. Anastasaki, V. Nikolaou, A. Simula, G. Nurumbetov, P. Wilson, K. Kempe and D. M. Haddleton, *Macromolecules*, 2015, **48**, 5517-5525.
62. F. Alsubaie, A. Anastasaki, V. Nikolaou, A. Simula, G. Nurumbetov, P. Wilson, K. Kempe and D. M. Haddleton, *Macromolecules*, 2015, **48**, 6421-6432.
63. D. Konkolewicz, Y. Wang, M. Zhong, P. Krys, A. A. Isse, A. Gennaro and K. Matyjaszewski, *Macromolecules*, 2013, **46**, 8749-8772.
64. G. Moad, E. Rizzardo and S. H. Thang, *Acc. Chem. Res.*, 2008, **41**, 1133-1142.
65. V. Coessens, T. Pintauer and K. Matyjaszewski, *Prog. Polym. Sci.*, 2001, **26**, 337-377.
66. G. Moad, E. Rizzardo and S. H. Thang, *Aust. J. Chem.*, 2005, **58**, 379-410.
67. H. Willcock and R. K. O'Reilly, *Polym. Chem.*, 2010, **1**, 149-157.
68. G. Moad, E. Rizzardo and S. H. Thang, *Polym. Int.*, 2011, **60**, 9-25.
69. M. Semsarilar and S. Perrier, *Nat. Chem.*, 2010, **2**, 811-820.
70. D. J. Keddie, G. Moad, E. Rizzardo and S. H. Thang, *Macromolecules*, 2012, **45**, 5321-5342.
71. M. K. Georges, R. P. N. Veregin, P. M. Kazmaier and G. K. Hamer, *Macromolecules*, 1993, **26**, 2987-2988.
72. C. J. Hawker, *J. Am. Chem. Soc.*, 1994, **116**, 11185-11186.

73. J. Nicolas, Y. Guillaneuf, C. Lefay, D. Bertin, D. Gigmes and B. Charleux, *Prog. Polym. Sci.*, 2013, **38**, 63-235.
74. R. Mülhaupt, *Angew. Chem. Int. Ed.*, 2004, **43**, 1054-1063.
75. M. Wei, Y. Gao, X. Li and M. J. Serpe, *Polym. Chem.*, 2017, **8**, 127-143.
76. F. Liu and M. W. Urban, *Prog. Polym. Sci.*, 2010, **35**, 3-23.
77. D. A. Davis, A. Hamilton, J. Yang, L. D. Cremar, D. Van Gough, S. L. Potisek, M. T. Ong, P. V. Braun, T. J. Martinez, S. R. White, J. S. Moore and N. R. Sottos, *Nature*, 2009, **459**, 68-72.
78. J. Thevenot, H. Oliveira, O. Sandre and S. Lecommandoux, *Chem. Soc. Rev.*, 2013, **42**, 7099-7116.
79. T. Tanaka, I. Nishio, S.-T. Sun and S. Ueno-Nishio, *Science*, 1982, **218**, 467-469.
80. T. Shimoboji, E. Larenas, T. Fowler, S. Kulkarni, A. S. Hoffman and P. S. Stayton, *Proc. Natl. Acad. Sci. U. S. A.*, 2002, **99**, 16592-16596.
81. M. Irie, *Pure Appl. Chem.*, 1990, **62**, 1495.
82. A. Schmalz, M. Hanisch, H. Schmalz and A. H. E. Müller, *Polymer*, 2010, **51**, 1213-1217.
83. S. Dai, P. Ravi and K. C. Tam, *Soft Matter*, 2008, **4**, 435-449.
84. D. Roy, W. L. A. Brooks and B. S. Sumerlin, *Chem. Soc. Rev.*, 2013, **42**, 7214-7243.
85. Y. L. Colson and M. W. Grinstaff, *Adv. Mater.*, 2012, **24**, 3878-3886.
86. J. Hu and S. Liu, *Macromolecules*, 2010, **43**, 8315-8330.
87. A. K. Bajpai, S. K. Shukla, S. Bhanu and S. Kankane, *Prog. Polym. Sci.*, 2008, **33**, 1088-1118.
88. D. Parasuraman and M. J. Serpe, *ACS Appl. Mater. Interfaces*, 2011, **3**, 4714-4721.
89. M. Ma, L. Guo, D. G. Anderson and R. Langer, *Science*, 2013, **339**, 186-189.
90. Q. Zhao, J. W. C. Dunlop, X. Qiu, F. Huang, Z. Zhang, J. Heyda, J. Dzubiella, M. Antonietti and J. Yuan, *Nat. Commun.*, 2014, **5**, 4293.
91. H. Koerner, G. Price, N. A. Pearce, M. Alexander and R. A. Vaia, *Nat. Mater.*, 2004, **3**, 115-120.
92. F. Wang, Y.-H. Lai and M.-Y. Han, *Macromolecules*, 2004, **37**, 3222-3230.

93. F. Seker, P. R. L. Malenfant, M. Larsen, A. Alizadeh, K. Conway, A. M. Kulkarni, G. Goddard and R. Garaas, *Adv. Mater.*, 2005, **17**, 1941-1945.
94. G. Charlet and G. Delmas, *Polymer*, 1981, **22**, 1181-1189.
95. M. Heskins and J. E. Guillet, *J. Macromol. Sci., Part A: Pure Appl.Chem.*, 1968, **2**, 1441-1455.
96. I. Bischofberger and V. Trappe, *Sci. Rep.*, 2015, **5**, 15520.
97. Y. Okada and F. Tanaka, *Macromolecules*, 2005, **38**, 4465-4471.
98. A. Milewska, J. Szydlowski and L. P. N. Rebelo, *J. Polym. Sci., Part B: Polym. Phys.*, 2003, **41**, 1219-1233.
99. S. Hirotsu, Y. Hirokawa and T. Tanaka, *J. Chem. Phys.*, 1987, **87**, 1392-1395.
100. R. Liu, M. Fraylich and B. R. Saunders, *Colloid. Polym. Sci.*, 2009, **287**, 627-643.
101. X. Gao, Y. Cao, X. Song, Z. Zhang, C. Xiao, C. He and X. Chen, *J. Mater. Chem. B*, 2013, **1**, 5578-5587.
102. F. Liu and M. W. Urban, *Macromolecules*, 2008, **41**, 6531-6539.
103. F. A. Plamper, M. Ruppel, A. Schmalz, O. Borisov, M. Ballauff and A. H. E. Müller, *Macromolecules*, 2007, **40**, 8361-8366.
104. M. L. Tebaldi, H. Charan, L. Mavliutova, A. Böker and U. Glebe, *Macromol. Chem. Phys.*, 2017, DOI: 10.1002/macp.201600529.
105. H. Charan, U. Glebe, D. Anand, J. Kinzel, L. Zhu, M. Bocola, T. M. Garakani, U. Schwaneberg and A. Boker, *Soft Matter*, 2017, DOI: 10.1039/C1036SM02520J.
106. D. Roy and B. S. Sumerlin, *Macromol. Rapid Commun.*, 2014, **35**, 174-179.
107. L. Long, W. D. Habicher, D. Kuckling and H. J. Adler, *Des. Monomers Polym.*, 1999, **2**, 351-358.
108. F. C. De Schryver, N. Boens and G. Smets, *J. Polym. Sci., Part A: Polym. Chem.*, 1972, **10**, 1687-1699.
109. J. Finter, E. Widmer and H. Zweifel, *Angew. Makromol. Chem.*, 1984, **128**, 71-97.
110. J. Gaitzsch, D. Appelhans, L. Wang, G. Battaglia and B. Voit, *Angew. Chem. Int. Ed.*, 2012, **51**, 4448-4451.
111. S. Seiffert, W. Oppermann and K. Saalwächter, *Polymer*, 2007, **48**, 5599-5611.
112. D. Kuckling, H.-J. P. Adler, K.-F. Arndt, L. Ling and W. D. Habicher, *Macromol. Symp.*, 1999, **145**, 65-74.

113. C. D. Vo, D. Kuckling, H. J. P. Adler and M. Schönhoff, *Colloid. Polym. Sci.*, 2002, **280**, 400-409.
114. D. Kuckling, C. D. Vo, H. J. P. Adler, A. Völkel and H. Cölfen, *Macromolecules*, 2006, **39**, 1585-1591.
115. M. S. S. de Samaniego and A. F. Miller, *Macromol. Symp.*, 2007, **256**, 167-174.
116. P. van Rijn, N. C. Mougin, D. Franke, H. Park and A. Böker, *Chem. Commun.*, 2011, **47**, 8376-8378.
117. N. C. Mougin, P. van Rijn, H. Park, A. H. E. Müller and A. Böker, *Adv. Funct. Mater.*, 2011, **21**, 2470-2476.
118. A. Habicht, W. Schmolke, F. Lange, K. Saalwächter and S. Seiffert, *Macromol. Chem. Phys.*, 2014, **215**, 1116-1133.
119. T. Johannes, M. R. Simurdiak and H. Zhao, in *Encyclopedia of Chemical Processing*, 2006, pp. 101-110.
120. K. M. Koeller and C.-H. Wong, *Nature*, 2001, **409**, 232-240.
121. R. A. Gross, A. Kumar and B. Kalra, *Chem. Rev.*, 2001, **101**, 2097-2124.
122. F. Hollmann and I. W. C. E. Arends, *Polymers*, 2012, **4**, 759.
123. J. R. Cherry and A. L. Fidantsef, *Curr. Opin. Biotechnol.*, 2003, **14**, 438-443.
124. P. V. Iyer and L. Ananthanarayan, *Process Biochem.*, 2008, **43**, 1019-1032.
125. B. G. Davis and V. Boyer, *Nat. Prod. Rep.*, 2001, **18**, 618-640.
126. N. U. Nair, W. Lin Tang, D. T. Eriksen and H. Zhao, in *Manual of Industrial Microbiology and Biotechnology, Third Edition*, American Society of Microbiology, 2010.
127. C. Mateo, J. M. Palomo, G. Fernandez-Lorente, J. M. Guisan and R. Fernandez-Lafuente, *Enzyme Microb. Technol.*, 2007, **40**, 1451-1463.
128. K. M. Polizzi, A. S. Bommarius, J. M. Broering and J. F. Chaparro-Riggers, *Curr. Opin. Chem. Biol.*, 2007, **11**, 220-225.
129. S. Basak, V. D. Punetha, G. Bisht, S. S. Bisht, N. G. Sahoo and J. W. Cho, *Polym. Rev. (Philadelphia, PA, U. S.)*, 2015, **55**, 163-198.
130. U. T. Bornscheuer, *Angew. Chem. Int. Ed.*, 2003, **42**, 3336-3337.
131. L. Cao, in *Carrier-bound Immobilized Enzymes*, Wiley-VCH Verlag GmbH & Co. KGaA, 2006, pp. 1-52.
132. W. Liu and P. Wang, *Biotechnol. Adv.*, 2007, **25**, 369-384.

133. R. A. Sheldon, *Adv. Synth. Catal.*, 2007, **349**, 1289-1307.
134. K. L. Heredia and H. D. Maynard, *Org. Biomol. Chem.*, 2007, **5**, 45-53.
135. J. Nicolas, G. Mantovani and D. M. Haddleton, *Macromol. Rapid Commun.*, 2007, **28**, 1083-1111.
136. M. A. Gauthier and H.-A. Klok, *Chem. Commun.*, 2008, **23**, 2591-2611.
137. B. Le Droumaguet and J. Nicolas, *Polym. Chem.*, 2010, **1**, 563-598.
138. R. M. Broyer, G. N. Grover and H. D. Maynard, *Chem. Commun.*, 2011, **47**, 2212-2226.
139. Y. Qi and A. Chilkoti, *Polym. Chem.*, 2014, **5**, 266-276.
140. J. D. Wallat, K. A. Rose and J. K. Pokorski, *Polym. Chem.*, 2014, **5**, 1545-1558.
141. I. Cobo, M. Li, B. S. Sumerlin and S. Perrier, *Nat. Mater.*, 2015, **14**, 143-159.
142. G. Fuhrmann, A. Grotzky, R. Lukic, S. Matoori, P. Luciani, H. Yu, B. Zhang, P. Walde, A. D. Schluter, M. A. Gauthier and J. C. Leroux, *Nat. Chem.*, 2013, **5**, 582-589.
143. C. Cummings, H. Murata, R. Koepsel and A. J. Russell, *Biomacromolecules*, 2014, **15**, 763-771.
144. R. Duncan, *Nat. Rev. Cancer*, 2006, **6**, 688-701.
145. J. Y. Shu, B. Panganiban and T. Xu, *Annu. Rev. Phys. Chem.*, 2013, **64**, 631-657.
146. X. Huang, M. Li, D. C. Green, D. S. Williams, A. J. Patil and S. Mann, *Nat. Commun.*, 2013, **4**, 2239.
147. D. Bontempo and H. D. Maynard, *J. Am. Chem. Soc.*, 2005, **127**, 6508-6509.
148. K. L. Heredia, D. Bontempo, T. Ly, J. T. Byers, S. Halstenberg and H. D. Maynard, *J. Am. Chem. Soc.*, 2005, **127**, 16955-16960.
149. B. S. Lele, H. Murata, K. Matyjaszewski and A. J. Russell, *Biomacromolecules*, 2005, **6**, 3380-3387.
150. G. Yasayan, A. O. Saeed, F. Fernandez-Trillo, S. Allen, M. C. Davies, A. Jangher, A. Paul, K. J. Thurecht, S. M. King, R. Schweins, P. C. Griffiths, J. P. Magnusson and C. Alexander, *Polym. Chem.*, 2011, **2**, 1567-1578.
151. Y. Qi, M. Amiram, W. Gao, D. G. McCafferty and A. Chilkoti, *Macromol. Rapid Commun.*, 2013, **34**, 1256-1260.

152. H. Murata, C. S. Cummings, R. R. Koepsel and A. J. Russell, *Biomacromolecules*, 2014, **15**, 2817-2823.
153. B. Le Droumaguet and K. Velonia, *Angew. Chem. Int. Ed.*, 2008, **47**, 6263-6266.
154. J. Nicolas, V. S. Miguel, G. Mantovani and D. M. Haddleton, *Chem. Commun.*, 2006, 4697-4699.
155. P. De, M. Li, S. R. Gondi and B. S. Sumerlin, *J. Am. Chem. Soc.*, 2008, **130**, 11288-11289.
156. H. Li, M. Li, X. Yu, A. P. Bapat and B. S. Sumerlin, *Polym. Chem.*, 2011, **2**, 1531-1535.
157. X. Li, L. Wang, G. Chen, D. M. Haddleton and H. Chen, *Chem. Commun.*, 2014, **50**, 6506-6508.
158. J. Xu, K. Jung, N. A. Corrigan and C. Boyer, *Chem. Sci.*, 2014, **5**, 3568-3575.
159. N. Vanparijs, R. De Coen, D. Laplace, B. Louage, S. Maji, L. Lybaert, R. Hoogenboom and B. G. De Geest, *Chem. Commun.*, 2015, **51**, 13972-13975.
160. S. Averick, A. Simakova, S. Park, D. Konkolewicz, A. J. D. Magenau, R. A. Mehl and K. Matyjaszewski, *ACS Macro Lett.*, 2012, **1**, 6-10.
161. A. Simakova, S. E. Averick, D. Konkolewicz and K. Matyjaszewski, *Macromolecules*, 2012, **45**, 6371-6379.
162. Q. Zhang, M. Li, C. Zhu, G. Nurumbetov, Z. Li, P. Wilson, K. Kempe and D. M. Haddleton, *J. Am. Chem. Soc.*, 2015, **137**, 9344-9353.
163. Q. Zhang, Z. Li, P. Wilson and D. M. Haddleton, *Chem. Commun.*, 2013, **49**, 6608-6610.
164. H. Murata, C. S. Cummings, R. R. Koepsel and A. J. Russell, *Biomacromolecules*, 2013, **14**, 1919-1926.
165. M. Li, H. Li, P. De and B. S. Sumerlin, *Macromol. Rapid Commun.*, 2011, **32**, 354-359.
166. J. K. Pokorski, K. Breitenkamp, L. O. Liepold, S. Qazi and M. G. Finn, *J. Am. Chem. Soc.*, 2011, **133**, 9242-9245.
167. J. Lucon, S. Qazi, M. Uchida, G. J. Bedwell, B. LaFrance, P. E. Prevelige and T. Douglas, *Nat. Chem.*, 2012, **4**, 781-788.
168. J. Lucon, E. Edwards, S. Qazi, M. Uchida and T. Douglas, *Eur. Polym. J.*, 2013, **49**, 2976-2985.

169. M. L. Hovlid, J. L. Lau, K. Breitenkamp, C. J. Higginson, B. Laufer, M. Manchester and M. G. Finn, *ACS Nano*, 2014, **8**, 8003-8014.
170. S. Mann, *Angew. Chem. Int. Ed.*, 2013, **52**, 155-162.
171. A. Harish and G. Caetano-Anollés, *PLoS One*, 2012, **7**, e32776.
172. C. Nardin, S. Thoeni, J. Widmer, M. Winterhalter and W. Meier, *Chem. Commun.*, 2000, 1433-1434.
173. M. Nallani, S. Benito, O. Onaca, A. Graff, M. Lindemann, M. Winterhalter, W. Meier and U. Schwaneberg, *J. Biotechnol.*, 2006, **123**, 50-59.
174. P. Tanner, O. Onaca, V. Balasubramanian, W. Meier and C. G. Palivan, *Chem. Eur. J.*, 2011, **17**, 4552-4560.
175. X. Huang, A. J. Patil, M. Li and S. Mann, *J. Am. Chem. Soc.*, 2014, **136**, 9225-9234.
176. S. Sun, M. Li, F. Dong, S. Wang, L. Tian and S. Mann, *Small*, 2016, **12**, 1920-1927.
177. X. Liu, P. Zhou, Y. Huang, M. Li, X. Huang and S. Mann, *Angew. Chem. Int. Ed.*, 2016, **55**, 7095-7100.
178. Z. Liu, C. Dong, X. Wang, H. Wang, W. Li, J. Tan and J. Chang, *ACS Appl. Mater. Interfaces*, 2014, **6**, 2393-2400.
179. X. Huang, M. Li and S. Mann, *Chem. Commun.*, 2014, **50**, 6278-6280.
180. S. F. M. van Dongen, M. Nallani, J. J. L. M. Cornelissen, R. J. M. Nolte and J. C. M. van Hest, *Chem. Eur. J.*, 2009, **15**, 1107-1114.
181. P. van Rijn, H. Park, K. Özlem Nazli, N. C. Mougin and A. Böker, *Langmuir*, 2013, **29**, 276-284.
182. Y. Chevalier and M.-A. Bolzinger, *Colloids Surf., A*, 2013, **439**, 23-34.
183. J. Gaitzsch, X. Huang and B. Voit, *Chem. Rev.*, 2016, **116**, 1053-1093.
184. M. Kumar, M. Grzelakowski, J. Zilles, M. Clark and W. Meier, *Proc. Natl. Acad. Sci. U. S. A.*, 2007, **104**, 20719-20724.
185. M. Nallani, O. Onaca, N. Gera, K. Hildenbrand, W. Hoheisel and U. Schwaneberg, *Biotechnol. J.*, 2006, **1**, 828-834.
186. W. Meier, C. Nardin and M. Winterhalter, *Angew. Chem. Int. Ed.*, 2000, **39**, 4599-4602.

187. T. Einfalt, R. Goers, I. A. Dinu, A. Najer, M. Spulber, O. Onaca-Fischer and C. G. Palivan, *Nano Lett.*, 2015, **15**, 7596-7603.
188. P. Tanner, P. Baumann, R. Enea, O. Onaca, C. Palivan and W. Meier, *Acc. Chem. Res.*, 2011, **44**, 1039-1049.
189. C. G. Palivan, O. Fischer-Onaca, M. Delcea, F. Itel and W. Meier, *Chem. Soc. Rev.*, 2012, **41**, 2800-2823.
190. B. Yameen, M. Ali, R. Neumann, W. Ensinger, W. Knoll and O. Azzaroni, *Nano Lett.*, 2009, **9**, 2788-2793.
191. Z. Liu, W. Wang, R. Xie, X.-J. Ju and L.-Y. Chu, *Chem. Soc. Rev.*, 2016, **45**, 460-475.
192. P. van Rijn, M. Tutus, C. Kathrein, L. Zhu, M. Wessling, U. Schwaneberg and A. Boker, *Chem. Soc. Rev.*, 2013, **42**, 6578-6592.
193. T. Xu, N. Zhao, F. Ren, R. Hourani, M. T. Lee, J. Y. Shu, S. Mao and B. A. Helms, *ACS Nano*, 2011, **5**, 1376-1384.
194. Y. Wang and F. Li, *Adv. Mater.*, 2011, **23**, 2134-2148.
195. P. K. Smith, R. I. Krohn, G. T. Hermanson, A. K. Mallia, F. H. Gartner, M. D. Provenzano, E. K. Fujimoto, N. M. Goeke, B. J. Olson and D. C. Klenk, *Anal. Biochem.*, 1985, **150**, 76-85.
196. ThermoScientific, *Instructions: Pierce BCA protein Assay kit, 23225 23227*, 1-8.
197. K. J. Wiechelman, R. D. Braun and J. D. Fitzpatrick, *Anal. Biochem.*, 1988, **175**, 231-237.
198. R. J. Simpson, *Cold Spring Harbor Protocols*, 2010, **2010**, pdb.prot5413.
199. C. Winkler, K. Denker, S. Wortelkamp and A. Sickmann, *Electrophoresis*, 2007, **28**, 2095-2099.
200. T. Rabilloud, *Electrophoresis*, 1990, **11**, 785-794.
201. J. R. Lakowicz, *Principles of Fluorescence Spectroscopy*, Springer Science, 2006.
202. V. I. Dodero and P. V. Messina, in *Proteins in Solution and at Interfaces*, John Wiley & Sons, Inc., 2013, pp. 73-98.
203. M. K. Sharon and C. P. Nicholas, *Curr. Protein Pept. Sci.*, 2000, **1**, 349-384.
204. K. Wuthrich, *Nat Struct Mol Biol*, 2001, **8**, 923-925.
205. A. Barth, *Biochim. Biophys. Acta, Bioenerg.*, 2007, **1767**, 1073-1101.

206. Q. Zhang, P. Wilson, Z. Li, R. McHale, J. Godfrey, A. Anastasaki, C. Waldron and D. M. Haddleton, *J. Am. Chem. Soc.*, 2013, **135**, 7355-7363.
207. P. van Rijn, N. C. Mougin and A. Böker, *Polymer*, 2012, **53**, 6045-6052.
208. G. T. Hermanson, *Bioconjugate Techniques*, Elsevier Science, 2013.
209. J. Pyun and K. Matyjaszewski, *Chem. Mater.*, 2001, **13**, 3436-3448.
210. D. L. Kyluik-Price and M. D. Scott, *Biomaterials*, 2016, **74**, 167-177.
211. O. Onaca, M. Nallani, S. Ihle, A. Schenk and U. Schwaneberg, *Biotechnol. J.*, 2006, **1**, 795-805.
212. S.-J. Tenne, J. Kinzel, M. Arlt, F. Sibilla, M. Bocola and U. Schwaneberg, *J. Chromatogr. B*, 2013, **937**, 13-17.
213. T. Dworeck, A. K. Petri, N. Muhammad, M. Fioroni and U. Schwaneberg, *Protein Expression Purif.*, 2011, **77**.
214. C. Michaux, N. C. Pomroy and G. G. Privé, *J. Mol. Biol.*, 2008, **375**, 1477-1488.
215. F. Philippart, M. Arlt, S. Gotzen, S.-J. Tenne, M. Bocola, H.-H. Chen, L. Zhu, U. Schwaneberg and J. Okuda, *Chem. Eur. J.*, 2013, **19**, 13865-13871.
216. D. F. Sauer, M. Bocola, C. Broglia, M. Arlt, L.-L. Zhu, M. Brocker, U. Schwaneberg and J. Okuda, *Chem. - Asian J.*, 2015, **10**, 177-182.
217. J. C. Carrington and W. G. Dougherty, *Proc. Natl. Acad. Sci. U. S. A.*, 1988, **85(10)**, 3391-3395.
218. I. M. Fearnley and J. E. Walker, *Biochem. Soc. Trans.*, 1996, **24**, 912-917.
219. J. Whitelegge, F. Halgand, P. Souda and V. Zabrouskov, *Expert Rev. Proteomics*, 2006, **3**, 585-596.
220. J. W. Jr., *Annu. Rev. Biophys. Biophys. Chem.*, 1988, **17**, 145-166.
221. F. Lorandi, M. Fantin, A. A. Isse and A. Gennaro, *Polymer*, 2015, **72**, 238-245.
222. C. Boyer, V. Bulmus, J. Liu, T. P. Davis, M. H. Stenzel and C. Barner-Kowollik, *J. Am. Chem. Soc.*, 2007, **129**, 7145-7154.
223. J. Lebowitz, M. S. Lewis and P. Schuck, *Protein Sci.*, 2002, **11**, 2067-2079.
224. C. Breyton, A. Flayhan, F. Gabel, M. Lethier, G. Durand, P. Boulanger, M. Chami and C. Ebel, *J. Biol. Chem.*, 2013, **288**, 30763-30772.
225. J. Thoma, P. Bosshart, M. Pfreundschuh and Daniel J. Müller, *Structure*, 2012, **20**, 2185-2190.

226. V. Gotor-Fernández, E. Busto and V. Gotor, *Adv. Synth. Catal.*, 2006, **348**, 797-812.
227. T. G. Mosbacher, M. Mueller and G. E. Schulz, *FEBS J.*, 2005, **272**, 6067-6076.
228. C. M. Wong, K. H. Wong and X. D. Chen, *Appl. Microbiol. Biotechnol.*, 2008, **78**, 927-938.
229. H. G. Schild, *Prog. Polym. Sci.*, 1992, **17**, 163-249.
230. N. C. Mougin, A. H. E. Müller and A. Böker, *PMSE Prepr.*, 2008, **99**, 99.
231. A. Nagai, K. Kokado, J. Miyake and Y. Chujo, *J. Polym. Sci., Part A: Polym. Chem.*, 2010, **48**, 1849-1849.
232. H. Osseili, D. F. Sauer, K. Beckerle, M. Arlt, T. Himiyama, T. Polen, A. Onoda, U. Schwaneberg, T. Hayashi and J. Okuda, *Beilstein J. Org. Chem.*, 2016, **12**, 1314-1321.
233. M. Bonhivers, M. Desmadril, G. S. Moeck, P. Boulanger, A. Colomer-Pallas and L. Letellier, *Biochemistry*, 2001, **40**, 2606-2613.
234. J. D. Berry, M. J. Neeson, R. R. Dagastine, D. Y. C. Chan and R. F. Tabor, *J. Colloid Interface Sci.*, 2015, **454**, 226-237.
235. N. A. Alexandrov, K. G. Marinova, T. D. Gurkov, K. D. Danov, P. A. Kralchevsky, S. D. Stoyanov, T. B. J. Blijdenstein, L. N. Arnaudov, E. G. Pelan and A. Lips, *J. Colloid Interface Sci.*, 2012, **376**, 296-306.
236. M. J. Richter, A. Schulz, T. Subkowski and A. Böker, *J. Colloid Interface Sci.*, 2016, **479**, 199-206.
237. J. Maldonado-Valderrama, V. B. Fainerman, E. Aksenenko, M. Jose Gálvez-Ruiz, M. A. Cabrerizo-Vílchez and R. Miller, *Colloids Surf., A*, 2005, **261**, 85-92.
238. G. Yampolskaya and D. Platikanov, *Adv. Colloid Interface Sci.*, 2006, **128–130**, 159-183.
239. M. B. Linder, *Curr. Opin. Colloid Interface Sci.*, 2009, **14**, 356-363.
240. J.-F. Gohy, S. Antoun and R. Jérôme, *Macromolecules*, 2001, **34**, 7435-7440.
241. M. Lucius, R. Falatach, C. McGlone, K. Makaroff, A. Danielson, C. Williams, J. C. Nix, D. Konkolewicz, R. C. Page and J. A. Berberich, *Biomacromolecules*, 2016, **17**, 1123-1134.
242. P. B. Lawrence and J. L. Price, *Curr. Opin. Chem. Biol.*, 2016, **34**, 88-94.

243. E. M. Pelegri-O'Day, E.-W. Lin and H. D. Maynard, *J. Am. Chem. Soc.*, 2014, **136**, 14323-14332.

244. D. J. Miller, S. Kasemset, D. R. Paul and B. D. Freeman, *J. Membr. Sci.*, 2014, **454**, 505-515.

245. C.-C. Ho and A. L. Zydney, *J. Membr. Sci.*, 2002, **209**, 363-377.